

1 **The SPPL3-defined glycosphingolipid repertoire modulates immune responses by improving**
2 **HLA class I access**

3
4 Marlieke L.M. Jongsma^{1,2,3}, Antonius A. de Waard^{1,2,#}, Matthijs Raaben^{4,#}, Tao Zhang^{5,#}, Birol
5 Cabukusta³, René Platzer⁶, Vincent A. Blomen⁴, Anastasia Xagara^{1,2}, Tamara Verkerk^{1,2}, Sophie
6 Bliss^{1,2}, Xiangrui Kong^{1,2}, Carolin Gerke^{7,8,9,10}, Lennert Janssen^{3,11}, Elmer Stickel⁴, Stephanie Holst⁵,
7 Rosina Plomp⁵, Arend Mulder¹², Soldano Ferrone¹³, Frans H.J. Claas¹², Mirjam H.M. Heemskerk¹⁴,
8 Marieke Griffioen¹⁴, Anne Halenius^{7,8}, Hermen Overkleeft¹⁵, Johannes B. Huppa⁶, Manfred Wuhrer⁵,
9 Thijn R. Brummelkamp^{4,16,17}, Jacques Neefjes^{3,11}, Robbert M. Spaapen^{1,2,11}

10
11
12 ¹Department of Immunopathology, Sanquin Research, Amsterdam, The Netherlands, ²Landsteiner
13 Laboratory, Amsterdam UMC, University of Amsterdam, Amsterdam, The Netherlands; ³Oncode
14 Institute and Department of Cell and Chemical Biology, LUMC, Leiden, The Netherlands; ⁴Oncode
15 Institute, Division of Biochemistry, the Netherlands Cancer Institute, Amsterdam, The Netherlands;
16 ⁵Center for Proteomics and Metabolics, LUMC, Leiden, The Netherlands; ⁶Institut für Hygiene und
17 Angewandte Immunologie, Vienna, Austria; ⁷Institute of Virology, Medical Center University of
18 Freiburg, Freiburg, Germany; ⁸Faculty of Medicine, University of Freiburg, Freiburg, Germany;
19 ⁹Spemann Graduate School of Biology and Medicine, University of Freiburg, Freiburg, Germany;
20 ¹⁰Faculty of Biology, University of Freiburg, Freiburg, Germany; ¹¹Department of Cell Biology II, The
21 Netherlands Cancer Institute, Amsterdam, The Netherlands; ¹²Department of Immunohaematology
22 and Blood Transfusion, LUMC, Leiden, The Netherlands; ¹³Department of Surgery, Massachusetts
23 General Hospital, Harvard Medical School, Boston, MA, United States; ¹⁴Department of Hematology,
24 Leiden University Medical Center, Leiden, The Netherlands; ¹⁵Leiden Institute of Chemistry, Leiden
25 University, Leiden, The Netherlands; ¹⁶CeMM Research Center for Molecular Medicine of the Austrian
26 Academy of Sciences, Vienna, Austria; ¹⁷Cancer Genomics Center, Amsterdam, The Netherlands.

27
28 # These authors contributed equally to this paper

29
30
31 **Running title:** Glycosphingolipids regulate HLA class I function

32 **Keywords:** HLA class I; MHC class I; glycosphingolipids; B3GNT5; SPPL3; T cell activation; antigen
33 presentation; immunotherapy; immune recognition

34
35
36
37 **Corresponding Author:** Robbert Spaapen, PhD, Sanquin Research, Department of
38 Immunopathology, Plesmanlaan 125, 1066CX, Amsterdam, The Netherlands. Phone: +31
39 610906464; e-mail: r.spaapen@sanquin.nl

1 **Summary**

2 HLA class I (HLA-I) drives immune responses by presenting antigen-derived peptides to cognate
3 CD8⁺ T cells. This process is often hijacked by tumors and pathogens for immune evasion. Since
4 therapeutic options for restoring HLA-I antigen presentation are limited, we aimed to identify new
5 HLA-I pathway targets. By iterative genome-wide screens we uncovered that the cell surface
6 glycosphingolipid (GSL) repertoire determines effective HLA-I antigen presentation. We show that
7 absence of the protease SPPL3 augments B3GNT5 enzyme activity, resulting in upregulated levels of
8 surface (neo)lacto-series GSLs. These GSLs sterically impede molecular interactions with HLA-I and
9 diminish CD8⁺ T cell activation. Furthermore, a disturbed SPPL3-B3GNT5 pathway in glioma
10 correlates with decreased patient survival. Importantly, we show that the immunomodulatory effect
11 can be reversed through GSL synthesis inhibition using clinically approved drugs. Overall, our study
12 identifies a GSL signature that inhibits immune recognition and represents a potential therapeutic
13 target in cancer, infection and autoimmunity.

14

15

1 **Introduction**

2 Human Leukocyte Antigen class I (HLA-I) proteins are the primary modules recognized by CD8⁺ T
3 cells determining both the induction and effector phase of immune responses. Their primary function
4 is to present peptide fragments from degraded proteins to the T cell receptor (TCR) of cytotoxic CD8⁺
5 T cells, leading to T cell-mediated elimination of target cells (Neefjes et al., 2011; Unanue and
6 Cerottini, 1989). Because HLA-I molecules on tumor cells also present tumor antigen-derived
7 peptides to cognate T cells, they play a major role in the anti-tumor activity of T cells unleashed by
8 current immunotherapeutic strategies (Schumacher and Schreiber, 2015). As a consequence, tumors
9 often escape from immune surveillance by downregulating one or multiple molecules critical in HLA-I
10 antigen presentation (Chowell et al., 2018; Gettinger et al., 2017; Restifo et al., 1996; Sade-Feldman
11 et al., 2017; Zaretsky et al., 2016). This reduction is often reversible, for example by interferon
12 stimulation, ionizing radiation or inhibition of histone deacetylases, which has led to various
13 experimental therapies aimed at increasing tumor HLA-I surface expression (Haworth et al., 2015;
14 Reits et al., 2006; Thor Straten and Garrido, 2016). Moreover, sensitizing tumor cells as immune
15 targets can act synergistically with T cell (re)activating strategies, thereby increasing the therapeutic
16 potential of enhancing HLA-I availability (Hahnel et al., 2008). Active suppression of HLA-I surface
17 expression to escape T cell surveillance is also employed by a wide array of pathogens, such as
18 Epstein-Barr virus, cytomegalovirus and SARS-CoV-2 (Hansen and Bouvier, 2009; Yewdell and Hill,
19 2002; Zhang, 2020). These examples underscore the broad relevance of HLA-I based interventions,
20 necessitating a thorough understanding of the molecular mechanisms underpinning the HLA-I
21 pathway.

22 Over the last 35 years, several key elements in HLA-I expression and antigen presentation have been
23 identified and extensively studied. A protein complex directed by the transcriptional regulator NLRC5
24 drives HLA-I expression in selected tissues while HLA-I translation and glycosylation are currently
25 thought to be executed by general enzymes and mechanisms (Jongsma et al., 2019; Ryan and Cobb,
26 2012). In the ER, the HLA-I heavy chain and its light chain beta-2 microglobulin (B2M) assemble and
27 are stabilized by a unique combination of the ER chaperone proteins tapasin, ERp57 and calreticulin
28 (CALR) (Rock et al., 2016). These HLA-I chaperone complexes bind the peptide transporter TAP to
29 form the so-called peptide loading complex (PLC), which drives efficient ER import and loading of
30 peptides into the HLA-I peptide-binding groove (Blees et al., 2017). Subsequently, mature trimeric
31 complexes of HLA-I heavy chain, B2M and peptide are released from the PLC for transport to the cell
32 surface for peptide presentation to T cells (Garstka et al., 2015; Wearsch and Cresswell, 2008). Given
33 the multifactorial complexity of the HLA-I antigen presentation pathway, we hypothesized that
34 additional regulatory mechanisms of this central process in adaptive immunity must exist.

35 To uncover new components involved in successful HLA-I antigen presentation, we performed a
36 series of genome-wide haploid genetic screens. In addition to the factors described above, we
37 identified the enzyme signal peptide peptidase like 3 (SPPL3) as a new player in HLA-I antigen
38 presentation. We found that SPPL3 controls the composition of the cell surface glycosphingolipid
39 (GSL) repertoire by inhibiting the glycosyltransferase B3GNT5. In the absence of SPPL3, an increase
40 in B3GNT5 activity leads to high levels of complex negatively charged (neo)lacto-series GSLs

1 (nsGSLs), preventing HLA-I from being accessed by several immune cell receptors and interfering
2 with activation of CD8⁺ T cells. The GSL synthesis in several tumors including glioma is skewed
3 towards the nsGSL synthesis pathway. High activation of this pathway negatively correlates with
4 survival of glioma patients. We show that intervention of GSL synthesis in glioma cells by FDA-
5 approved drugs leads to improved anti-tumor immunity *in vitro*. In conclusion, we identified that
6 nsGSLs shield HLA-I molecules at the cell surface, which is an unexpected and targetable layer of
7 immune regulation.

8

1 Results

2 A haploid genetic screen provides a high-resolution map of the HLA-I antigen presentation 3 pathway

4 To identify unknown factors regulating HLA-I antigen presentation, we performed a genome-wide
5 insertional mutagenesis screen in haploid human HAP1 cells endogenously expressing HLA-I
6 (Brockmann et al., 2017; Carette et al., 2009). A heterogeneous pool of millions of cells, each
7 knockout (KO) for a random gene or set of genes, was generated by retroviral gene trap insertion and
8 expanded. Mutagenized cells that were poorest or best recognized by the HLA-I-specific W6/32
9 antibody were sorted by flow cytometry (Figure 1A). Subsequently, we determined the relative
10 enrichment of unique disruptive integrations per gene between both sorted populations using deep
11 sequencing. This provided an unbiased overview of genes involved in HLA-I antigen presentation at
12 an unprecedented resolution (Figure 1B). Among the highly significant positive modifiers were the
13 known key genes directing HLA-I expression, such as the transcriptional (co)activators NLRC5,
14 RFXAP and RFX5 (Jongsma et al., 2019) and essential components for post-transcriptional
15 assembly, glycosylation and peptide loading (B2M, MOGS (α -glucosidase I), GANAB (α -glucosidase
16 II), TAP1, TAP2, tapasin, ERp57 and CALR) (Figure 1B) (Wearsch and Cresswell, 2008). Thus, this
17 single genetic map identified the components in the HLA-I pathway previously discovered through
18 decades of research. In addition, HLA-I regulators identified in human B cell lymphoma CRISPR/Cas9
19 screens by Dersh et al. were also highly significant in our haploid genetic screen, such as SUSP6,
20 SND1, ANKRD33B, EZH2 (Dersh et al., submitted). The most prominent hit from our screen in the
21 W6/32^{low} sorted population was the gene encoding SPPL3, a protease that had never been described
22 before in the context of antigen presentation (Figure 1B). SPPL3 is an ER- and Golgi-localized
23 transmembrane protein of the family of intramembrane-cleaving aspartyl proteases (Fluhrer and
24 Haass, 2007).

25 26 **SPPL3 determines the accessibility of membrane proximal regions of HLA-I**

27 To validate that HLA-I cell surface expression was altered by SPPL3, we created SPPL3 KO HAP1
28 cells using CRISPR/Cas9 (Table S1) and performed flow cytometry using the W6/32 antibody. HLA-I
29 surface levels in the absence of SPPL3 turned out identical to those of wild type (WT) cells (Figure
30 S1A), an unexpected result in view of the screening data. Likewise, the total HLA-I content of SPPL3
31 KO and WT cells was similar as determined by western blot analysis (Figure S1B). Furthermore,
32 SPPL3 deficiency does not alter HLA-I turnover or stability of the peptide-HLA-I interaction (Figures
33 S1C and S1D). As the anti-HLA antibody W6/32 was used under non-saturating staining conditions in
34 the genome-wide screen, these seemingly contradictory outcomes may have resulted from a reduced
35 accessibility of the W6/32 epitope in the absence of SPPL3.

36 To test this hypothesis, we titrated the W6/32 antibody for binding to WT, SPPL3 KO and control HLA-I
37 I KO and tapasin KO cells (Table S1), which were individually color-barcoded and combined in a
38 single well for optimal comparison of staining intensity (Figure S1E). In contrast to saturating W6/32
39 concentrations, lower W6/32 concentrations resulted in decreased binding to SPPL3 KO cells
40 compared to WT cells, indicating that access of the HLA-I epitope recognized by W6/32 was indeed

1 hindered (Figures 1C and 1D). A similar result was apparent using monovalent W6/32 Fab fragments,
2 validating this conclusion (Figure S2A). To further define SPPL3-dependent HLA-I accessibility, we
3 performed additional titrations using 13 HLA-I-specific antibodies recognizing distinct HLA-I epitopes
4 and one targeting a B2M epitope (Figures 1C, S2A and Table S2). The binding of three antibodies
5 (clones W6/32, TP25.99, ROU9A6) was markedly affected by the absence of SPPL3 (Figures 1C, 1D
6 and S2A). By superimposing critical amino acid positions for binding of the individual antibodies onto
7 an HLA-I structure, we defined that the SPPL3-susceptible region is relatively proximal to the cellular
8 membrane, an area which is largely conserved among HLA-I alleles (Figure 1E). Binding of several
9 other antibodies (e.g. B1.23.2) was not affected by SPPL3, further supporting that HLA-I surface
10 levels are not targeted by SPPL3 and providing unique intra-molecular controls for further
11 experiments. To determine whether SPPL3 differentially affected HLA-A, -B or -C alleles, we
12 reconstituted HLA-A, -B and -C KO cells on a WT or SPPL3 KO background (Table S1) with the
13 single original HLA-I alleles and analyzed their accessibility. Each allele showed a comparable
14 difference in HLA-I accessibility between WT and SPPL3-deficient cells as detected by W6/32 (Figure
15 S2B). In addition, other cell lines exhibited a similar decrease in HLA-I accessibility after siRNA
16 knockdown or CRISPR/Cas9 KO of SPPL3, indicating that regulation of HLA-I accessibility is not
17 solely restricted to HAP1 cells or their HLA-I haplotype (Figures S2C, S2D and S2E).

18

19 **SPPL3 expression promotes HLA-I ligand binding and CD8⁺ T cell activation**

20 The fact that SPPL3 modulates antibody reactivity towards specific regions of HLA-I molecules raises
21 the question whether the HLA-I function is affected. The CD8 coreceptor, which on most T cells is
22 essential for sensitizing responsiveness through supporting TCR docking to its cognate peptide HLA-I
23 complex, ligates closely to the SPPL3-affected HLA-I region (Figures 1E and 2A) (Gao et al., 1997;
24 Purbhoo et al., 2004; Roszkowski et al., 2003). We evaluated whether SPPL3 enhances HLA-I
25 antigen presentation to CD8⁺ T cells by stimulating multiple HLA-A*02:01-restricted T cell clones
26 specific for different tumor-expressed antigens endogenously expressed by WT and SPPL3 KO cells
27 (Amir et al., 2011; van Bergen et al., 2007; Van Bergen et al., 2010). All clones were more reactive to
28 SPPL3 expressing WT cells, as determined by their IFN- γ or GM-CSF production (Figure 2B),
29 indicating that SPPL3 increases functional access to HLA-I. The effect of SPPL3 on T cell function
30 was further confirmed in ⁵¹Cr release assays showing reduced killing of SPPL3 KO cells compared to
31 WT cells (Figures 2C and S3A).

32 Disturbed accessibility of HLA-I may not only affect T cells, but also other immune cells that express
33 HLA-I interacting proteins, including the inhibitory leukocyte and killer cell Ig-like receptor (LIR and
34 KIR) families that suppress unwanted immune cell activation (Saverino et al., 2000; Valiante et al.,
35 1997). The defined SPPL3-susceptible region on HLA-I highly overlaps with the binding site of LIR-1,
36 which is expressed by monocytes, B cells and small subsets of NK cells and T cells (Borges et al.,
37 1997; Colonna et al., 1997; Cosman et al., 1997) (Figure 2A). Even more pronounced than for
38 SPPL3-affected antibodies, binding of a recombinant LIR-1 Fc fusion protein (Gonen-Gross et al.,
39 2010) to HLA-I was strongly decreased on SPPL3 KO cells compared to WT cells, suggesting that
40 various immune cell functions can be impacted by SPPL3 (Figures 2D and 2F). Similarly, we

1 investigated the NK cell receptors KIR2DL1 and KIR2DL2 by evaluating the binding of their
2 recombinant Fc fusion proteins to overexpressed HLA-C*05:01 on HLA-I KO and HLA-I SPPL3
3 quadruple KO cells (Figure S3B) (Anfossi et al., 2006; Moesta et al., 2008). Surprisingly, KIR2DL1
4 binding was not influenced by SPPL3 depletion, while KIR2DL2 binding was significantly reduced in
5 the absence of SPPL3 (Figures 2E and 2F). Thus, the effect of SPPL3 on KIR and LIR binding to
6 HLA-I is variable, indicating diverse, currently not further defined, effects on signaling towards
7 different immune cell subsets.

9 **HLA-I accessibility depends on SPPL3-mediated proteolytic cleavage of a novel target**

10 SPPL3 contains two aspartate residues embedded in conserved YD and GxGD motifs located in
11 transmembrane helices 6 and 7 respectively forming the catalytic unit for proteolysis (Voss et al.,
12 2013) (Figure 2G). To investigate whether SPPL3 catalytic activity was critical in controlling HLA-I
13 accessibility and function, we expressed wild type SPPL3 or a catalytically inactive SPPL3 mutant
14 (D271A) in SPPL3 KO cells (Voss et al., 2012). Flow cytometry analysis showed that only SPPL3
15 D271A failed to restore the accessibility of HLA-I for W6/32, indicating that SPPL3 proteolytic activity
16 is required for antibody access to HLA-I (Figures 2H and S3C). This lack of rescue was further
17 confirmed on a functional level since expression of active but not inactive SPPL3 in SPPL3 KO cells
18 partially restored their capacity to activate T cells (Figure 2I).

19 SPPL3 has previously been reported to affect protein *N*-glycosylation by proteolytic inactivation of
20 glycosyltransferases in the ER and Golgi (Kuhn et al., 2015; Voss et al., 2014). Variations in the *N*-
21 linked glycan of HLA-I, located at position N86 in close proximity to the SPPL3-susceptible region
22 (Figure S3D), can affect its accessibility (Barbosa et al., 1987; Neefjes et al., 1990). However, liquid
23 chromatography-mass spectrometry (RP nano LC-ESI-MS(/MS)) of HLA-I *N*-linked glycans revealed
24 no differences between WT and SPPL3 KO cells (Figure S3E), indicating that the HLA-I *N*-glycan
25 structure is not regulated by SPPL3 activity. To further exclude a contribution of the HLA-I *N*-glycan to
26 SPPL3-modulated HLA-I accessibility, we inhibited complex *N*-glycan formation on SPPL3 KO cells
27 using the α -mannosidase I and II inhibitors kifunensine and swainsonine. The decrease of complex *N*-
28 glycans failed to alter the accessibility of the W6/32 epitope on SPPL3 KO cells (Figures S3F and
29 S3G). This result was confirmed in cells genetically engineered to lack complex (HLA-I) *N*-
30 glycosylation through ablation of the gene encoding GANAB (Table S1), which resulted in lower
31 overall HLA-I surface levels as visualized by decreased W6/32 and B1.23.2 signals (Figure S3H).
32 Comparison of these antibody stainings between WT and SPPL3 KO cells showed that the HLA-I
33 accessibility was still impaired in the absence of SPPL3 (Figure S3H). As we ruled out a role for
34 protein glycosylation, our finding that SPPL3 activity affects HLA-I at the cell surface suggests the
35 involvement of at least one unknown SPPL3 target.

37 **SPPL3-controlled glycosphingolipids modulate HLA-I accessibility**

38 To elucidate how SPPL3 controls HLA-I accessibility, we followed two genome-wide screening
39 strategies to specifically identify targets that are either positively or negatively regulated by SPPL3.

1 An SPPL3-activated target affecting HLA-I accessibility would likely be a hit in the original W6/32
2 screen, just like SPPL3 (Figure 1B). However, the identification of such a target was complicated by
3 the long list of significant hits. To distinguish SPPL3-activated targets from other candidates, we
4 complemented the original screen with a new genome-wide haploid screen using a different HLA-I-
5 specific antibody that was significantly less affected by the absence of SPPL3 (antibody BB7.2)
6 (Figures 3A and S2A). This additional screen yielded another high-resolution snapshot of HLA-I
7 antigen presentation (Figure S4A). A comparison of the two screens showed that SPPL3 was the only
8 factor selectively affecting W6/32 binding, implying that no other gene was as strongly required for
9 accessibility of HLA-I (Figure 3B).

10 We then searched for potential genes negatively regulated by SPPL3 to affect HLA-I. To this end, we
11 performed a genome-wide haploid screen in SPPL3 KO HAP1 cells. In these cells, which potentially
12 lacked SPPL3-mediated suppression of the sought target, gene trap mutagenesis of such a target or
13 its associated pathway should improve W6/32 access to HLA-I (Figure 3C). The hits from this screen
14 converged to the glycosphingolipid (GSL) synthesis pathway (Figure 3D). The enzymes UGCG,
15 B4GALT5 and B3GNT5 catalyze the synthesis of GSLs in the Golgi membrane by consecutive
16 linkage of sugar residues derived from UDP-glucose, UDP-galactose and UDP-*N*-acetylglucosamine
17 donors on ceramide molecules (Figure 3E) (Allende and Proia, 2014). The latter two carbohydrate
18 donors are transported from the cytoplasm into the Golgi by SLC35A2 and SLC35A3 respectively,
19 which were also identified in the screen (Figure 3D) (Caffaro and Hirschberg, 2006). Other hits from
20 the screen included proteins and complexes associated with Golgi homeostasis such as the members
21 of the component of oligomeric Golgi (COG) and Golgi associated retrograde protein (GARP)
22 complexes that further facilitate GSL synthesis and trafficking (Frohlich et al., 2015; Kingsley et al.,
23 1986) (Figure 3D). Of note, none of these hits related to GSL metabolism emerged in the original
24 screen with W6/32 on SPPL3-containing WT cells, strongly suggesting that in WT cells the GSL
25 synthesis or transport pathway is suppressed by SPPL3 (Figure S4B). Collectively, these
26 observations revealed the existence of a pathway comprising GSL-mediated regulation of HLA-I
27 access and function controlled by SPPL3.

28 To validate that SPPL3 reduces HLA-I accessibility through manipulation of GSL synthesis, we
29 generated GSL-deficient SPPL3 KO cells by additionally knocking out the first enzyme of the GSL
30 synthesis pathway, UGCG (Table S1). In these SPPL3/UGCG double KO cells we observed full
31 rescue of the W6/32 HLA-I epitope accessibility without affecting the SPPL3-independent B1.23.2
32 staining (Figure 3F) pointing towards an essential role for GSLs in HLA-I accessibility. Importantly,
33 GSL-deficient SPPL3 KO cells regained the capacity to engage the HLA-I ligand LIR-1 (Figure 3G),
34 underscoring the physiological relevance of GSL-mediated modulation of HLA-I accessibility.

35

36 **B3GNT5 tunes the capacity of HLA-I to interact with its natural receptors**

37 The synthesis of GSLs is probably best illustrated as a chain of sugar moiety transfers catalyzed by
38 different Golgi enzymes (Figure 3E). UGCG initiates the GSL synthesis pathway by transferring a
39 glucose to a ceramide on the cytosolic leaflet of the Golgi membrane (Allende and Proia, 2014). After
40 this glucosylceramide is flipped into the Golgi lumen, a galactose moiety is added by B4GALT5 or

1 B4GALT6 to generate lactosylceramide. This neutral GSL then serves as a substrate for various
2 glycosyltransferases responsible for the generation of different GSL-series: A4GALT (globo-series),
3 A3GALT2 (isoglobo-series), B3GNT5 ((neo)lacto-series; nsGSLs), B4GALNT1 (gangliosides, o-
4 series) and ST3GAL5 (gangliosides, a-,b-,c-series) (Figure 3E) (Allende and Proia, 2014; Zhang et
5 al., 2019). Our screening data suggest that specifically nsGSL production by means of B3GNT5
6 activity can diminish HLA-I accessibility (Figures 3D and S4A). To confirm this specificity, we
7 generated polyclonal cell lines on the SPPL3 KO background, each CRISPR/Cas9-targeting one of
8 the five branching enzymes, and analyzed W6/32 epitope accessibility by flow cytometry. HLA-I
9 accessibility in SPPL3 KO cells was restored only by ablation of B3GNT5 or control UGCG,
10 confirming B3GNT5 as the sole branching enzyme involved in HLA-I epitope shielding (Figures 4A,
11 4B and S4C). This effect was selective for SPPL3-deficient cells as HLA-I accessibility was unaffected
12 on WT cells with corresponding gene KOs (Figures 4C and S4D). Single cell derived B3GNT5 KO and
13 SPPL3/B3GNT5 double KO cell lines were generated to further corroborate a pivotal role for B3GNT5
14 in HLA-I accessibility (Table S1). As expected, additional B3GNT5 KO in SPPL3 KO cells not only
15 restored W6/32 binding to its epitope, but also the accessibility of other SPPL3-susceptible epitopes
16 recognized by TP25.99 and ROU9A6 (Figure 4D). Accessibility to SPPL3-independent epitopes and
17 total HLA-I surface expression were not affected by additional KO of B3GNT5 (Figure 4D). Most
18 importantly, the lack of B3GNT5 expression in SPPL3 KO cells restored both binding of the ligand
19 LIR-1 to HLA-I as well as their potential to activate T cells (Figures 4E and 4F). Taken together our
20 results suggest that active SPPL3 disrupts the B3GNT5 protein, which tunes the capacity of HLA-I to
21 interact with its ligands.

22

23 **SPPL3 controls the generation of (neo)lacto-series GSLs by proteolytically inactivating** 24 **B3GNT5**

25 To detect a direct interaction between SPPL3 and its putative target B3GNT5, we performed
26 coimmunoprecipitation of overexpressed epitope-tagged proteins. We coisolated B3GNT5
27 predominantly with the catalytically inactive SPPL3 D271A mutant suggesting a transient interaction
28 between SPPL3 and its substrate (Figure 5A). Cleavage of B3GNT5 by the intramembrane protease
29 SPPL3 was confirmed in total lysate by a small reduction in the molecular weight of B3GNT5 reflecting
30 proteolytic removal of the 1.5-4kD cytosolic tail and by the presence of luminal B3GNT5 fragments in
31 the supernatant (Figures 5A and 5B). Two other branching enzymes of the GSL synthesis pathway,
32 B4GALNT1 and ST3GAL5, were poorly coisolated with SPPL3 (Figure 5A). Furthermore, cleavage
33 products were not detected in the supernatant indicating that B3GNT5 is a specific substrate of
34 SPPL3 (Figure 5A).

35 To investigate whether SPPL3 affects B3GNT5 activity, we performed a B3GNT5 enzymatic assay.
36 Lysates of indicated WT and KO cells were incubated with a BODIPY-conjugated analog of the
37 B3GNT5-substrate lactosylceramide (LacCer) and the donor sugar UDP-*N*-acetylglucosamine,
38 followed by thin layer chromatography (TLC) of extracted GSLs. The B3GNT5 product
39 lactotriaosylceramide (BODIPY-Lc3Cer), as confirmed by LC-MS, was generated in increased
40 amounts in SPPL3 KO compared to WT cell lysates (Figures 5C, 5D and S5A). In addition, no Lc3Cer

1 was synthesized in lysates of B3GNT5 KO cells, demonstrating that B3GNT5 is the sole producer of
2 Lc3Cer in HAP1 cells. Since SPPL3 inhibits B3GNT5 activity, we next addressed the extent to which
3 SPPL3 defines the cellular GSL profile. Glycan portions of the GSL repertoire of WT, SPPL3 KO and
4 SPPL3/B3GNT5 double KO cells were isolated and analyzed by LC-MS. We found an extensive shift
5 in the relative GSL abundance towards B3GNT5-produced nsGSLs, from 44% in WT cells to 82% in
6 SPPL3 KO cells (Figures 5E, 5F and Table S3). The increase was most evident for complex nsGSLs
7 containing six or more sugar residues as determined by relative quantification of individual GSLs,
8 suggesting that epitope shielding of HLA-I is mediated by complex nsGSLs (Figure S5B and Table
9 S3). To validate the shift in GSL repertoire in living cells, we conducted flow cytometry-based
10 experiments using cholera toxin subunit B, which binds the ganglioside GM1, and an antibody against
11 the nsGSL SSEA-1 epitope. GSL-deficient UGCG KO cells were negative for all probes,
12 demonstrating probe specificity towards GSLs on our cells (Figure S5C). Compared to WT cells,
13 SPPL3 KO cells expressed increased levels of SSEA-1 nsGSLs, which were generated by B3GNT5,
14 and decreased levels of GM1 gangliosides (Figures 5G and S5C). Consistent with our relative
15 quantification of individual glycans detected by LC-MS, these data demonstrate that SPPL3 dictates
16 the composition of the GSL repertoire by inhibiting the nsGSL biosynthesis activity of B3GNT5.

17

18 **Sialic acid residues on nsGSLs are required for HLA-I shielding**

19 GSLs are major constituents of membrane microdomains (Sezgin et al., 2017). A change in GSL
20 composition may then disturb membrane protein localization, mobility and function. We therefore
21 investigated the mobility of HLA-I in SPPL3 KO cells by single particle tracking. The mobile fraction
22 and diffusion constant of BB7.2 Fab labeled HLA-I molecules were equal between SPPL3 KO and WT
23 cells, indicating that HLA-I membrane dynamics were not detectably affected by any potential
24 alterations in membrane microdomain organization nor by SPPL3 itself (Figures S6A, S6B, S6C and
25 S6D). This renders a scenario in which HLA-I associates with another protein in the absence of
26 SPPL3 unlikely, as this would reduce the HLA-I diffusion rate. Instead, our data highly suggest that
27 decreased HLA-I accessibility is a direct consequence of interactions with nsGSLs. Such GSL-protein
28 interactions can occur between gangliosides and hormone receptors through a charge-based linkage
29 of GSL-derived sialic acid with positively charged amino acids (D'Angelo et al., 2013). Further
30 analyses of the GSL signature of SPPL3 KO compared to WT cells revealed that the nsGSL glycan
31 chains more frequently contain α -2,3- and α -2,6-linked sialic acid residues, but also non-charged
32 fucoses (Figures 5D, 6A and Table S3). To test the requirement of these nsGSL-localized sugar
33 residues, we inhibited all sialyl- and fucosyl-transferase activity and found that dose-dependent
34 inhibition of sialylation but not fucosylation restores HLA-I accessibility in SPPL3 KO cells (Figures 6B,
35 6C, 6D and 6E). The requirement for sialic acids was further substantiated by the genetic KO of CMP-
36 sialic acid synthetase (CMAS), which recapitulated the recovery of HLA-I accessibility in SPPL3 KO
37 cells (Figures 6B and 6F). Finally, the enzymatic removal of sialic acid residues at the cell surface by
38 neuraminidase treatment also diminished HLA-I shielding (Figures 6B and 6G). Thus, the B3GNT5-
39 generated GSLs shield HLA-I through its sialic acids, likely via a direct charge-based interaction.

40

1 **Pharmacological inhibition of GSL synthesis in glioma enhances anti-tumor immune activation**
2 ***in vitro***

3 Having determined that nsGSL-rich target cells suppress T cell activity, we examined which tumors
4 have increased nsGSL expression or downmodulated SPPL3 activity. Because of the complexity
5 inherent to identifying (large) nsGSLs, there is currently only a limited amount of data available on
6 their tissue expression, including tumors (Merrill and Sullards, 2017; Zhang et al., 2019). Nonetheless,
7 elevated levels of nsGSLs or its synthesis enzyme B3GNT5 have been observed on several tumor
8 types including glioma, AML and adenocarcinomas (Furukawa et al., 2015; Hakomori, 1984; Wang et
9 al., 2012; Wikstrand et al., 1991). In addition, The Cancer Genome Atlas (TCGA) analyses
10 demonstrated that high B3GNT5 expression in low grade glioma correlates with decreased overall
11 patient survival (Figure 7A). In line with our findings, the reverse holds true for the B3GNT5-
12 suppressing SPPL3 (Figure 7B). Moreover, analyses of the combined effect of B3GNT5 and SPPL3
13 expression showed only lower survival rates for patients with high B3GNT5 and low SPPL3
14 expression (Figures 7C and S7A), probably reflecting that the nsGSL levels are only elevated in
15 tumors from this group. This indicates that gliomas possibly limit immune detection by exploiting the
16 SPPL3-B3GNT5 axis. We tested the role of SPPL3 in the glioblastoma cell line U373. Overexpression
17 of SPPL3 increased HLA-I accessibility to W6/32 without altering HLA-I expression (Figure 7D). Next,
18 we analyzed the role of GSLs in this process by genetic depletion of (ns)GSLs from WT U373 cells
19 and detected also here a specific increase in HLA-I accessibility (Figures 7E and S7B). Moreover, in
20 the absence of GSLs, U373 cells were better activators of T cells (Figure 7F).

21 To downregulate nsGSL expression in patients, the clinically approved GSL synthesis inhibitors
22 miglustat and eliglustat may be used (Stirnemann et al., 2017). These drugs are currently being used
23 in substrate reduction therapy in Gaucher disease. We first explored whether these small molecule
24 drugs affect accessibility of HLA-I epitopes that are shielded in SPPL3 KO cells. The miglustat mimics
25 MZ21 and MZ31 with fewer off-target effects were also included (Ghisaidoobe et al., 2014). All GSL
26 synthesis inhibitors fully restored HLA-I accessibility despite a small proportion of GSLs still being
27 detectable on the cell surface (Figures 7G, S7C, S7D, S7E and S7F). Moreover, these inhibitors
28 increased the capacity of SPPL3 KO cells to activate T cells (Figures 7H, 7I and S7G). This was also
29 observed for the U373 cells, of which HLA-I shielding was alleviated and their capacity to activate T
30 cells was increased (Figures 7J, 7K and S7H). Together these data demonstrate that these inhibitors
31 can boost immune responses against tumor cells that display an excess of nsGSLs.

1 Discussion

2 The process of HLA-I antigen presentation has been a topic of longstanding interest to the research
3 community, giving rise to a detailed understanding of various proteins governing this complex
4 pathway. We here add an unexpected element to the equation of successful antigen presentation,
5 namely the SPPL3-B3GNT5 pathway responsible for the production of a subset of GSLs. GSLs are
6 present on every cell, yet their functional roles in the cell membrane remain largely unknown. By
7 conducting sensitive genome-wide screens in an iterative fashion, we uncovered a role for a subset of
8 GSLs in immunity controlled by the aspartyl protease SPPL3. These so-termed nsGSLs shield HLA-I
9 molecules, limiting their interactions with several immune cell receptors and decreasing CD8⁺ T cell
10 responses. We identified SPPL3 as a new switch controlling the expression of nsGSLs through
11 proteolytic inhibition of the nsGSL synthesizing enzyme B3GNT5. Taken together, our study reveals a
12 novel layer of immune regulation which acts late in the HLA-I antigen presentation pathway through
13 shielding of critical HLA-I epitopes at the cell surface.

14
15 Understanding nsGSL function at a molecular level and in (patho)physiological settings is challenging
16 given that their isolation, analytical dissection and in particular their experimental manipulation are
17 extraordinarily demanding to date (Merrill and Sullards, 2017; Zhang et al., 2019). Hence, no
18 validated methods are available to study nsGSL-protein interactions restricting options to directly
19 probe the nsGSL-HLA-I interaction. Our current data indicate that the interaction between nsGSLs
20 and HLA-I molecules must be transient, since a high dose of antibody can overcome the decreased
21 accessibility. In addition, we show that this interplay is independent of carbohydrate-carbohydrate
22 interactions (D'Angelo et al., 2013) between nsGSLs and HLA-I *N*-glycans. The profound shielding of
23 large HLA-I patches by nsGSLs can however be explained by the fact that nsGSLs, in contrast to
24 other GSL subtypes, can carry huge glycan chains of up to 60 sugar residues (Miller-Podraza et al.,
25 1993; Miller-Podraza et al., 1997). These long carbohydrate trees may reach up to HLA-I domains
26 involved in the interaction with ligands such as LIR-1. The nsGSLs may sterically compete with
27 ligands for access to HLA-I, or restrict ligand access by altering HLA-I orientation towards the cellular
28 membrane (Mitra et al., 2004). In addition, our data do not exclude a direct interaction between the
29 GSL ceramide and the HLA-I transmembrane domain (Contreras et al., 2012), which could contribute
30 to the positioning the nsGSL glycan chain in close proximity of HLA-I. Finally, we show that sialic acid
31 residues on GSLs are essential for HLA-I shielding. The negatively charged sialylated nsGSLs may
32 establish ionic interactions with HLA-I, which has abundant positively charged patches at its molecular
33 surface (Li et al., 2012). Similar GSL-protein interactions have been found between sialic acids on
34 short GSL-glycans and exposed positively charged amino acid residues close to the plasma
35 membrane (D'Angelo et al., 2013). This points out that sialylated nsGSLs may also shield cell surface
36 receptors other than HLA-I and possibly affect their cognate interactions. This assumption is
37 supported by the fact that SPPL3 was also identified in recent genome-wide KO screens for surface
38 detection of BTN molecules by a functional V γ 9V δ 2⁺ $\gamma\delta$ TCR, or CD47 and CD59 by antibodies (Davis
39 et al., 2015; Logtenberg et al., 2019; Rigau et al., 2020). In these cases, the underlying molecular
40 mechanism of the SPPL3 effect was not resolved, yet they suggest that the newly identified SPPL3-

1 B3GNT5 pathway constitutes a novel mechanism to fine tune communication between cells, including
2 a functional tumor cell - T cell interaction as we report here.

3
4 Various malignant cells exhibit alterations in their GSL surface repertoire to which a number of
5 specific functions have been attributed. Some GSLs can serve as signaling molecules to control
6 cellular processes such as apoptosis and proliferation while other GSL species can confer anti-cancer
7 drug resistance by inhibiting proteins that facilitate their membrane transport (Liu et al., 2013;
8 Ogretmen and Hannun, 2004). We here propose that changes in the tumor GSL repertoire, in
9 particular increments of sialic acid-containing nsGSLs, limit HLA-I signaling to T cells as a means to
10 evade immune surveillance. In support of this hypothesis, our *in vitro* data show that GSLs diminish
11 the capacity of CD8⁺ T cells to respond to glioma, a tumor type with high levels of nsGSLs (Furukawa
12 et al., 2015). Furthermore, HLA-I-related NK cell activation against tumors lacking SPPL3 may be
13 restricted according to recent genome-wide KO screens (Pech et al., 2019). Thus, nsGSL
14 upregulation by tumors such as glioma might allow T cell escape, while marginalizing NK cell
15 recognition. In addition to *in vitro* experimentation, analyses involving glioma patients revealed worst
16 overall survival when the SPPL3 and B3GNT5 expression signature of the tumor suggests high
17 nsGSL synthesis. Such correlation with patient outcome may have been influenced by covariates,
18 which potentially include nsGSL-mediated shielding of other immune or nonimmune receptors or
19 membrane turnover (Catalaa et al., 2006; Righi et al., 2009). Other tumor types, including AML,
20 colorectal carcinoma, adenocarcinomas and ductal carcinomas in situ (DCIS) also overexpress
21 B3GNT5 and its product nsGSLs (Hakomori, 1984; Potapenko et al., 2015; Wang et al., 2012;
22 Wikstrand et al., 1991), suggesting that nsGSL overexpression is a general strategy for tumor
23 survival. Furthermore, pathogens such as cytomegalovirus, respiratory syncytial virus and HIV alter
24 the GSL composition of the host cell, potentially inducing/representing immune evasion through HLA-I
25 shielding (Fantini et al., 2000; Moore et al., 2008; Radsak and Wiegandt, 1984). Except for low
26 resolution data concerning cytomegalovirus-induced nsGSL expression upon infection (Andrews et
27 al., 1989; Radsak and Wiegandt, 1984), currently little is known about which viral infections influence
28 complex nsGSL expression.

29
30 In this study, we present GSLs as highly relevant molecules affecting the efficiency of immune
31 responses. nsGSLs and their molecular switch SPPL3 represent an unexplored avenue for
32 therapeutic intervention in cancer, infection and autoimmune diseases. Currently, two small molecule
33 drugs inhibiting GSL synthesis are registered, miglustat (Zavesca) and eliglustat (Cerdelga). These
34 structurally different UGCG inhibitors (Platt et al., 1994; Shayman, 2010) have been approved for the
35 treatment of patients with lysosomal storage disorders, such as type I Gaucher disease and Niemann-
36 Pick disease type C (Lachmann, 2003; Wraith and Imrie, 2009). Therapeutic application can therefore
37 efficiently be extended to include immune enhancement against tumors or pathogen-infected cells.
38 GSL synthesis inhibition may even be successfully combined with existing immunotherapies, such as
39 PD-1 blockade, because of the potential synergy between enhanced tumor cell immunogenicity and
40 simultaneous T cell activation. Hence our findings define a novel strategy to improve immunotherapy.

1 **Acknowledgments**

2 We thank Dr. R. Fluhrer (Ludwig Maximilians University, Germany) for providing SPPL3 plasmids, Dr.
3 M. Griffioen (LUMC, The Netherlands) for providing T cell clones, Dr. O. Mandelboim (Hebrew
4 University Hadassah Medical School, Israel) for providing LIR-1 Fc fusion protein, Dr. T. Rispens
5 (Sanquin, The Netherlands) for expert advice and assistance on protein purification and Fab
6 generation, E. Mul, S. Tol and M. Hoogenboezem (Sanquin) for assistance with flow cytometry, Dr. D.
7 Amsen (Sanquin) and Dr. I. Berlin (LUMC) for critical reading of the manuscript, Dr. Y. Rombouts
8 (Université de Toulouse, France) for discussions and contribution to MTBE extraction, and C.A.M.
9 Koeleman and A.L. Hipgrave Ederveen (LUMC) for technical support with LC-MS.

10 This work was supported by the Dutch Research Council (NWO-VENI 016.131.047, NWO-VIDI
11 91719369 and ZonMw-ETH 435004024; R.M.S.), KWF Alpe d’HuZes (Bas Mulder Award 2015-7982;
12 R.M.S.) and the Landsteiner Foundation for Blood Transfusion Research (LSBR fellowship 1842F;
13 R.M.S.). M.L.M.J. was supported by an EMBO short term fellowship (ASTF 10-2016). T.R.B. was
14 supported by NWO Vici Grant 016.Vici.170.033, KWF grant NKI2015-7609, the Cancer Genomics
15 Center (CGC.nl), and the Ammodo KNAW Award 2015 for Biomedical Sciences. R.P. was supported
16 by a predoctoral fellowship from the Boehringer Ingelheim Fond and J.B.H. by the Vienna Science
17 and Technology Fund (WWTF LS14-031). S.F. was supported by grants from DOD (W81XWMH-16-1-
18 0500) and NIH (R01DE028172, R03CA216114, RO3CA223886 and RO3CA231766).

19

20

1 **Author contribution statements**

2 Conceptualization and design, M.L.M.J and R.M.S. Data acquisition, analysis and interpretation,
3 M.L.M.J, M.R., A.A.W., T.Z., B.C., R.P., V.A.B., A.X., T.V., S.B., X.K., C.G., L.J., E.S., S.H., R.P. and
4 R.M.S. Resources and discussion, A.M., S.F., F.H.J.C., M.H.M.H., M.G., A.H. and H.O. Supervision
5 and conceptual discussion, J.B.H., M.W., T.R.B., J.N., R.M.S. Writing, M.L.M.J. and R.M.S. Editing,
6 J.B.H., M.R., A.A.W.,T.Z., M.W., J.N.

7

8 **Declarations of interests**

9 T.R.B. is a cofounder and SAB member of Haplogen GmbH and a cofounder and director of Scenic
10 Biotech B.V.. The other authors declare no competing interests.

1 **Figure Legends**

2 **Figure 1. A haploid genetic screen reveals SPPL3 as a novel regulator of accessibility to**
3 **membrane proximal HLA-I regions** (A) Schematic overview of genome-wide haploid genetic screen
4 using the W6/32 antibody against HLA-A, -B and -C alleles. (B) A fish-tail plot showing the mutation
5 index (ratio of integrations mapped per gene in the W6/32^{High} / W6/32^{Low} sorted populations) against
6 the total amount of mapped integrations per gene (W6/32^{High} + W6/32^{Low}). Positive and negative
7 regulators of HLA-I (*black/color*) were identified by two-sided Fisher's exact test, FDR (Benjamini-
8 Hochberg) corrected $p < 0.05$. Known HLA-I regulators are depicted in green, known HLA-I
9 transcriptional (co)activators in brown and the novel regulator SPPL3 in red. (C) (*left*) Representative
10 titration curves of W6/32, TP25.99, B1.23.2 and WK1D12 antibodies on mixed barcoded (see Figure
11 S1E) WT (*blue*), SPPL3 KO (*red*), tapasin KO (*black*) and HLA-I KO (*green*) HAP1 cells. The
12 individual antibody binding epitopes are depicted on the HLA-I structure. (*right*) Example FACS
13 histograms of non-saturating antibody stain (concentration chosen around EC50 value as indicated by
14 the arrow). (D) Titration-based EC50 values for WT and SPPL3 KO ('KO'), ratios are plotted. Data are
15 represented as mean \pm SD, n=5-8. (E) Crystal structure of HLA-I/B2M. SPPL3-susceptible epitopes
16 (*red*), mildly affected epitopes (*purple*) and SPPL3-independent epitopes (*blue*) are highlighted on the
17 structure (see Figures 1C and S2A for individual epitopes). *See also Figures S1 and S2.*

1 **Figure 2. SPPL3 expression promotes LIR-1 binding to HLA-I and enhances CD8⁺ T cell**
2 **activation** (A) CD8 interaction sites (*left, orange*) and LIR-1 interactions sites (*right, green*) mapped
3 on the crystal structure of HLA-I/B2M. (B) IFN- γ production by HLA-A*02:01-restricted T cells
4 recognizing endogenously derived USP11, VPS13B and ADIR peptides after overnight coculture with
5 WT (*blue*) or SPPL3 KO (*red*) HAP1 cells determined by ELISA. Data are represented as mean \pm SD,
6 n=3. (C) ⁵¹Chromium release depicted as specific lysis (%) of WT (*blue*), SPPL3 KO (*red*) and HLA-I
7 KO cells (*green*) by HLA-A*02:01-restricted T cells recognizing endogenously derived USP11 or
8 SSR1 peptides at indicated E:T ratios. Data are represented as mean \pm SD, n=3 (see also Figure
9 S3A). (D) (*left*) Representative titration curves of LIR-1 Fc fusion protein on WT (*blue*), SPPL3 KO
10 (*red*), tapasin KO (*black*) and HLA-I KO (*green*) HAP1 cells. (*right*) Representative histogram of LIR-1
11 Fc binding from the indicated concentration (arrow). n=2. (E) Representative histograms of non-
12 saturating concentration of KIR2DL1 Fc and KIR2DL2 Fc fusion proteins, binding to HLA-C*05:01
13 expressed in HLA-I KO (*blue*) and SPPL3/HLA-I dKO (*red*) cells. Unstained control is in gray. (F)
14 Normalized quantification (median fluorescence intensity; MFI) of HLA-I binding by indicated fusion
15 proteins (including data from experiments of Figures 2D, 2E, 3G and 4E). Data are represented as \pm
16 SD, n=3-6. (G) Predicted protein structure of SPPL3 with its catalytic residues magnified in the
17 detailed view. (H) Representative histogram of non-saturating W6/32 stain on HAP1 WT (*blue*) or
18 SPPL3 KO cells transduced with either RFP-empty vector (EV, *red*), RFP-SPPL3 (*green*) or
19 catalytically inactive RFP-SPPL3 D271A (*orange*). Unstained control is in gray. For transduced
20 samples, only cells from RFP⁺ gate are shown. See Figure S3C for SPPL3-independent B1.23.2
21 antibody stain. Quantified mean fluorescence intensity (MFI) ratios using the RFP- gate as reference
22 are represented as mean \pm SD, n=5. (I) IFN- γ secretion by HLA-A*02:01-restricted T cells recognizing
23 endogenously presented USP11 or FDPS peptides after overnight coculture with RFP⁺ FACS sorted
24 HAP1 SPPL3 KO cells that were transduced with either RFP-empty vector (EV, red), RFP-SPPL3
25 (green) or catalytically inactive RFP-SPPL3 D271A (orange), or with unsorted WT (blue) or unsorted
26 HLA-I KO (gray) cells, as determined by ELISA. Data are represented as mean \pm SD, n=2-3. See also
27 *Figure S3.*

1 **Figure 3. SPPL3-controlled glycosphingolipids modulate accessibility of HLA-I** (A) Schematic
2 outline showing that a combination of BB7.2 and W6/32 antibody screens will lead to the specific
3 identification of potential HLA-I regulators activated by SPPL3. (B) Rocket plot depicts the number of
4 unique disruptive integrations per gene in the BB7.2^{Low} sorted population plotted against the number
5 of unique disruptive integrations per gene in the W6/32^{Low} sorted population. Positive and negative
6 regulators of HLA-I (*black*) were determined by Fisher's exact test, FDR (Benjamini-Hochberg)
7 corrected $p < 0.05$. Highlighted are known HLA-I regulators (HLA-A $p < 0.05$; *green*), HLA-I
8 transcriptional (co)activators (*brown*), the regulator SPPL3 ($p < 0.05$; *red*), proteins involved in the
9 glycosphingolipid (GSL) synthesis pathway (*orange*) and members of the GARP and COG complexes
10 (*blue and purple, respectively*) (see also Figure S4A). (C) Schematic outline showing that a W6/32
11 antibody screen in SPPL3 KO cells will lead to the identification of potential HLA-I regulators that are
12 inactivated by SPPL3 activity in WT cells. (D) Fish-tail plot of the mutation index (ratio of integrations
13 per gene of W6/32^{High} / W6/32^{Low} populations) against the total amount of integrations per gene
14 (W6/32^{High} + W6/32^{Low}). Positive and negative regulators of HLA-I (*black/color*) were determined by
15 Fisher's exact test, FDR (Benjamini-Hochberg) corrected $p < 0.05$. Color legend as in (B) (see also
16 Figure S4B). (E) Schematic overview of the GSL synthesis pathway. The core enzymes UGCG and
17 B4GALT5 catalyze the first two steps of GSL synthesis. Five branching enzymes initiate the synthesis
18 of four different groups of GSLs: globo-, isoglobo-, (neo)lacto- and ganglio-series. The putative
19 SPPL3-targeted branch is shown in orange. PM, plasma membrane. (F) Representative histograms of
20 non-saturating W6/32 and B1.23.2 cell surface staining of WT (*blue*), SPPL3 KO (*red*), UGCG KO
21 (*blue dashed*) and SPPL3/UGCG double KO (dKO) HAP1 cells (*red dashed*). Quantification (MFI) is
22 represented as mean \pm SD, $n=3$, 'KO' is SPPL3 KO. Unstained control is in gray. (G) Representative
23 histogram of LIR-1 Fc fusion protein binding to WT (*blue*), SPPL3 KO (*red*), UGCG KO (*blue dashed*)
24 or SPPL3/UGCG double KO (dKO) HAP1 cells (*red dashed*), quantification (median fluorescence
25 intensity; MFI) is represented as mean \pm SD, $n=3$, 'KO' is SPPL3 KO. Unstained control is in gray.
26 *See also Figure S4.*

1 **Figure 4. B3GNT5 function determines the HLA-I visibility for its natural receptors** (A)
2 Representative histograms of non-saturating W6/32 cell surface staining of SPPL3 KO (GFP-: *red*,
3 *solid*) or polyclonal populations of SPPL3 KO cells additionally knocked out for the core enzyme
4 UGCG or the branching enzymes A3GALT2, A4GALT, B3GNT5, B4GALNT1 or ST3GAL5 (GFP+:
5 *red*, *dashed*) (gRNAs, see Table S4). (B) Normalized W6/32 (*left*) and B1.23.2 (*right*) MFI of SPPL3
6 KO cells additionally KO for UGCG or branching enzymes (GFP+) against non-transduced SPPL3 KO
7 cells in the same sample (GFP-). Data is represented as mean \pm SD, n=4-8 (see Figure S4C). (C)
8 Normalized W6/32 MFI of HAP1 WT cells as in (B). Data is represented as mean \pm SD, n=4-8 (see
9 Figure S4D). (D) Representative histograms of non-saturating cell surface stainings using three HLA-
10 I-specific antibodies recognizing SPPL3-susceptible epitopes (W6/32, TP25.99 and ROU9A6) and
11 three recognizing SPPL3-independent epitopes (SN230G6, WK4E3 and B1.23.2) on WT (*blue*),
12 SPPL3 KO (*red*), B3GNT5 KO (*blue dashed*) and SPPL3/B3GNT5 double KO (dKO) (*red dashed*)
13 HAP1 cells. Quantifications (MFI) are represented as mean \pm SD, n=4-7, 'KO' is SPPL3 KO. (E)
14 Representative histograms of LIR-1 Fc fusion protein binding to WT (*blue*), SPPL3 KO (*red*), B3GNT5
15 KO (*blue dashed*) and SPPL3/B3GNT5 double KO (dKO) (*red dashed*) HAP1 cells. Quantification
16 (median fluorescence intensity; MFI) is represented as mean \pm SD, n=2, 'KO' is SPPL3 KO. (F) IFN- γ
17 or GM-CSF secretion by HLA-A*02:01-restricted USP11- or SSR1-specific T cells after overnight
18 coculture with WT (*blue*), SPPL3 KO (*red*), B3GNT5 KO (*blue dashed*), SPPL3/B3GNT5 double KO
19 (dKO) (*red dashed*) or HLA-I KO (*gray*) HAP1 cells was determined by ELISA. Data are represented
20 as mean \pm SD, n=3. For flow cytometry data, the gray histogram represents an unstained control cell
21 line. See also Figure S4.

1 **Figure 5. SPPL3 controls the generation of nsGSLs by targeting B3GNT5** (A)
2 Coimmunoprecipitation of B3GNT5-FLAG, B4GALNT1-FLAG or ST3GAL5-FLAG with either empty
3 vector RFP (RFP), RFP-SPPL3 (R-SPPL3) or RFP-SPPL3 D271A (R-D271A) using RFP-Trap beads.
4 TL, total lysate; Sup, total supernatant. Representative of n=2 is shown. (B) Schematic representation
5 of B3GNT5 proteolysis by the intramembrane protease SPPL3. (C/D) B3GNT5 activity in cell lysates
6 from WT, SPPL3 KO, B3GNT5 KO or SPPL3/B3GNT5 double KO (dKO) HAP1 cells using UDP-
7 GlcNac donor sugar, BODIPY-Lactosylceramide substrate or both, analyzed by thin layer
8 chromatography. (C) Quantification of B3GNT5-produced BODIPY-Lc3 and (D) an example
9 chromatogram are shown. Data are represented as mean \pm SD, n=3 (see Figure S5A for LC-MS
10 validation). (E) Base peak chromatograms of PGC LC-MS on total GSL glycans isolated from WT
11 (*blue*), SPPL3 KO (*red*) or SPPL3/B3GNT5 double KO (dKO) cells (*black*). The proposed glycan
12 structures, their relative abundance and standard deviation are listed in Table S3 and Figure S5B.
13 Representative of n=3 is shown. (F) Quantified relative abundance of the three subtypes of GSL
14 glycans derived from WT (*blue*), SPPL3 KO (*red*) and SPPL3/B3GNT5 dKO cells (*white*). Data are
15 represented as mean \pm SD, n=3. (G) Representative histograms of cholera toxin B (CTB; anti-GM1)
16 and C3D-1 (anti-SSEA-1) cell surface staining of WT (*blue*), SPPL3 KO (*red*), B3GNT5 KO (*blue*
17 *dashed*) and SPPL3/B3GNT5 double KO (dKO) (*red dashed*) HAP1 cells. Unstained control is in gray.
18 Quantification (MFI) of is represented as mean \pm SD, n=3, 'KO' is SPPL3 KO (see also Figure S5C).
19 *See also Figure S5.*

20

1 **Figure 6. Sialic acid residues on nsGSLs are required for HLA-I shielding** (A) Quantification of
2 the percentage of sialylated and fucosylated nsGSLs relative to total GSLs present in WT or SPPL3
3 KO HAP1 cells. Data are represented as mean \pm SD, n=3. Experiment from Figure 5E. (B) Schematic
4 model of several targetable steps in the sialylation and fucosylation of nsGSLs. NA, neuraminidase;
5 PM, plasma membrane. (C) Non-saturating W6/32 (*left*) and B1.23.2 (*right*) cell surface staining of WT
6 (*blue*) and SPPL3 KO (*red*) HAP1 cells cultured in the presence of a serial dilution of indicated
7 sialyltransferase (SiaT; *top*) or fucosyltransferase (FucT; *bottom*) inhibitors. (D) Representative
8 histograms of non-saturating W6/32 (*left*) and B1.23.2 (*right*) cell surface staining of WT (*blue*) or
9 SPPL3 KO (*red*) HAP1 cells precultured with (*dashed*) or without (*continuous*) indicated sialyl- (*upper*)
10 or fucosyltransferase (*bottom*) inhibitors (100 μ M). (E) Quantification of histograms shown in (D), MFI
11 are represented as mean \pm SD, n=6, 'KO' is SPPL3 KO. (F) Representative histograms of non-
12 saturating W6/32 and B1.23.2 cell surface stainings of WT (*blue*), SPPL3 KO (*red*), CMAS KO (*blue*
13 *dashed*) and SPPL3/CMAS double KO (dKO) (*red dashed*) HAP1 cells. CMAS KO cells were
14 puromycin selected before staining. Quantification (MFI) is represented as mean \pm SD, n=2, 'KO' is
15 SPPL3 KO. (G) Representative histograms of non-saturating W6/32 and B1.23.2 cell surface staining
16 of WT (*blue*) and SPPL3 KO (*red*) HAP1 cells treated with (*dashed*) or without (*solid*) 225mU
17 Neuraminidase (NA) for 1h at 37°C. Quantification (MFI) is represented as mean \pm SD, n=4, 'KO' is
18 SPPL3 KO. For flow cytometry data, the unstained control is gray.

19

20

1 **Figure 7. Pharmacological inhibition of GSL synthesis in glioma enhances anti-tumor immune**
2 **responses** (A/B) TCGA (The Cancer Genome Atlas) derived Kaplan-Meier curve showing the
3 percentage survival of patients that have tumors expressing high (*black*) or low (*gray*) levels of
4 B3GNT5 (A) or SPPL3 (B). (C) Kaplan-Meier curves for four groups based on B3GNT5/SPPL3 low
5 and high expression levels (see Figure S7A for expression distribution). (D) Representative
6 histograms of non-saturating W6/32 (*left*) and B1.23.2 (*right*) cell surface staining of U373
7 glioblastoma cells overexpressing GFP-SPPL3 (*green*) or RFP empty vector control (*black*), mixed
8 and analyzed in a single well. Quantification (MFI GFP+ cells / MFI RFP+ cells) is shown including
9 GFP empty vector control as mean \pm SD, n=5. (E) Representative histograms of non-saturating
10 W6/32 and B1.23.2 cell surface staining of WT (*black*) and UGCG KO (*red*) U373 cells. UGCG KO
11 cells were puromycin selected resulting in a pooled population of KO cells. Quantification (MFI) is
12 represented as mean \pm SD, n=4-5 (see Figure S7B). (F) IFN- γ secretion by HLA-A*02:01-restricted T
13 cells recognizing USP11 peptides after overnight coculture with U373 WT (*black*) or UGCG KO (*red*)
14 cells as determined by ELISA, data is represented as mean \pm SD, n=3. (G) Normalized W6/32 (*left*)
15 and B1.23.2 (*right*) MFI of SPPL3 KO cells (*red*) precultured with the UGCG inhibitors miglustat (Migl),
16 eliglustat (Eligl), MZ21 or MZ31 (*red dashed*) against WT HAP1 cells (*blue*). Quantifications (MFI) are
17 represented as mean \pm SD, n=2-7 (see also Figures S7C, S7D, S7E and S7F). (H/I) IFN- γ or GM-
18 CSF secretion by HLA-A*02:01-restricted T cells specific for endogenously derived USP11 (H) or
19 SSR1 (I) antigens in an overnight coculture with HAP1 WT (*blue*) or SPPL3 KO cells (*red*) each
20 precultured with (*dashed*) or without (*solid*) the indicated UGCG inhibitor (MZ31 or miglustat (Migl)) as
21 determined by ELISA. Data is represented as mean \pm SD, n=3 (see Figure S7G for more T cell
22 clones). (J) Representative histogram of non-saturating W6/32 cell surface staining of WT (*black*,
23 *solid*) U373 cells precultured with UGCG inhibitors eliglustat (*black, dashed*) or MZ31 (*black, dotted*).
24 Quantification (MFI) is represented as mean \pm SD, n=3 (see also Figure S7H). (K) IFN- γ secretion by
25 HLA-A*02:01-restricted USP11-specific T cells after overnight coculture with untreated (*black*) or
26 depicted UGCG inhibitor pretreated (*dashed*) U373 cells as determined by ELISA, data is represented
27 as mean \pm SD, n=3. For flow cytometry data, the gray histogram represents an unstained control cell
28 line. See also Figure S7.

29

1 **STAR Methods**

2

3 **KEY RESOURCE TABLE**

4 See separate Word file.

5

6 **RESOURCE AVAILABILITY**

7 **Lead Contact:** Further information and requests for resources and reagents should be directed to
8 and will be fulfilled by the Lead Contact, Robbert Spaapen, Ph.D (r.spaapen@sanquin.nl).

9 **Materials Availability:** Plasmids and knock-out cell lines generated in this study will be available from
10 the lead contact with a completed Material Transfer Agreement (MTA).

11 **Data and Code availability:** The published article includes all data generated or analyzed during this
12 study, except for the processed screen results, which are accessible in an interactive database
13 (<https://phenosaurus.nki.nl/>). The raw sequence data of the screens have been deposited in the NCBI
14 Sequence Read Archive under study number PRJNA665349 with bioSample accession number
15 SAMN16252402.

16

17 **EXPERIMENTAL MODEL AND SUBJECT DETAILS**

18 **Mammalian cell lines and T cell clones:** HAP1 (HLA-A*02:01, HLA-B*40:01 and HLA-Cw*03:04,
19 near-haploid, male chronic myeloid leukemia), MelJuSo (HLA-A*01:01, B*08:01 and C*07:01, female
20 melanoma authenticated at Eurofins), SW620 (HLA-A*24:02, A*02:01, B*07, B*15 and C*07:04, male
21 colon, derived from metastatic site: lymph node) (kindly provided by Dr. T. de Gruijl (Amsterdam
22 UMC, The Netherlands)) and U373 (HLA-A*02:01, male glioblastoma) (kindly provided by Dr. H.
23 Versteeg (LUMC)) cell lines were cultured in IMDM (Gibco and Lonza) supplemented with 10% FCS
24 and antibiotics (PenStrep; Invitrogen) at 37°C and 5% CO₂. HEK293T (ATCC Cat# CRL-3216, RRID:
25 CVCL_0063) and its derivative Phoenix amphi (female embryonic kidney) cells were cultured in
26 similarly supplemented DMEM (Gibco). The HLA-A*02:01-restricted CD8⁺ T cell clones reactive
27 against peptides derived from the tumor-expressed proteins USP11, FDPS, VPS13B, ADIR, and
28 SSR1 were previously described (Amir et al., 2011; van Bergen et al., 2007; Van Bergen et al., 2010)
29 and expanded using a feeder cell-cytokine mixture in medium with human serum (Sanquin) as
30 described (Oostvogels et al., 2014).

31

32 **METHOD DETAILS**

33 **Haploid genetic screening:** Genome-wide knockout screening was performed in either early
34 passage WT or CRISPR/Cas9 generated SPPL3 KO HAP1 cells using directly conjugated W6/32 or
35 BB7.2 antibodies. Retroviral mutagenesis was performed on ~100 x 10⁶ cells using GT-GFP or GT-
36 BFP plasmids as previously described (Brockmann et al., 2017). 2 x 10⁹ expanded mutagenized cells
37 were fixed, stained and sorted into two separate populations based on the fluorescent intensity of the
38 respective HLA-I antibody staining (Brockmann et al., 2017). Gene trap integration sites were
39 amplified using a LAM-PCR with a biotinylated primer on genomic DNA isolated from sorted cells.
40 Biotinylated products were captured on streptavidin-coated beads followed by a single-stranded DNA

1 linker ligation and a subsequent amplification step using two primers to generate fragments that
2 include a genomic region flanking the insertion site in addition to adaptors for deep sequencing. Deep
3 sequencing reads were aligned to the human genome (hg19) and intersected with protein coding
4 genes to obtain the numbers of unique disruptive integrations mapped per gene in both populations
5 either lowly or highly recognized by the respective HLA-I antibody. Enrichment of mutations in genes
6 was assessed using a Fisher's exact test corrected for false discovery (Benjamini-Hochberg). The
7 approach is described in detail in (Brockmann et al., 2017).

8
9 **Plasmids:** pMXs-puro vector (Cell Biolabs) was equipped with a novel multiple cloning site with or
10 without N- or C-terminal tags (RFP, GFP and FLAG). SPPL3 and its inactive mutant SPPL3 D271A
11 (kind gift from Dr. R. Flührer) (Voss et al., 2012) were recloned into pMXs-puro-RFP or -GFP using
12 XhoI/BamHI restriction sites. B3GNT5 and B4GALNT1 were PCR amplified from IMAGE:202800754
13 and IMAGE:202800771 and cloned into pMXs-puro-FLAG-C or -N by EcoRI/BamHI restriction sites.
14 ST3GAL5 was amplified from IMAGE:202759803 and cloned into pMXs-puro-FLAG-C using
15 EcoRI/BclI digestion into an EcoRI/BamHI digested plasmid. The pLZRS-based retroviral vectors
16 containing HLA-A*02:01/B*40:01/C*03:03-IRES-ΔNGFR were described before (Griffioen et al., 2012;
17 Van Bergen et al., 2010). Generation of retroviral supernatants and transduction of cells were
18 performed as described (Spaapen et al., 2008). HLA-C*05:01 (IMGT/HLA database) with a mutated
19 signal peptide from HLA-A*02:01 (M4V) was purchased as a gBlock gene fragment (Integrated DNA
20 Technologies, Inc.) and used as a template for amplification. The PCR product was cloned into the
21 puc2CL6IN lentiviral vector using NheI and BamHI. gRNAs (Table S4) were cloned into the pX330
22 expression vector or the lentiviral vectors lentiCRISPR_v2 or pLCRISPR.efs.GFP (Addgene) as
23 described (Heckl et al., 2014; Sanjana et al., 2014).

24
25 **Genome editing:** SPPL3 KO and tapasin KO HAP1 cells were created by in frame integration of a
26 blasticidin-resistance gene after cotransfection of pX330 with TIA-2Ablast (using Extremegene HP,
27 Sigma) as described for other targets (Blomen et al., 2015; de Waard et al., 2020). Clones growing
28 after blasticidin selection (10µg/mL, Life Technologies) were sequence verified for specific genome
29 editing by Sanger sequencing (primers in Table S5). Lentiviral constructs containing gRNAs targeting
30 SPPL3, UGCG, CMAS and the five core GSL-enzymes were cotransfected into HEK293T with the
31 packaging enzymes psPAX2, pVSVg, pAdVantage using polyethylenimine (PEI; Polyscience) for
32 virus production. Filtered viral supernatants were used for transduction by spinoculation in the
33 presence of 8µg/mL protamine sulfate. Cells were selected using puromycin (0.25µg/mL; Gibco),
34 blasticidin (10µg/mL; Gibco), geneticin (550µg/mL; Formedium) or gated on based on the
35 coexpression of GFP or RFP. Polyclonal KO populations after selection were used for flow cytometry
36 (SPPL3, CMAS and core GSL-enzymes) or KO clones were made by limiting dilution and sequence
37 verified. HLA-A, -B and -C KO cells were generated by pX330 transfection followed by single cell
38 FACS sort using W6/32 and sequence verification of clones (de Waard et al., 2020).

39
40 **Sanger sequencing:** Constructs were sequenced using BigDye Terminator Kit (Applied Biosystems).

1 Genomic DNA isolated from cell lines using DirectPCR (Cell) lysis reagent (Viagen) supplemented
2 with Proteinase K (Sigma) was amplified using primers mentioned in Table S5 and directly sequenced
3 using BigDye Terminator Kit (Applied Biosystems). Sequences were analyzed using Snapgene (GSL
4 Biotech). Sequence decomposition to assess the size of deletions or insertions of genome-edited
5 diploid cells was performed using Tide (Brinkman et al., 2014).

6

7 **siRNA transfections:** Gene silencing was performed in a 96F well plate using 5 μ L siRNA (500nM
8 stock) mixed with 0.1 μ L DharmaFECT1 #1 (Dharmacon) in 4.9 μ L IMDM. The mixture was incubated
9 for 20min on a shaker at RT and mixed with 4700 cells/200ul. After three days cells were analyzed
10 using flow cytometry. siGENOME human SPPL3 (D-006042, Dharmacon) and B2M (M-004366,
11 Dharmacon) siRNAs were used to silence SPPL3 and B2M respectively. Non-targeting siRNA
12 (siCTRL, D-001206-13-20, Dharmacon) was used as a negative control.

13

14 **Inhibitors and enzymes:** UGCG inhibitors MZ31 (used concentration: 2 μ M), MZ21 (2 μ M), miglustat
15 (100 μ M) were produced as previously described (Ghisaidoobe et al., 2014) and eliglustat (200nM)
16 was obtained from Bio-Connect. Swainsonine (20 μ g/mL) and kifunensine (25 μ M) were obtained from
17 Sigma. *N*-glycosylation inhibitor activity was confirmed by incubating W6/32 immunoprecipitated HLA-
18 I molecules with Endoglycosidase H (Sigma) in a 20 μ l reaction mixture (50 μ M Sodiumcitrate (pH5.5),
19 0.2% SDS, 2 μ l Endoglycosidase H and protease inhibitors) for 18h at 37°C followed by HLA-I
20 detection on western blot. Sialyltransferase inhibitor (3Fax-peracetyl Neu5Ac, 100 μ M) was obtained
21 from Sigma and fucosyltransferase inhibitor (2-Deoxy-2-fluoro-L-fucose, 100 μ M) was obtained from
22 Carbosynth. Cells were cultured for 2 or 3 days at 37°C with inhibitors and analyzed by flow
23 cytometry. Cells were incubated with neuraminidase (N2876, Sigma, 225mU/mL) for 1h at 37°C.

24

25 **Fab fragment production and labeling:** W6/32 Fab fragments were prepared by 1h pepsin (1 μ g/ μ L,
26 pH3.5) treatment at 37°C in a pH3.5 buffer containing citric acid (0.07M) and sodium citrate (0.03M),
27 followed by reduction using DTT (2.5mM, Sigma-Aldrich). BB7.2 Fab fragments were prepared using
28 a papain:antibody ratio of 1:100 (16 μ g/mL papain) for 20h at 37°C. All Fab fragments were purified by
29 gel filtration (Superdex 200, 10/300 GL, GE Healthcare Life Sciences). Monomeric Fab fragments
30 were either conjugated to Alexa Fluor® 555 NHS Ester (AF555; ThermoFisher Scientific) or Alexa
31 Fluor® 647 NHS Ester (AF647; ThermoFisher Scientific) according to the manufacturer's labeling
32 protocol. To remove unconjugated fluorophores, the labeled Fab fragments were further purified by
33 gel filtration (Superdex 75, 10/300 GL, GE Healthcare Life Sciences). Fractions containing monomeric
34 fluorophore-conjugated Fab fragments were concentrated to a protein concentration of 0.2-0.5mg/mL
35 using Amicon Ultra-4 centrifugal filters (10 kDa cut off, Merck Millipore) and then stored in 50%
36 glycerol at -20°C. The protein to dye ratios were determined by spectrophotometry at 280nm and the
37 corresponding absorption maximum of the dyes at 555nm and 650nm. The protein to dye ratio of the
38 randomly conjugated Fab fragments were 1.0 (BB7.2 Fab-AF555), 0.94 (W6/32 Fab-AF647) and 0.4
39 (W6/32 Fab-AF555).

40

1 **Flow cytometry using antibodies:** Trypsinized cells were incubated with specific antibodies diluted
2 in PBS for 30min at 4°C and washed up to five times in PBS (with or without 0.5% BSA) before
3 incubation with secondary antibodies if required (30min at 4°C). Stained cells were fixed in PBS
4 containing 1% formaldehyde (Merck). DAPI (1µM, Sigma-Aldrich) was used to exclude dead cells
5 from analyses. Cells were fluorescently barcoded using the fluorescent dyes CFSE (125nM,
6 Invitrogen), Alexa Fluor 350 NHS Ester (40µM, Thermo Fisher Scientific) or Violet proliferation dye
7 450 (2.5µM, BD Horizon) diluted in PBS. Cells were incubated with a fluorescent dye for 15min
8 (vortexed every 5min) and washed three times in ice-cold complete IMDM (see above). Barcoded
9 cells were mixed prior to plating in 96V-bottom wells for antibody staining. Stained samples (barcoded
10 or not) were analyzed or sorted on BD flow cytometers (Canto II, Fortessa, LSR II or ARIA II). FACS
11 data was analyzed using FlowJo (Tree Star, Inc).

12

13 **Flow cytometry using other proteins:** Fusion proteins LIR-1 Fc (kindly provided by Ofer
14 Mandelboim), KIR2DL1-Fc and KIR2DL2-Fc (R&D Biosystems) were reconstituted in PBS
15 (100µg/mL) and stored at -80°C. Cholera toxin B subunit (CTB)-FITC (Sigma) was reconstituted in
16 sterile water (500µg/ml) and used at 10 µg/mL. Trypsinized cells were washed in PBS with 3% FCS or
17 0.5% BSA and stained in 40µL (fusion) protein dilution for 30min to 2h on ice. For fusion proteins,
18 cells were washed twice and incubated on ice in 40µl secondary antibody APC AffiniPure F(ab')₂
19 Fragment Goat Anti-Human IgG, Fcγ fragment specific (Jackson ImmunoResearch) (KIR2DL1,
20 KIR2DL2) or mouse anti-human IgG (MH161-1, Sanquin) in-house conjugated to DL650 (Thermo
21 Fisher Scientific) for 30-45min. After two washes cells were resuspended in PBS/3%FCS containing
22 DAPI and analysed on BD flow cytometers.

23

24 **T cell assays:** Target cells were cocultured with T cells in a 1:1 ratio for 18h as previously described
25 (Spaapen et al., 2008). Cytokine content of cell free supernatants was determined using standard
26 sandwich ELISA according to the manufacturer's instructions (IFN-γ and GM-CSF; Sanquin and
27 Biolegend). Some target cells were precultured for 2 days in the presence or absence of UGCG
28 inhibitors. For cytotoxicity experiments, target cells were loaded with 100 µCi ⁵¹Cr (Perkin-Elmer) for
29 90min at 37°C and then washed twice with PBS. 4000 target cells were then cocultured with T cells at
30 indicated effector target (E:T) ratios for 4-6h in round-bottom plates after which 30 µL of the
31 supernatant was harvested and analyzed for radioactivity using a gamma counter (Wallac). Medium
32 and 0.1% triton X-100 served as spontaneous and maximal release controls. The percentage of
33 specific lysis was calculated as [(experimental cpm – spontaneous cpm) / (maximal cpm –
34 spontaneous cpm)] × 100%.

35

36 **Immunoprecipitation:** The medium of transiently transfected HEK293T cells was filtered through a
37 puradisc 30 syringe filter (0.2µm, FP 30/0.2) to remove cell material. Before sample buffer was added.
38 HEK293T or CRISPR/Cas9 edited HAP1 cells (confluent 6cm dish) were lysed for 20min in lysis
39 buffer containing 0.8% NP-40, 10% glycerol, 150mM NaCl, 50mM Tris-HCl pH8.0, 1mM EDTA, 5mM
40 MgCl₂ and protease inhibitors (Roche Diagnostics, EDTA free). Lysate was centrifuged for 20min at

1 12.000rpm and the supernatant was incubated with RFP-Trap beads (Chromotek) or antibody coated
2 Protein-G sepharose beads for 2h. Beads were washed four times in lysis buffer before addition of
3 Laemmli Sample Buffer (containing 5% β -mercaptoethanol) followed by 5min incubation at 95°C.
4 Coimmunoprecipitated proteins were separated by SDS-PAGE for Western blotting and detected by
5 antibody staining.

6

7 **SDS-PAGE and Western blotting:** Samples were separated by SDS-PAGE (10% or 12% acrylamide
8 gel) and transferred to a PVDF membrane (Immobilon-P, 0.45 μ m, Millipore) at 300mA for 3h. The
9 membranes were blocked in PBS/5% Milk (Skim milk powder, Oxoid) and incubated with a primary
10 antibody for 1h diluted in PBS/0.1% Tween/5% Milk, washed thrice for 10min in PBS/0.1% Tween and
11 incubated with the secondary antibody for 45min diluted in PBS/0.1% Tween/5% Milk and washed
12 thrice again in PBS/0.1% Tween. The filter was incubated with ECL reagent (SuperSignal West Dura
13 Extended Duration Substrate, Thermo Fisher Scientific) and the signal was detected using the
14 Chemidoc XRS+ imager (Bio-Rad) or Amersham Imager 600.

15

16 **BFA assay:** To determine HLA-I turnover, HAP1 cells were seeded in 96w plates (80% confluent)
17 and cultured in the presence of Brefeldin A (0.5 μ g/mL BFA, Sigma Aldrich) at 37°C for indicated
18 times. BFA containing medium was removed and the cells were washed in cold PBS, trypsinized and
19 harvested in PBS/0.5% BSA. Cells were kept on ice and stained for flow cytometry using non-
20 saturating amounts of W6/32 and B1.23.2 antibodies (*see flow cytometry section*).

21

22 **Crystal structures:** Structural prediction software Phyre2 was used to create a model of SPPL3
23 using the primary consensus sequence CCDS9208.1 (Kelley et al., 2015). Models of HLA-A*02:01
24 were made using the crystal structure 3MRG courtesy of the RCSB PDB (Reiser et al., 2014; Winn et
25 al., 2011). The structure 3QZW was used in conjunction with the CCP4 program ARIAIMOL (Berman
26 et al., 2000) to determine the hydrogen bonding contacts between human HLA-A*24:02 and human
27 CD8 alpha-alpha dimer (Shi et al., 2011). A similar method was used to assess the contacts between
28 LIR-1 and HLA-A*02:01 using the structure 1P7Q (Berman et al., 2000; Willcox et al., 2003). All
29 figures have been produced using the PyMOL molecular graphics software (Version 2.0 Schrödinger,
30 LLC).

31

32 **B3GNT5 activity assay:** 5 x 10⁶ HAP1 cells were harvested by trypsinization and cells were lysed in
33 lysis buffer (2% TritonX-100, 50mM sodium cacodylate pH7.4, 10mM MnCl₂, and protease inhibitors
34 (Roche Diagnostics, EDTA free)) by incubating on ice for 30min. Nuclei were precipitated by
35 centrifugation at 15,000xg. Equal volumes of lysis buffer containing 2 μ M BODIPY-C5-
36 Lactosylceramide complexed to BSA (Thermo Fisher Scientific) and/or 1mM UDP-N-acetyl-D-
37 glucosamine (Santa Cruz) were added to post-nuclear supernatants containing equal amounts of
38 protein in 50 μ L lysis buffer. Samples were incubated at 37°C for 4h and subjected to lipid extraction
39 using Bligh-Dyer method (Bligh and Dyer, 1959). 100 μ L 2% NaCl, 250 μ L chloroform, and 500 μ L
40 methanol were added to the reactions and samples were vortexed. Phase separation was induced by

1 addition of 250µl 0.45% NaCl and 250µL chloroform and lower phases were collected. Upper phases
2 were re-extracted twice more and collected lower phases were dried under a nitrogen flow. Dried
3 lipids were resuspended in chloroform:methanol (2:1 v/v) solution and spotted on TLC plates. TLC
4 plates were developed in chloroform:methanol:water (60:25:4 v/v/v) and imaged using Typhoon
5 FLA9500 (GE Healthcare) scanner equipped with a 473nm laser and BPB1 filter (530DF30). Identity
6 of BODIPY-Lc3Cer was confirmed by MS/MS. Structures were assigned based on MS/MS
7 fragmentation pattern in negative mode following nomenclature from Domon and Costello (Domon
8 and Costello, 1988).

9
10 **GSL extraction and purification by RP-SPE:** GSLs were extracted from 1 x 10⁷ HAP1 WT, SPPL3
11 KO and B3GNT5/SPPL3 double KO cell lines in triplicate in glass vials equipped with a Teflon-lined
12 screw cap. Cells were washed three times in 1mL of water followed by centrifugation at 2000xg for
13 30min. The supernatant was removed and replaced by 300µL of 2-propanol. The samples were
14 vortexed for 5min and incubated for 15min at 75°C. A volume of 350µL of MTBE (Sigma-Aldrich) was
15 added to the samples followed by 15min sonication. 200µL of water was added to the cell pellets and
16 incubated for 4h with shaking at room temperature. The upper phase containing GSLs was collected
17 after centrifugation at 2700xg for 20min. Then, 400µL of MTBE was added, followed by sonication
18 and centrifugation. The upper phase was collected and pooled to the previous sample. The process of
19 adding MTBE, sonication, centrifugation and removing upper phase was repeated another two times.
20 The combined upper phases were dried under vacuum in an Eppendorf Concentrator 5301
21 (Eppendorf) at 30°C. Before purification of the GSLs using RP-solid phase extraction (SPE), the
22 samples were dissolved in 200µL methanol and vortexed for 10min, followed by addition of 400µL
23 water. TC18-RP-cartridges were prewashed with 2mL of chloroform/methanol (2:1, v/v), 2mL of
24 methanol followed by equilibration with 2mL methanol/water (1:2, v/v). The extracted GSLs were
25 loaded to the cartridge for 3 times and washed with 3mL methanol/water (1:2, v/v). The GSLs were
26 eluted from the column with 2mL methanol and 2mL chloroform/methanol (2:1, v/v). The samples
27 containing the eluate were evaporated under nitrogen for 1h and dried under vacuum in an Eppendorf
28 Concentrator at 30°C. The collection and dry of GSLs eluate were performed in glass tube.

29
30 **GSL glycan release by EGCCase I and purification:** To release the glycans from the GSLs, a
31 mixture of 2µL Endoglycoceramidase I (EGCase I recombinant clone derived from *Rhodococcus*
32 *triatomea* and expressed in *Escherichia coli* (12mU, NEB)), 4µL 10x EGCCase I buffer (500mM
33 HEPES, 1M NaCl, 20mM DTT and 0.1% Brij 35, pH5.2, NEB) and 34µL water (pH5.2) was added to
34 each sample and incubated for 16h at 37°C. The released glycans were collected and applied to a
35 TC18-RP-cartridges (Waters) which was preconditioned with 2mL of methanol and 2mL of water. The
36 sample vials were washed with 200µL of water and residual glycans were loaded to the cartridge.
37 Then, 500µL of water was added to the cartridge to wash the glycans from the column. The flow-
38 through and wash fractions were pooled and dried in an Eppendorf Concentrator at 30°C.

39
40 **Reduction, desalting and carbon SPE cleanup of GSL glycans:** The reduction was carried out as

1 described previously with slight modifications (Jensen et al., 2012). In brief, GSL glycans were
2 reduced to alditols in 20 μ L of sodium borohydride (500mM, Sigma-Aldrich) in potassium hydroxide
3 (50mM, Sigma-Aldrich) for 2h at 50°C. Subsequently, 2 μ L of 100% glacial acetic acid was added to
4 neutralize the solution and quench the reaction. The desalting of GSL glycans was performed on
5 cation exchange columns (Sigma-Aldrich) which consist of 60 μ L of AG50W-X8 resin beads deposited
6 onto reversed phase μ C18 ZipTips (Perfect Pure, Millipore) as previously described (Jensen et al.,
7 2012). Glycan alditols were eluted with 50 μ L of water twice. The combined flow-through and eluate
8 were pooled and dried under vacuum in an Eppendorf Concentrator at 30°C. The carbon SPE clean-
9 up was performed and the purified glycan alditols were resuspended in 10 μ L water for porous
10 graphitized carbon (PGC) LC-ESI-MS/MS analysis.

11

12 **Analysis of GSL glycans using PGC LC-ESI-MS/MS:** Porous graphitized carbon (PGC) LC-ESI-
13 MS/MS analysis of GSL glycan alditols was performed on a Dionex Ultimate 3000 nano-LC system
14 equipped with a Hypercarb PGC trap column (5 μ m Hypercarb Kappa, 32 μ m x 30mm, Thermo Fisher
15 Scientific) and a Hypercarb PGC nano-column (3 μ m Hypercarb Kappa, 75 μ m x 100mm, Thermo
16 Fisher Scientific) coupled to an amaZon speed ion trap mass spectrometer (Bruker Daltonics). Mobile
17 phase A consisted of 10mM ammonium bicarbonate (Sigma-Aldrich). Mobile phase B was 60% (v/v)
18 acetonitrile (Biosolve) / 10mM ammonium bicarbonate (Sigma-Aldrich). To analyze glycans, 2 μ L
19 injections were performed and separation was achieved with a gradient of B (1-71% at 0.7%/min)
20 followed by a 10min wash step using 95% of B at a flow rate of 0.6 μ L/min. MS scans from *m/z* 340
21 to 1700 were recorded in enhanced mode using negative ion mode. MS/MS spectra were recorded
22 selecting the top 3 highest intensity peaks. Glycan structures were assigned based on glycan
23 composition obtained from accurate mass, relative PGC elution position, MS/MS fragmentation
24 pattern in negative-ion mode and general glycobiochemical knowledge (Karlsson et al., 2004), with help
25 of Glycoworkbench (Ceroni et al., 2008) and Glycomod (Cooper et al., 2001) software tools. Extracted
26 ion chromatograms were used to integrate area under the curve (AUC) for each individual glycan
27 isomer using Compass Data Analysis software v.5.0. The most abundant peaks in the glycan profile
28 were manually picked and integrated. Relative quantitation of individual glycans was performed on the
29 total area of all included glycans within one sample normalizing it to 100%.

30 **HLA-I glycan analysis, in-gel tryptic digestion:** The glycopeptide generation and analysis were
31 performed as described previously with slight modifications (Plomp et al., 2014). BB7.2
32 immunoprecipitated samples were loaded on SDS PAGE. Bands containing HLA-I were excised and
33 cut into pieces. The gel pieces were washed with 25mM ammonium bicarbonate, dehydrated with
34 acetonitrile (ACN) and reduced in-gel for 30min at 55°C with 100 μ L 10mM DTT in 25mM ammonium
35 bicarbonate solution. Thereafter they were dehydrated in ACN followed by cysteine alkylation for
36 20min with 100 μ L of a 55mM iodoacetamide (Sigma-Aldrich) in 25mM ammonium bicarbonate
37 solution in the dark for 45min. This was repeated twice, and the gel pieces were subsequently dried in
38 a centrifugal vacuum concentrator at 30°C for 10min. Enzymatic digestion of trypsin was performed
39 by adding 50 μ L of 25mM ammonium bicarbonate containing 0.6 μ g of trypsin (sequencing grade
40 modified trypsin, Promega) to the dried gel particles. The samples were kept on ice for 1h and were

1 subsequently incubated overnight at 37°C. The solution surrounding the gel pieces was collected and
2 stored at -20°C. 20µL of 25mM ammonium bicarbonate was added to the remaining gel pieces, and
3 incubated at 37°C for another hour. The solution was again collected and added to the first fraction
4 prior to freezing.

5
6 **Glycopeptide analysis by reverse-phase (RP) nanoLC-ESI-MS(/MS):** Glycopeptides were
7 analyzed by RP nanoLC-ESI-MS(/MS) on an Ultimate 3000 RSLCnano system (Dionex / Thermo
8 Fisher Scientific) coupled to an HCTUltra-ESI-ion trap-MS (Bruker Daltonics). 5µL sample was
9 injected and concentrated on a trap column (Acclaim PepMap100 C18 column, 100µm × 2cm, C18
10 particle size 5µm, pore size 100Å, Dionex / Thermo Fisher Scientific) before separation on an Acclaim
11 PepMap RSLC nanocolumn (75µm × 15cm, C18 particle size 2µm, pore size 100Å, Dionex / Thermo
12 Fisher Scientific). A flow rate of 700nL/min was applied. Solvent A consisted of 0.1% formic acid in
13 water; solvent B, 0.1% formic acid in 95% ACN and 5% water. A linear gradient was applied with the
14 following conditions: $t = 0\text{min}$, 3% solvent B; $t = 5\text{min}$, 3% solvent B; $t = 20\text{min}$, 27% solvent B; $t =$
15 21min , 70% solvent B; $t = 23\text{min}$, 70% solvent B; $t = 24\text{min}$, 3% solvent B; $t = 43\text{min}$, 3% solvent B.
16 Samples were ionized in positive ion mode with an online nanospray source (4500V) using fused-
17 silica capillaries and a Distal Coated SilicaTip Emitter (New Objective) with an internal diameter of
18 20µm (10µm at the tip) and a length of 5cm. Solvent evaporation was performed at 220°C with a
19 nitrogen flow of 3L/min. For the detection of glycopeptides, the MS ion detection window was set at
20 m/z 500-1800, and the MS/MS detection window at m/z 140-2200, with automated selection of the
21 three highest peaks in the spectrum for MS/MS analysis. The LC-MS/MS results were analyzed using
22 DataAnalysis 4.0 software (Bruker Daltonics) and screened manually for the masses of common
23 oxonium fragment ions (m/z 366.1, [1 hexose + 1 GlcNAc + H]⁺; m/z 657.2, [1 hexose + 1 GlcNAc + 1
24 *N*-acetylneuraminic acid + H]⁺; m/z 528.2, [2 hexoses + 1 GlcNAc + H]⁺), which are characteristic for
25 fragmentation spectra of glycopeptides. Glycopeptide MS/MS spectra were further analyzed manually
26 to derive the oligosaccharide structure and the mass of the peptide moiety.

27
28 **Preparation of fibronectin-coated glass slides for single particle tracking experiments:** Glass
29 slides (24mm x 50mm #1.5 borosilicate, VWR) were immersed in a 1:1 mixture of concentrated
30 sulfuric acid (Sigma) and 30% hydrogen peroxide (Sigma) for at least 30min, rinsed with deionized
31 water, air dried and glued with picodent twinsil extrahart (Picodent) to the bottom of 8-well LabTek
32 chambers (Nunc). Slides were coated with 20µg/mL fibronectin (Sigma-Aldrich) in PBS for 1-2h at
33 37°C and rinsed with 1 X PBS.

34
35 **Single particle tracking of HLA-I molecules on HAP1 WT and SPPL3 KO cells:** 0.2×10^6 HAP1
36 WT and SPPL3 KO cells were stained with a single molecule dilution of the BB7.2-Fab-AF555 on ice
37 for 30min and washed twice in imaging buffer (HBSS, Gibco, 1% FCS, 2mM MgCl₂ and CaCl₂). Cells
38 were kept on ice or seeded onto fibronectin-coated glass slides for imaging at room temperature (23-
39 27°C) and in TIRF mode. AF555 was excited with a 532 nm laser (Obis) with a power density of
40 0.8kW/cm² and the emission channel was cleaned up with a TRITC filter (605/52) installed within the

1 fast emission filter wheel (Sutter Instrument Company). We recorded single HLA-I (BB7.2 Fab-AF555)
2 trajectories over 500 frames with an illumination time of 16ms and a total time lag of 20.6ms between
3 two adjacent images (100 X 100 pixel ROI size). Microscopy images were processed and analyzed
4 with the open-source image processing package Fiji (Schindelin et al., 2012). XY localization,
5 intensity and positional accuracy of single fluorescence emitters was calculated with the Fiji plugin
6 ThunderSTORM (Ovesny et al., 2014). After determining the localization of every fluorophore in the
7 image stack we combined these localizations to trajectories based on a published approach (Gao and
8 Kilfoil, 2009) with custom-made algorithms written in Matlab (MathWorks). We calculated the mean
9 square displacement (MSD) describing the average of the square displacements between two points
10 of the trajectory according to $MSD(t_{lag}) = \langle (r(t + t_{lag}) - r(t))^2 \rangle$. The first three MSD values as a function
11 of time lag (t_{lag}) were used to calculate the diffusion coefficient (D) for each trajectory according by
12 fitting $MSD = 4 \cdot D \cdot t_{lag} + 4 \cdot \sigma_{xy}^2$, with σ_{xy} representing the localization precision (Wieser et al., 2007).
13 Multiple fractions (i.e. a fast and a slow moving fraction of molecules) were discriminated by analyzing
14 the step-size distributions of square displacements for several time lags (Schutz et al., 1997). By
15 assuming free Brownian motion of one mobile fraction, the cumulative probability for finding a square
16 displacement smaller than r^2 is given by $P = 1 - \exp\left(-\frac{r^2}{4Dt_{lag}}\right)$; two different fractions α and $(1-\alpha)$ with
17 diffusion coefficients D1 (e.g. fast) and D2 (e.g. slow/immobile) can be distinguished by fitting the bi-
18 exponential function $P = 1 - \alpha \cdot \exp\left(-\frac{r^2}{4D_1t_{lag}}\right) - (1 - \alpha) \cdot \exp\left(-\frac{r^2}{4D_2t_{lag}}\right)$. We calculated the fraction of
19 mobile and slow/immobile molecules, the diffusion rate of mobile molecules and the diffusion rate of
20 slow/immobile molecules of all HLA-I trajectories present on a single cell (Bramshuber et al., 2018).

21

22 QUANTIFICATION AND STATISTICAL ANALYSIS

23 All error bars correspond to the standard deviation of the mean. For quantifications of flow cytometry
24 data we plotted data from median fluorescent intensities (fusion proteins, no normal distribution) or
25 mean fluorescent intensities (antibody and CTB stainings) as clarified in the legends. Data from
26 genome-wide screens were analyzed using two-sided Fisher's exact test followed by FDR (Benjamini-
27 Hochberg) correction of the p-value. Other statistical evaluations were done by a Student's t-test
28 (analysis of two data groups), one-way ANOVA (three groups or more), two-way ANOVA (two
29 variables), Mann-Whitney U test (non-parametric analyses) or Log-rank (survival analyses) with
30 Prism-Graphpad software (<http://www.graphpad.com>). TCGA survival and expression data were
31 retrieved from OncoLnc.org (Anaya, 2016). * $p < 0.05$, ** $p < 0.01$, *** $p < 0.001$ and ns (= not significant).
32 EC50 values of titrations were calculated using non-linear four parameter fit modeling with Prism
33 software.

34

1 References

- 2 Achdout, H., Manaster, I., and Mandelboim, O. (2008). Influenza virus infection augments NK cell
3 inhibition through reorganization of major histocompatibility complex class I proteins. *J Virol* *82*, 8030-
4 8037.
- 5 Allende, M.L., and Proia, R.L. (2014). Simplifying complexity: genetically resculpting glycosphingolipid
6 synthesis pathways in mice to reveal function. *Glycoconj J* *31*, 613-622.
- 7 Amir, A.L., van der Steen, D.M., Hagedoorn, R.S., Kester, M.G., van Bergen, C.A., Drijfhout, J.W., de
8 Ru, A.H., Falkenburg, J.H., van Veelen, P.A., and Heemskerk, M.H. (2011). Allo-HLA-reactive T cells
9 inducing graft-versus-host disease are single peptide specific. *Blood* *118*, 6733-6742.
- 10 Anaya, J. (2016). OncoLnc: linking TCGA survival data to mRNAs, miRNAs, and lncRNAs. *Peer J*
11 *Computer Science* *2*:e67.
- 12 Andrews, P.W., Gonczol, E., Fenderson, B.A., Holmes, E.H., O'Malley, G., Hakomori, S., and Plotkin,
13 S. (1989). Human cytomegalovirus induces stage-specific embryonic antigen 1 in differentiating
14 human teratocarcinoma cells and fibroblasts. *J Exp Med* *169*, 1347-1359.
- 15 Anfossi, N., Andre, P., Guia, S., Falk, C.S., Roeytynck, S., Stewart, C.A., Bresio, V., Frassati, C.,
16 Reviron, D., Middleton, D., *et al.* (2006). Human NK cell education by inhibitory receptors for MHC
17 class I. *Immunity* *25*, 331-342.
- 18 Barbosa, J.A., Santos-Aguado, J., Mentzer, S.J., Strominger, J.L., Burakoff, S.J., and Biro, P.A.
19 (1987). Site-directed mutagenesis of class I HLA genes. Role of glycosylation in surface expression
20 and functional recognition. *J Exp Med* *166*, 1329-1350.
- 21 Berman, H.M., Westbrook, J., Feng, Z., Gilliland, G., Bhat, T.N., Weissig, H., Shindyalov, I.N., and
22 Bourne, P.E. (2000). The Protein Data Bank. *Nucleic Acids Res* *28*, 235-242.
- 23 Blees, A., Janulienė, D., Hofmann, T., Koller, N., Schmidt, C., Trowitzsch, S., Moeller, A., and Tampe,
24 R. (2017). Structure of the human MHC-I peptide-loading complex. *Nature* *551*, 525-528.
- 25 Bligh, E.G., and Dyer, W.J. (1959). A rapid method of total lipid extraction and purification. *Can J*
26 *Biochem Physiol* *37*, 911-917.
- 27 Blomen, V.A., Majek, P., Jae, L.T., Bigenzahn, J.W., Nieuwenhuis, J., Staring, J., Sacco, R., van
28 Diemen, F.R., Olk, N., Stukalov, A., *et al.* (2015). Gene essentiality and synthetic lethality in haploid
29 human cells. *Science* *350*, 1092-1096.
- 30 Borges, L., Hsu, M.L., Fanger, N., Kubin, M., and Cosman, D. (1997). A family of human lymphoid
31 and myeloid Ig-like receptors, some of which bind to MHC class I molecules. *J Immunol* *159*, 5192-
32 5196.
- 33 Brameshuber, M., Kellner, F., Rosboth, B.K., Ta, H., Alge, K., Sevcsik, E., Gohring, J., Axmann, M.,
34 Baumgart, F., Gascoigne, N.R.J., *et al.* (2018). Monomeric TCRs drive T cell antigen recognition. *Nat*
35 *Immunol* *19*, 487-496.
- 36 Brinkman, E.K., Chen, T., Amendola, M., and van Steensel, B. (2014). Easy quantitative assessment
37 of genome editing by sequence trace decomposition. *Nucleic Acids Res* *42*, e168.
- 38 Brockmann, M., Blomen, V.A., Nieuwenhuis, J., Stickel, E., Raaben, M., Bleijerveld, O.B., Altelaar,
39 A.F.M., Jae, L.T., and Brummelkamp, T.R. (2017). Genetic wiring maps of single-cell protein states
40 reveal an off-switch for GPCR signalling. *Nature* *546*, 307-311.
- 41 Caffaro, C.E., and Hirschberg, C.B. (2006). Nucleotide sugar transporters of the Golgi apparatus: from
42 basic science to diseases. *Acc Chem Res* *39*, 805-812.
- 43 Carette, J.E., Guimaraes, C.P., Varadarajan, M., Park, A.S., Wuethrich, I., Godarova, A., Kotecki, M.,
44 Cochran, B.H., Spooner, E., Ploegh, H.L., *et al.* (2009). Haploid genetic screens in human cells
45 identify host factors used by pathogens. *Science* *326*, 1231-1235.
- 46 Catalaa, I., Henry, R., Dillon, W.P., Graves, E.E., McKnight, T.R., Lu, Y., Vigneron, D.B., and Nelson,
47 S.J. (2006). Perfusion, diffusion and spectroscopy values in newly diagnosed cerebral gliomas. *NMR*
48 *Biomed* *19*, 463-475.
- 49 Ceroni, A., Maass, K., Geyer, H., Geyer, R., Dell, A., and Haslam, S.M. (2008). GlycoWorkbench: a
50 tool for the computer-assisted annotation of mass spectra of glycans. *J Proteome Res* *7*, 1650-1659.
- 51 Chowell, D., Morris, L.G.T., Grigg, C.M., Weber, J.K., Samstein, R.M., Makarov, V., Kuo, F., Kendall,
52 S.M., Requena, D., Riaz, N., *et al.* (2018). Patient HLA class I genotype influences cancer response
53 to checkpoint blockade immunotherapy. *Science* *359*, 582-587.
- 54 Colonna, M., Navarro, F., Bellon, T., Llano, M., Garcia, P., Samaridis, J., Angman, L., Cella, M., and
55 Lopez-Botet, M. (1997). A common inhibitory receptor for major histocompatibility complex class I
56 molecules on human lymphoid and myelomonocytic cells. *J Exp Med* *186*, 1809-1818.
- 57 Contreras, F.X., Ernst, A.M., Haberkant, P., Bjorkholm, P., Lindahl, E., Gonen, B., Tischer, C.,
58 Elofsson, A., von Heijne, G., Thiele, C., *et al.* (2012). Molecular recognition of a single sphingolipid
59 species by a protein's transmembrane domain. *Nature* *481*, 525-529.
- 60 Cooper, C.A., Gasteiger, E., and Packer, N.H. (2001). GlycoMod--a software tool for determining

1 glycosylation compositions from mass spectrometric data. *Proteomics* 1, 340-349.

2 Cosman, D., Fanger, N., Borges, L., Kubin, M., Chin, W., Peterson, L., and Hsu, M.L. (1997). A novel
3 immunoglobulin superfamily receptor for cellular and viral MHC class I molecules. *Immunity* 7, 273-
4 282.

5 D'Angelo, G., Capasso, S., Sticco, L., and Russo, D. (2013). Glycosphingolipids: synthesis and
6 functions. *FEBS J* 280, 6338-6353.

7 Davis, E.M., Kim, J., Menasche, B.L., Sheppard, J., Liu, X., Tan, A.C., and Shen, J. (2015).
8 Comparative Haploid Genetic Screens Reveal Divergent Pathways in the Biogenesis and Trafficking
9 of Glycophosphatidylinositol-Anchored Proteins. *Cell Rep* 11, 1727-1736.

10 de Groot, N.G., Heijmans, C.M., van der Wiel, M.K., Blokhuis, J.H., Mulder, A., Guethlein, L.A.,
11 Doxiadis, G.G., Claas, F.H., Parham, P., and Bontrop, R.E. (2016). Complex MHC Class I Gene
12 Transcription Profiles and Their Functional Impact in Orangutans. *J Immunol* 196, 750-758.

13 de Waard, A.A., Verkerk, T., Jongsma, M.L.M., Hoefakker, K., Sethumadhavan, S., Gerke, C., Bliss,
14 S., Janssen, G.M.C., de Ru, A.H., Claas, F.H.J., *et al.* (2020). PAKC: A novel Panel of HLA class I
15 Antigen presentation machinery Knockout Cells from the same genetic origin. *bioRxiv*
16 2020.01.24.917807.

17 Desai, S.A., Wang, X., Noronha, E.J., Zhou, Q., Rebmann, V., Grosse-Wilde, H., Moy, F.J., Powers,
18 R., and Ferrone, S. (2000). Structural relatedness of distinct determinants recognized by monoclonal
19 antibody TP25.99 on beta 2-microglobulin-associated and beta 2-microglobulin-free HLA class I
20 heavy chains. *J Immunol* 165, 3275-3283.

21 Doench, J.G., Fusi, N., Sullender, M., Hegde, M., Vaimberg, E.W., Donovan, K.F., Smith, I., Tothova,
22 Z., Wilen, C., Orchard, R., *et al.* (2016). Optimized sgRNA design to maximize activity and minimize
23 off-target effects of CRISPR-Cas9. *Nat Biotechnol* 34, 184-191.

24 Domon, B., and Costello, C.E. (1988). Structure elucidation of glycosphingolipids and gangliosides
25 using high-performance tandem mass spectrometry. *Biochemistry* 27, 1534-1543.

26 Duquesnoy, R.J., Marrari, M., Jelenik, L., Zeevi, A., Claas, F.H., and Mulder, A. (2013). Structural
27 aspects of HLA class I epitopes reacting with human monoclonal antibodies in Ig-binding, C1q-binding
28 and lymphocytotoxicity assays. *Hum Immunol* 74, 1271-1279.

29 Duquesnoy, R.J., Marrari, M., Mulder, A., Claas, F.H., Mostecky, J., and Balazs, I. (2012). Structural
30 aspects of human leukocyte antigen class I epitopes detected by human monoclonal antibodies. *Hum*
31 *Immunol* 73, 267-277.

32 Fantini, J., Hammache, D., Pieroni, G., and Yahi, N. (2000). Role of glycosphingolipid microdomains
33 in CD4-dependent HIV-1 fusion. *Glycoconj J* 17, 199-204.

34 Fluhrer, R., and Haass, C. (2007). Signal peptide peptidases and gamma-secretase: cousins of the
35 same protease family? *Neurodegener Dis* 4, 112-116.

36 Frohlich, F., Petit, C., Kory, N., Christiano, R., Hannibal-Bach, H.K., Graham, M., Liu, X., Ejsing, C.S.,
37 Farese, R.V., and Walther, T.C. (2015). The GARP complex is required for cellular sphingolipid
38 homeostasis. *Elife* 4.

39 Furukawa, J., Tsuda, M., Okada, K., Kimura, T., Piao, J., Tanaka, S., and Shinohara, Y. (2015).
40 Comprehensive Glycomics of a Multistep Human Brain Tumor Model Reveals Specific Glycosylation
41 Patterns Related to Malignancy. *PLoS One* 10, e0128300.

42 Gao, G.F., Tormo, J., Gerth, U.C., Wyer, J.R., McMichael, A.J., Stuart, D.I., Bell, J.I., Jones, E.Y., and
43 Jakobsen, B.K. (1997). Crystal structure of the complex between human CD8alpha(alpha) and HLA-
44 A2. *Nature* 387, 630-634.

45 Gao, Y., and Kilfoil, M.L. (2009). Accurate detection and complete tracking of large populations of
46 features in three dimensions. *Opt Express* 17, 4685-4704.

47 Garstka, M.A., Fish, A., Celie, P.H., Joosten, R.P., Janssen, G.M., Berlin, I., Hoppes, R., Stadnik, M.,
48 Janssen, L., Ovaa, H., *et al.* (2015). The first step of peptide selection in antigen presentation by MHC
49 class I molecules. *Proc Natl Acad Sci U S A* 112, 1505-1510.

50 Gettinger, S., Choi, J., Hastings, K., Truini, A., Datar, I., Sowell, R., Wurtz, A., Dong, W., Cai, G.,
51 Melnick, M.A., *et al.* (2017). Impaired HLA Class I Antigen Processing and Presentation as a
52 Mechanism of Acquired Resistance to Immune Checkpoint Inhibitors in Lung Cancer. *Cancer Discov*
53 7, 1420-1435.

54 Ghisaidoobe, A.T., van den Berg, R.J., Butt, S.S., Strijland, A., Donker-Koopman, W.E., Scheij, S.,
55 van den Nieuwendijk, A.M., Koomen, G.J., van Loevezijn, A., Leemhuis, M., *et al.* (2014).
56 Identification and development of biphenyl substituted iminosugars as improved dual
57 glucosylceramide synthase/neutral glucosylceramidase inhibitors. *J Med Chem* 57, 9096-9104.

58 Gonen-Gross, T., Goldman-Wohl, D., Huppertz, B., Lankry, D., Greenfield, C., Natanson-Yaron, S.,
59 Hamani, Y., Gilad, R., Yagel, S., and Mandelboim, O. (2010). Inhibitory NK receptor recognition of
60 HLA-G: regulation by contact residues and by cell specific expression at the fetal-maternal interface.

1 PLoS One 5, e8941.
2 Griffioen, M., Honders, M.W., van der Meijden, E.D., van Luxemburg-Heijs, S.A., Lurvink, E.G.,
3 Kester, M.G., van Bergen, C.A., and Falkenburg, J.H. (2012). Identification of 4 novel HLA-B*40:01
4 restricted minor histocompatibility antigens and their potential as targets for graft-versus-leukemia
5 reactivity. *Haematologica* 97, 1196-1204.
6 Hahnel, P.S., Thaler, S., Antunes, E., Huber, C., Theobald, M., and Schuler, M. (2008). Targeting
7 AKT signaling sensitizes cancer to cellular immunotherapy. *Cancer Res* 68, 3899-3906.
8 Hakomori, S. (1984). Tumor-associated carbohydrate antigens. *Annu Rev Immunol* 2, 103-126.
9 Hansen, T.H., and Bouvier, M. (2009). MHC class I antigen presentation: learning from viral evasion
10 strategies. *Nat Rev Immunol* 9, 503-513.
11 Haworth, K.B., Leddon, J.L., Chen, C.Y., Horwitz, E.M., Mackall, C.L., and Cripe, T.P. (2015). Going
12 back to class I: MHC and immunotherapies for childhood cancer. *Pediatr Blood Cancer* 62, 571-576.
13 Heckl, D., Kowalczyk, M.S., Yudovich, D., Belizaire, R., Puram, R.V., McConkey, M.E., Thielke, A.,
14 Aster, J.C., Regev, A., and Ebert, B.L. (2014). Generation of mouse models of myeloid malignancy
15 with combinatorial genetic lesions using CRISPR-Cas9 genome editing. *Nat Biotechnol* 32, 941-946.
16 Hiby, S.E., Apps, R., Sharkey, A.M., Farrell, L.E., Gardner, L., Mulder, A., Claas, F.H., Walker, J.J.,
17 Redman, C.W., Morgan, L., *et al.* (2010). Maternal activating KIRs protect against human reproductive
18 failure mediated by fetal HLA-C2. *J Clin Invest* 120, 4102-4110.
19 Hogan, K.T., and Brown, S.L. (1992). Localization and characterization of serologic epitopes on HLA-
20 A2. *Hum Immunol* 33, 185-192.
21 Hsu, P.D., Scott, D.A., Weinstein, J.A., Ran, F.A., Konermann, S., Agarwala, V., Li, Y., Fine, E.J., Wu,
22 X., Shalem, O., *et al.* (2013). DNA targeting specificity of RNA-guided Cas9 nucleases. *Nat Biotechnol*
23 31, 827-832.
24 Jensen, P.H., Karlsson, N.G., Kolarich, D., and Packer, N.H. (2012). Structural analysis of N- and O-
25 glycans released from glycoproteins. *Nat Protoc* 7, 1299-1310.
26 Jongsma, M.L.M., Guarda, G., and Spaapen, R.M. (2019). The regulatory network behind MHC class
27 I expression. *Mol Immunol* 113, 16-21.
28 Karlsson, N.G., Wilson, N.L., Wirth, H.J., Dawes, P., Joshi, H., and Packer, N.H. (2004). Negative ion
29 graphitised carbon nano-liquid chromatography/mass spectrometry increases sensitivity for
30 glycoprotein oligosaccharide analysis. *Rapid Commun Mass Spectrom* 18, 2282-2292.
31 Kelley, L.A., Mezulis, S., Yates, C.M., Wass, M.N., and Sternberg, M.J. (2015). The Phyre2 web portal
32 for protein modeling, prediction and analysis. *Nat Protoc* 10, 845-858.
33 Kingsley, D.M., Kozarsky, K.F., Segal, M., and Krieger, M. (1986). Three types of low density
34 lipoprotein receptor-deficient mutant have pleiotropic defects in the synthesis of N-linked, O-linked,
35 and lipid-linked carbohydrate chains. *J Cell Biol* 102, 1576-1585.
36 Kuhn, P.H., Voss, M., Haug-Kroper, M., Schroder, B., Schepers, U., Brase, S., Haass, C.,
37 Lichtenhaler, S.F., and Fluhrer, R. (2015). Secretome analysis identifies novel signal Peptide
38 peptidase-like 3 (Sppl3) substrates and reveals a role of Sppl3 in multiple Golgi glycosylation
39 pathways. *Mol Cell Proteomics* 14, 1584-1598.
40 Lachmann, R.H. (2003). Miglustat. *Oxford GlycoSciences/Actelion. Curr Opin Investig Drugs* 4, 472-
41 479.
42 Ladasky, J.J., Shum, B.P., Canavez, F., Seuanez, H.N., and Parham, P. (1999). Residue 3 of beta2-
43 microglobulin affects binding of class I MHC molecules by the W6/32 antibody. *Immunogenetics* 49,
44 312-320.
45 Li, L., Muzahim, Y., and Bouvier, M. (2012). Crystal structure of adenovirus E3-19K bound to HLA-A2
46 reveals mechanism for immunomodulation. *Nat Struct Mol Biol* 19, 1176-1181.
47 Liu, Y.Y., Hill, R.A., and Li, Y.T. (2013). Ceramide glycosylation catalyzed by glucosylceramide
48 synthase and cancer drug resistance. *Adv Cancer Res* 117, 59-89.
49 Logtenberg, M.E.W., Jansen, J.H.M., Raaben, M., Toebes, M., Franke, K., Brandsma, A.M., Matlung,
50 H.L., Fauster, A., Gomez-Eerland, R., Bakker, N.A.M., *et al.* (2019). Glutaminyl cyclase is an
51 enzymatic modifier of the CD47- SIRPalpha axis and a target for cancer immunotherapy. *Nat Med* 25,
52 612-619.
53 Marrari, M., Mostecky, J., Mulder, A., Claas, F., Balazs, I., and Duquesnoy, R.J. (2010). Human
54 monoclonal antibody reactivity with human leukocyte antigen class I epitopes defined by pairs of
55 mismatched eplets and self-eplets. *Transplantation* 90, 1468-1472.
56 Merrill, A.H., Jr., and Sullards, M.C. (2017). Opinion article on lipidomics: Inherent challenges of
57 lipidomic analysis of sphingolipids. *Biochim Biophys Acta Mol Cell Biol Lipids* 1862, 774-776.
58 Miller-Podraza, H., Andersson, C., and Karlsson, K.A. (1993). New method for the isolation of
59 polyglycosylceramides from human erythrocyte membranes. *Biochim Biophys Acta* 1168, 330-339.
60 Miller-Podraza, H., Stenhagen, G., Larsson, T., Andersson, C., and Karlsson, K.A. (1997). Screening

1 for the presence of polyglycosylceramides in various tissues: partial characterization of blood group-
2 active complex glycosphingolipids of rabbit and dog small intestines. *Glycoconj J* 14, 231-239.

3 Mitra, A.K., Celia, H., Ren, G., Luz, J.G., Wilson, I.A., and Teyton, L. (2004). Supine orientation of a
4 murine MHC class I molecule on the membrane bilayer. *Curr Biol* 14, 718-724.

5 Moesta, A.K., Norman, P.J., Yawata, M., Yawata, N., Gleimer, M., and Parham, P. (2008). Synergistic
6 polymorphism at two positions distal to the ligand-binding site makes KIR2DL2 a stronger receptor for
7 HLA-C than KIR2DL3. *J Immunol* 180, 3969-3979.

8 Moore, M.L., Chi, M.H., Goleniewska, K., Durbin, J.E., and Peebles, R.S., Jr. (2008). Differential
9 regulation of GM1 and asialo-GM1 expression by T cells and natural killer (NK) cells in respiratory
10 syncytial virus infection. *Viral Immunol* 21, 327-339.

11 Mulder, A., Kardol, M.J., Arn, J.S., Eijnsink, C., Franke, M.E., Schreuder, G.M., Haasnoot, G.W.,
12 Doxiadis, I., Sachs, D.H., Smith, D.M., *et al.* (2010). Human monoclonal HLA antibodies reveal
13 interspecies crossreactive swine MHC class I epitopes relevant for xenotransplantation. *Mol Immunol*
14 47, 809-815.

15 Neefjes, J., Jongsma, M.L., Paul, P., and Bakke, O. (2011). Towards a systems understanding of
16 MHC class I and MHC class II antigen presentation. *Nat Rev Immunol* 11, 823-836.

17 Neefjes, J.J., De Bruijn, M.L., Boog, C.J., Nieland, J.D., Boes, J., Melief, C.J., and Ploegh, H.L.
18 (1990). N-linked glycan modification on antigen-presenting cells restores an allospecific cytotoxic T
19 cell response. *J Exp Med* 171, 583-588.

20 Ogretmen, B., and Hannun, Y.A. (2004). Biologically active sphingolipids in cancer pathogenesis and
21 treatment. *Nat Rev Cancer* 4, 604-616.

22 Oostvogels, R., Lokhorst, H.M., Minnema, M.C., van Elk, M., van den Oudenalder, K., Spierings, E.,
23 Mutis, T., and Spaapen, R.M. (2014). Identification of minor histocompatibility antigens based on the
24 1000 Genomes Project. *Haematologica* 99, 1854-1859.

25 Ovesny, M., Krizek, P., Borkovec, J., Svindrych, Z., and Hagen, G.M. (2014). ThunderSTORM: a
26 comprehensive ImageJ plug-in for PALM and STORM data analysis and super-resolution imaging.
27 *Bioinformatics* 30, 2389-2390.

28 Pech, M.F., Fong, L.E., Villalta, J.E., Chan, L.J., Kharbanda, S., O'Brien, J.J., McAllister, F.E.,
29 Firestone, A.J., Jan, C.H., and Settleman, J. (2019). Systematic identification of cancer cell
30 vulnerabilities to natural killer cell-mediated immune surveillance. *Elife* 8.

31 Platt, F.M., Neises, G.R., Dwek, R.A., and Butters, T.D. (1994). N-butyldeoxynojirimycin is a novel
32 inhibitor of glycolipid biosynthesis. *J Biol Chem* 269, 8362-8365.

33 Plomp, R., Hensbergen, P.J., Rombouts, Y., Zauner, G., Dragan, I., Koeleman, C.A., Deelder, A.M.,
34 and Wuhrer, M. (2014). Site-specific N-glycosylation analysis of human immunoglobulin e. *J*
35 *Proteome Res* 13, 536-546.

36 Potapenko, I.O., Luders, T., Russnes, H.G., Helland, A., Sorlie, T., Kristensen, V.N., Nord, S.,
37 Lingjaerde, O.C., Borresen-Dale, A.L., and Haakensen, V.D. (2015). Glycan-related gene expression
38 signatures in breast cancer subtypes; relation to survival. *Mol Oncol* 9, 861-876.

39 Purbhoo, M.A., Irvine, D.J., Huppa, J.B., and Davis, M.M. (2004). T cell killing does not require the
40 formation of a stable mature immunological synapse. *Nat Immunol* 5, 524-530.

41 Radsak, K., and Wiegandt, H. (1984). Glycosphingolipid synthesis in human fibroblasts infected by
42 cytomegalovirus. *Virology* 138, 300-309.

43 Reiser, J.B., Legoux, F., Gras, S., Trudel, E., Chouquet, A., Leger, A., Le Gorrec, M., Machillot, P.,
44 Bonneville, M., Saulquin, X., *et al.* (2014). Analysis of relationships between peptide/MHC structural
45 features and naive T cell frequency in humans. *J Immunol* 193, 5816-5826.

46 Reits, E.A., Hodge, J.W., Herberts, C.A., Groothuis, T.A., Chakraborty, M., Wansley, E.K.,
47 Camphausen, K., Luiten, R.M., de Ru, A.H., Neijssen, J., *et al.* (2006). Radiation modulates the
48 peptide repertoire, enhances MHC class I expression, and induces successful antitumor
49 immunotherapy. *J Exp Med* 203, 1259-1271.

50 Restifo, N.P., Marincola, F.M., Kawakami, Y., Taubenberger, J., Yannelli, J.R., and Rosenberg, S.A.
51 (1996). Loss of functional beta 2-microglobulin in metastatic melanomas from five patients receiving
52 immunotherapy. *J Natl Cancer Inst* 88, 100-108.

53 Rigau, M., Ostrouska, S., Fulford, T.S., Johnson, D.N., Woods, K., Ruan, Z., McWilliam, H.E.G.,
54 Hudson, C., Tutuka, C., Wheatley, A.K., *et al.* (2020). Butyrophilin 2A1 is essential for
55 phosphoantigen reactivity by gammadelta T cells. *Science* 367.

56 Righi, V., Roda, J.M., Paz, J., Mucci, A., Tugnoli, V., Rodriguez-Tarduchy, G., Barrios, L., Schenetti,
57 L., Cerdan, S., and Garcia-Martin, M.L. (2009). 1H HR-MAS and genomic analysis of human tumor
58 biopsies discriminate between high and low grade astrocytomas. *NMR Biomed* 22, 629-637.

59 Rock, K.L., Reits, E., and Neefjes, J. (2016). Present Yourself! By MHC Class I and MHC Class II
60 Molecules. *Trends Immunol* 37, 724-737.

1 Roszkowski, J.J., Yu, D.C., Rubinstein, M.P., McKee, M.D., Cole, D.J., and Nishimura, M.I. (2003).
2 CD8-independent tumor cell recognition is a property of the T cell receptor and not the T cell. *J*
3 *Immunol* *170*, 2582-2589.

4 Ryan, S.O., and Cobb, B.A. (2012). Roles for major histocompatibility complex glycosylation in
5 immune function. *Semin Immunopathol* *34*, 425-441.

6 Sade-Feldman, M., Jiao, Y.J., Chen, J.H., Rooney, M.S., Barzily-Rokni, M., Eliane, J.P., Bjorgaard,
7 S.L., Hammond, M.R., Vitzthum, H., Blackmon, S.M., *et al.* (2017). Resistance to checkpoint blockade
8 therapy through inactivation of antigen presentation. *Nat Commun* *8*, 1136.

9 Sanjana, N.E., Shalem, O., and Zhang, F. (2014). Improved vectors and genome-wide libraries for
10 CRISPR screening. *Nat Methods* *11*, 783-784.

11 Saverino, D., Fabbi, M., Ghiotto, F., Merlo, A., Bruno, S., Zarcone, D., Tenca, C., Tiso, M., Santoro,
12 G., Anastasi, G., *et al.* (2000). The CD85/LIR-1/ILT2 inhibitory receptor is expressed by all human T
13 lymphocytes and down-regulates their functions. *J Immunol* *165*, 3742-3755.

14 Schindelin, J., Arganda-Carreras, I., Frise, E., Kaynig, V., Longair, M., Pietzsch, T., Preibisch, S.,
15 Rueden, C., Saalfeld, S., Schmid, B., *et al.* (2012). Fiji: an open-source platform for biological-image
16 analysis. *Nature methods* *9*, 676-682.

17 Schumacher, T.N., and Schreiber, R.D. (2015). Neoantigens in cancer immunotherapy. *Science* *348*,
18 69-74.

19 Schutz, G.J., Schindler, H., and Schmidt, T. (1997). Single-molecule microscopy on model
20 membranes reveals anomalous diffusion. *Biophys J* *73*, 1073-1080.

21 Sezgin, E., Levental, I., Mayor, S., and Eggeling, C. (2017). The mystery of membrane organization:
22 composition, regulation and roles of lipid rafts. *Nat Rev Mol Cell Biol* *18*, 361-374.

23 Shayman, J.A. (2010). ELIGLUSTAT TARTRATE: Glucosylceramide Synthase Inhibitor Treatment of
24 Type 1 Gaucher Disease. *Drugs Future* *35*, 613-620.

25 Shi, Y., Qi, J., Iwamoto, A., and Gao, G.F. (2011). Plasticity of human CD8alpha binding to
26 peptide-HLA-A*2402. *Mol Immunol* *48*, 2198-2202.

27 Spaapen, R.M., Lokhorst, H.M., van den Oudenalder, K., Otterud, B.E., Dolstra, H., Leppert, M.F.,
28 Minnema, M.C., Bloem, A.C., and Mutis, T. (2008). Toward targeting B cell cancers with CD4+ CTLs:
29 identification of a CD19-encoded minor histocompatibility antigen using a novel genome-wide
30 analysis. *J Exp Med* *205*, 2863-2872.

31 Stirnemann, J., Belmatoug, N., Camou, F., Serratrice, C., Froissart, R., Caillaud, C., Levade, T.,
32 Astudillo, L., Serratrice, J., Brassier, A., *et al.* (2017). A Review of Gaucher Disease Pathophysiology,
33 Clinical Presentation and Treatments. *Int J Mol Sci* *18*.

34 Taketani, S., Krangel, M.S., Pious, D., and Strominger, J.L. (1983). Structural analysis of HLA-A2
35 antigen from immunoselected mutant 8.6.1: further definition of an HLA-A2-specific serological
36 determinant. *J Immunol* *131*, 2935-2938.

37 Thor Straten, P., and Garrido, F. (2016). Targetless T cells in cancer immunotherapy. *J Immunother*
38 *Cancer* *4*, 23.

39 Trymbulak, W.P., Jr., and Zeff, R.A. (1997). Mutants of human beta2-microglobulin map an
40 immunodominant epitope within the three-stranded beta-pleated sheet. *Transplantation* *64*, 640-645.

41 Unanue, E.R., and Cerottini, J.C. (1989). Antigen presentation. *FASEB J* *3*, 2496-2502.

42 Valiante, N.M., Uhrberg, M., Shilling, H.G., Lienert-Weidenbach, K., Arnett, K.L., D'Andrea, A.,
43 Phillips, J.H., Lanier, L.L., and Parham, P. (1997). Functionally and structurally distinct NK cell
44 receptor repertoires in the peripheral blood of two human donors. *Immunity* *7*, 739-751.

45 van Bergen, C.A., Kester, M.G., Jedema, I., Heemskerk, M.H., van Luxemburg-Heijs, S.A.,
46 Kloosterboer, F.M., Marijt, W.A., de Ru, A.H., Schaafsma, M.R., Willemze, R., *et al.* (2007). Multiple
47 myeloma-reactive T cells recognize an activation-induced minor histocompatibility antigen encoded by
48 the ATP-dependent interferon-responsive (ADIR) gene. *Blood* *109*, 4089-4096.

49 Van Bergen, C.A., Rutten, C.E., Van Der Meijden, E.D., Van Luxemburg-Heijs, S.A., Lurvink, E.G.,
50 Houwing-Duistermaat, J.J., Kester, M.G., Mulder, A., Willemze, R., Falkenburg, J.H., *et al.* (2010).
51 High-throughput characterization of 10 new minor histocompatibility antigens by whole genome
52 association scanning. *Cancer Res* *70*, 9073-9083.

53 Voss, M., Fukumori, A., Kuhn, P.H., Kunzel, U., Klier, B., Grammer, G., Haug-Kroper, M., Kremmer,
54 E., Lichtenthaler, S.F., Steiner, H., *et al.* (2012). Foamy virus envelope protein is a substrate for signal
55 peptide peptidase-like 3 (SPPL3). *J Biol Chem* *287*, 43401-43409.

56 Voss, M., Kunzel, U., Higel, F., Kuhn, P.H., Colombo, A., Fukumori, A., Haug-Kroper, M., Klier, B.,
57 Grammer, G., Seidl, A., *et al.* (2014). Shedding of glycan-modifying enzymes by signal peptide
58 peptidase-like 3 (SPPL3) regulates cellular N-glycosylation. *EMBO J* *33*, 2890-2905.

59 Voss, M., Schroder, B., and Fluhrer, R. (2013). Mechanism, specificity, and physiology of signal
60 peptide peptidase (SPP) and SPP-like proteases. *Biochim Biophys Acta* *1828*, 2828-2839.

1 Wang, Z., Wen, L., Ma, X., Chen, Z., Yu, Y., Zhu, J., Wang, Y., Liu, Z., Liu, H., Wu, D., *et al.* (2012).
2 High expression of lactotriaosylceramide, a differentiation-associated glycosphingolipid, in the bone
3 marrow of acute myeloid leukemia patients. *Glycobiology* 22, 930-938.
4 Wearsch, P.A., and Cresswell, P. (2008). The quality control of MHC class I peptide loading. *Curr*
5 *Opin Cell Biol* 20, 624-631.
6 Wieser, S., Moertelmaier, M., Fuertbauer, E., Stockinger, H., and Schutz, G.J. (2007). (Un)confined
7 diffusion of CD59 in the plasma membrane determined by high-resolution single molecule
8 microscopy. *Biophys J* 92, 3719-3728.
9 Wikstrand, C.J., He, X.M., Fuller, G.N., Bigner, S.H., Fredman, P., Svennerholm, L., and Bigner, D.D.
10 (1991). Occurrence of lacto series gangliosides 3'-isoLM1 and 3',6'-isoLD1 in human gliomas in vitro
11 and in vivo. *J Neuropathol Exp Neurol* 50, 756-769.
12 Willcox, B.E., Thomas, L.M., and Bjorkman, P.J. (2003). Crystal structure of HLA-A2 bound to LIR-1,
13 a host and viral major histocompatibility complex receptor. *Nat Immunol* 4, 913-919.
14 Winn, M.D., Ballard, C.C., Cowtan, K.D., Dodson, E.J., Emsley, P., Evans, P.R., Keegan, R.M.,
15 Krissinel, E.B., Leslie, A.G., McCoy, A., *et al.* (2011). Overview of the CCP4 suite and current
16 developments. *Acta Crystallogr D Biol Crystallogr* 67, 235-242.
17 Wraith, J.E., and Imrie, J. (2009). New therapies in the management of Niemann-Pick type C disease:
18 clinical utility of miglustat. *Ther Clin Risk Manag* 5, 877-887.
19 Yewdell, J.W., and Hill, A.B. (2002). Viral interference with antigen presentation. *Nat Immunol* 3,
20 1019-1025.
21 Zaretsky, J.M., Garcia-Diaz, A., Shin, D.S., Escuin-Ordinas, H., Hugo, W., Hu-Lieskovan, S., Torrejon,
22 D.Y., Abril-Rodriguez, G., Sandoval, S., Barthly, L., *et al.* (2016). Mutations Associated with Acquired
23 Resistance to PD-1 Blockade in Melanoma. *N Engl J Med* 375, 819-829.
24 Zhang, T., de Waard, A.A., Wuhrer, M., and Spaapen, R.M. (2019). The Role of Glycosphingolipids in
25 Immune Cell Functions. *Front Immunol* 10, 90.
26 Zhang, Y., Zhang, J., Chen, Y., Luo, B., Yuan, Y., Huang, F., Yang, T., Yu, F., Liu, J., Liu, B., Song,
27 Z., Chen, J., Pan, T., Zhang, X., Li, Y., Li, R., Huang, W., Xiao, F., Zhang, H. (2020). The ORF8
28 Protein of SARS-CoV-2 Mediates Immune Evasion through Potently Downregulating MHC-I. *bioRxiv*
29 *2020.05.24.111823*.
30

KEY RESOURCES TABLE

REAGENT or RESOURCE	SOURCE	IDENTIFIER
Antibodies		
Mouse monoclonal anti-HLA-ABC-PerCP-eFluor710 (W6/32)	Thermo Fisher Scientific	Cat# 46-9983-42, RRID:AB_10804486
Mouse monoclonal anti-HLA-BC-APC (B1.23.2)	Thermo Fisher Scientific	Cat# 17-5935-42, RRID:AB_11151509
Mouse monoclonal anti-HLA-A2-APC (BB7.2)	Thermo Fisher Scientific	Cat# 17-9876-42, RRID:AB_11149299
Mouse monoclonal anti-CD15-FITC (C3D-1)	Millipore	Cat# FCMAB182F, RRID:AB_11214339
Goat anti-mouse IgG (H+L) - Alexa Fluor 647	Thermo Fisher Scientific	Cat# A28181, RRID:AB_2536165
Mouse APC anti-human IgM (MHM-88)	Biologend	Cat# 314510, RRID:AB_493011
Mouse monoclonal anti-human IgG (MH161-1)	Sanquin home made	Hybridoma
Rabbit polyclonal anti-RFP	Netherlands Cancer Institute home made	Rocha et al., 2009
Mouse monoclonal anti-HLA-I (W6/32)	Dr. J. Neefjes (NKI, The Netherlands)	Hybridoma
Mouse monoclonal anti-HLA-I (HC10)	Dr. J. Neefjes (NKI, The Netherlands)	Hybridoma
Mouse monoclonal anti-HLA-I (HCA2)	Dr. J. Neefjes (NKI, The Netherlands)	Hybridoma
Mouse monoclonal anti-HLA-I (BB7.2)	Dr. M. Heemskerk (LUMC, The Netherlands)	Hybridoma
Mouse monoclonal anti-FLAG (M2)	Sigma-Aldrich	Cat# F3165, RRID:AB_259529
Mouse monoclonal anti-b-actin (AC-15)	Sigma-Aldrich	Cat# A5441, RRID:AB_476744
Mouse monoclonal anti-NGFR(CD271)-PE/Cy7 (ME20.4)	Biologend	Cat# 345109, RRID:AB_11204073
Goat anti-rabbit IgG (H+L)-HRP	Thermo Fisher Scientific	Cat# G-21234, RRID:AB_2536530
Mouse monoclonal anti-FLAG M2-HRP antibody	Sigma-Aldrich	Cat# A8592, RRID:AB_439702
APC AffiniPure F(ab') ₂ Fragment Goat Anti-Human IgG, Fcy fragment specific	Jackson ImmunoResearch	Cat# 109-136-098, RRID:AB_2337693
HLA-I/B2M specific antibodies, see <i>Table S3</i>		
Bacterial and Virus Strains		
Biological Samples		
Chemicals, Peptides, and Recombinant Proteins		
LIR-1 Fc fusion protein (human IgG1)	Dr. O. Mandelboim (Hebrew University Hadassah Medical School, Israel)	Gonen-Gross et al., 2010
Recombinant human KIR2DL1/CD158a Fc chimera protein	R&D systems	Cat# 1844-KR

Recombinant human KIR2DL2/CD158b1 Fc chimera protein	R&D systems	Cat# 3015-KR
Alexa Fluor® 555 NHS Ester	Thermo Fisher Scientific	Cat# A20009
Alexa Fluor® 647 NHS Ester	Thermo Fisher Scientific	Cat# A37573
CFSE	Invitrogen	Cat# C1157
Alexa Fluor 350 NHS Ester	Thermo Fisher Scientific	Cat# A10168
Violet proliferation dye 450	BD Horizon	Cat# 562158
DyLight 650 NHS ester	Thermo Fisher Scientific	Cat# 62265
Cholera Toxin B Subunit from <i>Vibrio cholerae</i> -FITC	Sigma	Cat# C1655, CAS: 131096-89-4
Animal-Free Recombinant Human IFN- γ	Peprtech	Cat# AF-300-02
Sialyltransferase inhibitor (3Fax-peracetyl Neu5Ac)	Sigma	Cat# 566224, CAS: 117405-58-0
Fucosyltransferase inhibitor (2-Deoxy-2-fluoro-L-fucose)	Carbosynth	MD06089, CAS: 70763-62-1
Neuraminidase from <i>Clostridium perfringens</i>	Sigma-Aldrich	N2876, CAS: 9001-67-6
Endoglycoceramidase I	New England Biolabs	Cat# P0773S
Miglustat	Dr. H. Overkleeft (Leiden University, The Netherlands)	Ghisaidoobe et al., 2014
Eliglustat	Bio-Connect	Cat# HY-14885A
MZ21	Dr. H. Overkleeft (Leiden University, The Netherlands)	Ghisaidoobe et al., 2014
MZ31	Dr. H. Overkleeft (Leiden University, The Netherlands)	Ghisaidoobe et al., 2014
Kifunensine (mannosidase inhibitor)	Santa Cruz	Cat# sc-201364, CAS: 109944-15-2
Swainsonine	Sigma-Aldrich	Cat# S8195, CAS: 72741-87-8
Brefeldin A	Sigma-Aldrich	Cat#B7651, CAS: 20350-15-6
BODIPY™ FL C5-Lactosylceramide complexed to BSA	Thermo Fisher Scientific	Cat# B34402
UDP-N-acetyl-D-glucosamine disodium salt	Santa Cruz	Cat# sc-286851
Endoglycoceramidase I (derived from <i>Rhodococcus triatomea</i> and expressed in <i>Escherichia coli</i>)	New England Biolabs	Cat# P0773S
Endoglycosidase H from <i>Streptomyces plicatus</i>	Sigma-Aldrich	Cat# A0810, CAS: 37278-88-9
Critical Commercial Assays		
IFN- γ ELISA Kit	Sanquin	Cat# M9333
GMCSF-ELISA Kit	Biolegend	Cat# 432002
Deposited Data		
Experimental Models: Cell Lines		

Human: HAP1	Dr. T. Brummelkamp (NKI, The Netherlands)	
Human: MeJuSo	Dr. J. Neefjes (LUMC, The Netherlands)	Authenticated: 19 ZE 000486 (2019)
Human: U373	Laboratory of Dr. H. Versteeg (LUMC, The Netherlands)	
Human: SW620	Dr. T. de Gruijl (Amsterdam UMC, The Netherlands)	
Human: HEK293T	ATCC	Cat# CRL-3216 RRID:CVCL_0063
Human: Phoenix Ampho	Dr. J. Neefjes (LUMC, The Netherlands)	
Murine: BB7.2 cell line (hybridoma)	Dr. M. Heemskerk (LUMC, The Netherlands)	
Murine: W6/32 cell line (hybridoma)	Dr. J. Neefjes (LUMC, The Netherlands)	
Human: CD8+ T cell clone reactive to USP11 peptide	Dr. M. Heemskerk (LUMC, The Netherlands)	Amir et al., 2011
Human: CD8+ T cell clone reactive to FDPS peptide	Dr. M. Heemskerk (LUMC, The Netherlands)	Amir et al., 2011
Human: CD8+ T cell clone reactive to VPS13B peptide	Dr. M. Heemskerk (LUMC, The Netherlands)	Amir et al., 2011
Human: CD8+ T cell clone reactive to SSR1 peptide	Dr. M. Griffioen (LUMC, The Netherlands)	van Bergen et al., 2010
Human: CD8+ T cell clone reactive to ADIR peptide	Dr. M. Griffioen (LUMC, The Netherlands)	van Bergen et al., 2007
Experimental Models: Organisms/Strains		
Oligonucleotides		
siGENOME Human SPPL3 siRNA	Dharmacon	D-006042-02,03,04
siGENOME Human B2M siRNA (SMARTpool)	Dharmacon	M-004366-00
siGENOME Non-Targeting siRNA Pool#1	Dharmacon	D-001206-13
gRNA sequences used for CRISPR/Cas9 mediated genome editing, see <i>Table S4</i>	This paper	N/A
PCR and sequencing primers for KO validation, see <i>Table S5</i> .	This paper	N/A
Recombinant DNA		
pX330	Addgene	Plasmid #42230
TIA-2A-blast	Dr. T. Brummelkamp (NKI, The Netherlands)	Blomen et al., 2015
LentiCRISPR_v2	Addgene	Plasmid #52961
pL-CRISPR.EFS.GFP	Addgene	Plasmid #57818

pMXs-puro retroviral expression vector	Cell Biolabs	Cat# RTV-012
pMXs-puro-GFP	This paper	N/A
pMXs-puro-GFP-SPPL3	This paper	Voss et al., 2012
pMXs-puro-GFP-SPPL3DA	This paper	Voss et al., 2012
pMXs-puro-FLAG-N	This paper	N/A
pMXs-puro-FLAG-C	This paper	N/A
pMXs-puro-FLAG-B3GNT5	This paper	IMAGE:202800754
pMXs-puro-B3GNT5-FLAG	This paper	IMAGE:202800754
pMXs-puro-RFP	This paper	N/A
pMXs-puro-RFP-SPPL3	This paper	Voss et al., 2012
pMXs-puro-RFP-SPPL3DA	This paper	Voss et al., 2012
pMXs-puro-FLAG-B4GALNT1	This paper	IMAGE:202800771
pMXs-puro-FLAG-ST3GAL5	This paper	IMAGE:202759803
puc2CL6IN-HLA-C*05:01 (with mutated signal peptide from HLA-A*02:01 [M4V])	Dr. A. Halenius (University Medical Center Freiburg)	N/A
pLZRS-HLA-A*02:01-IRES-ΔNGFR	Dr. M. Griffioen (LUMC, The Netherlands)	(Griffioen et al., 2012; Van Bergen et al., 2010)
pLZRS-HLA-B*40:01-IRES-ΔNGFR	Dr. M. Griffioen (LUMC, The Netherlands)	(Griffioen et al., 2012; Van Bergen et al., 2010)
pLZRS-HLA-C*03:03-IRES-ΔNGFR	Dr. M. Griffioen (LUMC, The Netherlands)	(Griffioen et al., 2012; Van Bergen et al., 2010)
Software and Algorithms		
Phyre2	http://www.sbg.bio.ic.ac.uk/	Kelley et al., 2015
PyMOL v2.0	http://pymol.org	Schrödinger, LLC
Compass Data Analysis v4.0 and v5.0 software	http://www.bruker.com	Bruker Daltonics
FlowJo Single Cell Analysis v10 software	http://www.flowjo.com	FlowJo, LLC
Fiji – plugin ThunderSTORM		Ovesny et al., 2014
Glycoworkbench		Ceroni et al., 2008
Glycomod		Cooper et al., 2001
TCGA survival and expression data	http://oncoLnc.org	Anaya, 2016
Graphpad Prism	http://www.graphpad.com	
Other		
RFP-Trap_A antibody	ChromoTek	Cat# rta-20, RRID:AB_2631362
Acclaim PepMap100 C18 column, 100μm × 2cm, C18 particle size 5μm, pore size 100Å.	Dionex/Thermo Fisher Scientific	Cat# 164199
Acclaim PepMap RSLC nanocolumn, 75μm × 15cm, C18 particle size 2μm, pore size 100Å	Dionex/Thermo Fisher Scientific	Cat# TF164534
⁵¹ Cr, sodium chromate in normal saline (pH 8-10)	Perkin-Elmer	Cat# NEZ030
Hypercarb™ KAPPA Column, 30 × 0.32 mm, particle size 5μm, pore size 250Å.	Thermo Scientific	Cat# 03170480
Hypercarb™ KAPPA Column, 100 mm × 75 μm, particle size 3μm, pore size 250Å.	Thermo Scientific	Cat# 03170480

Figure 1

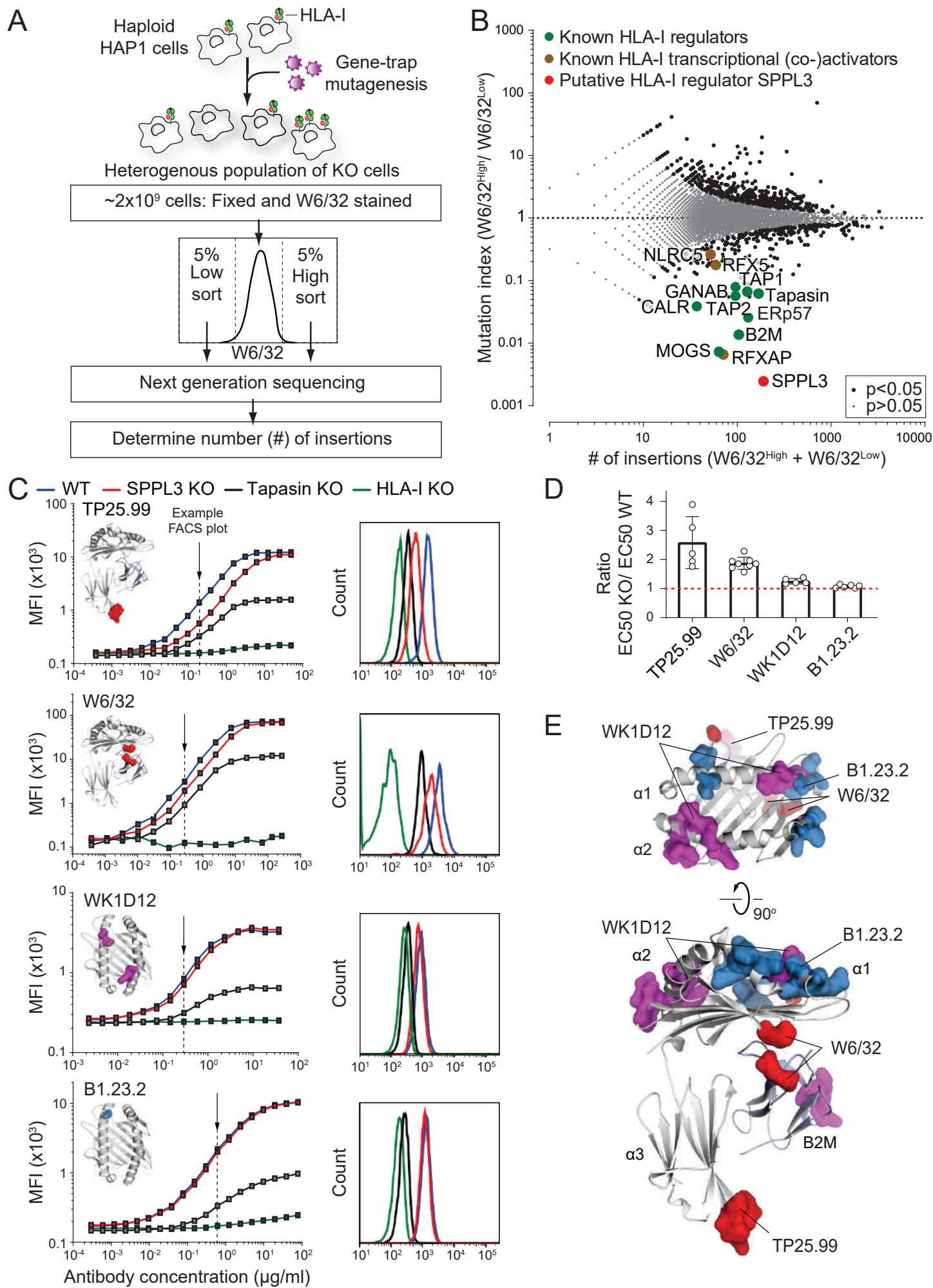


Figure 2

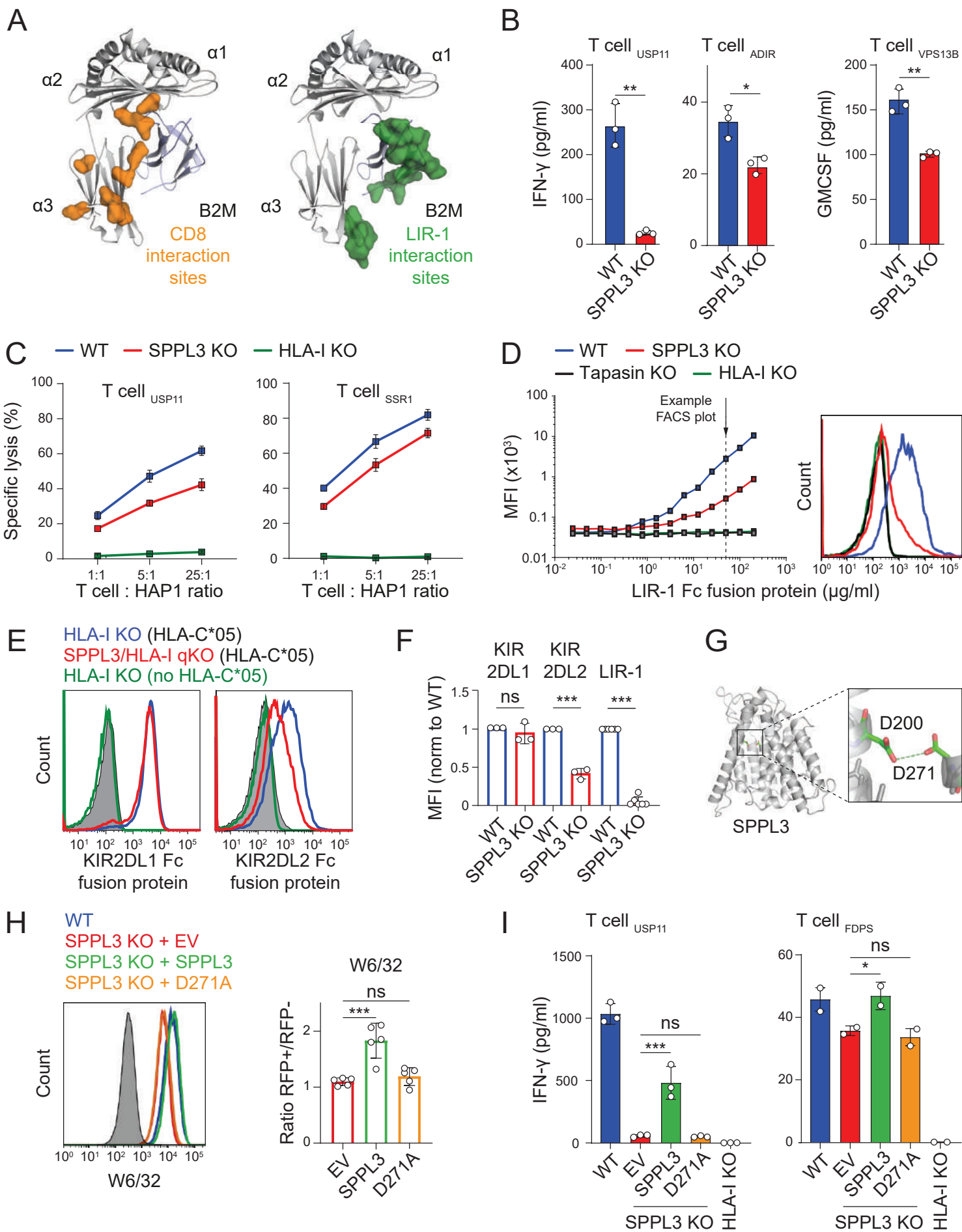


Figure 3

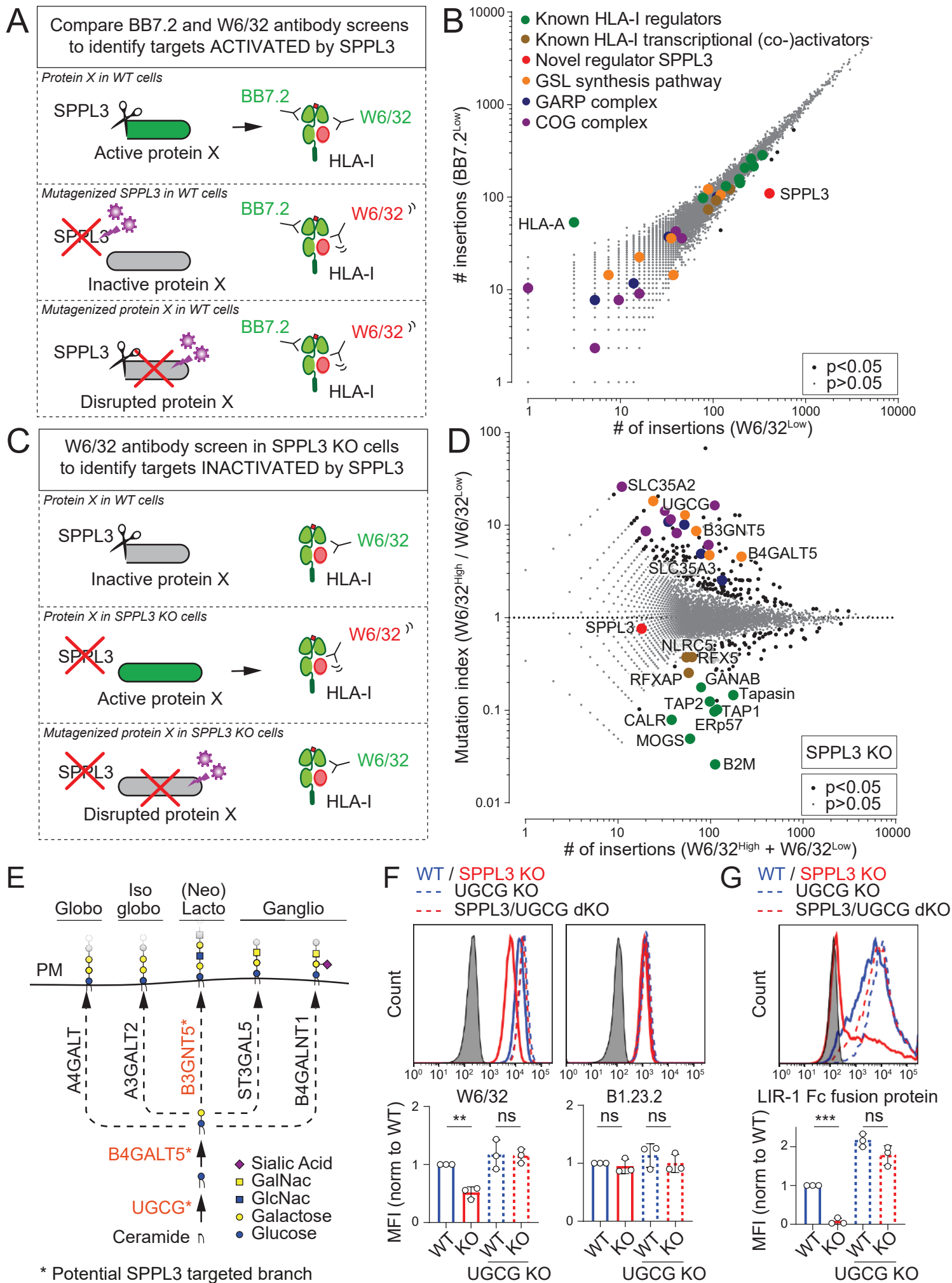


Figure 4

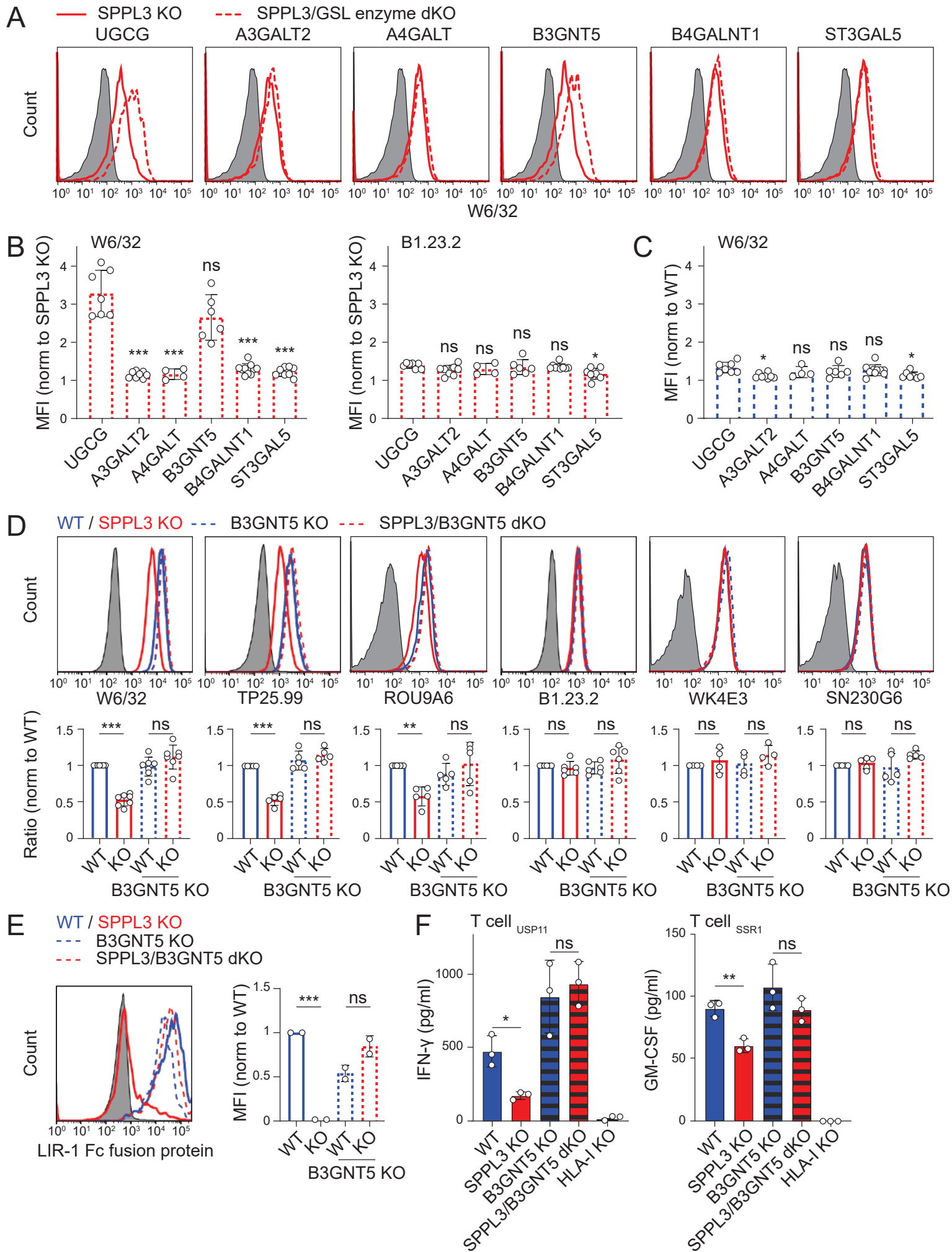


Figure 5

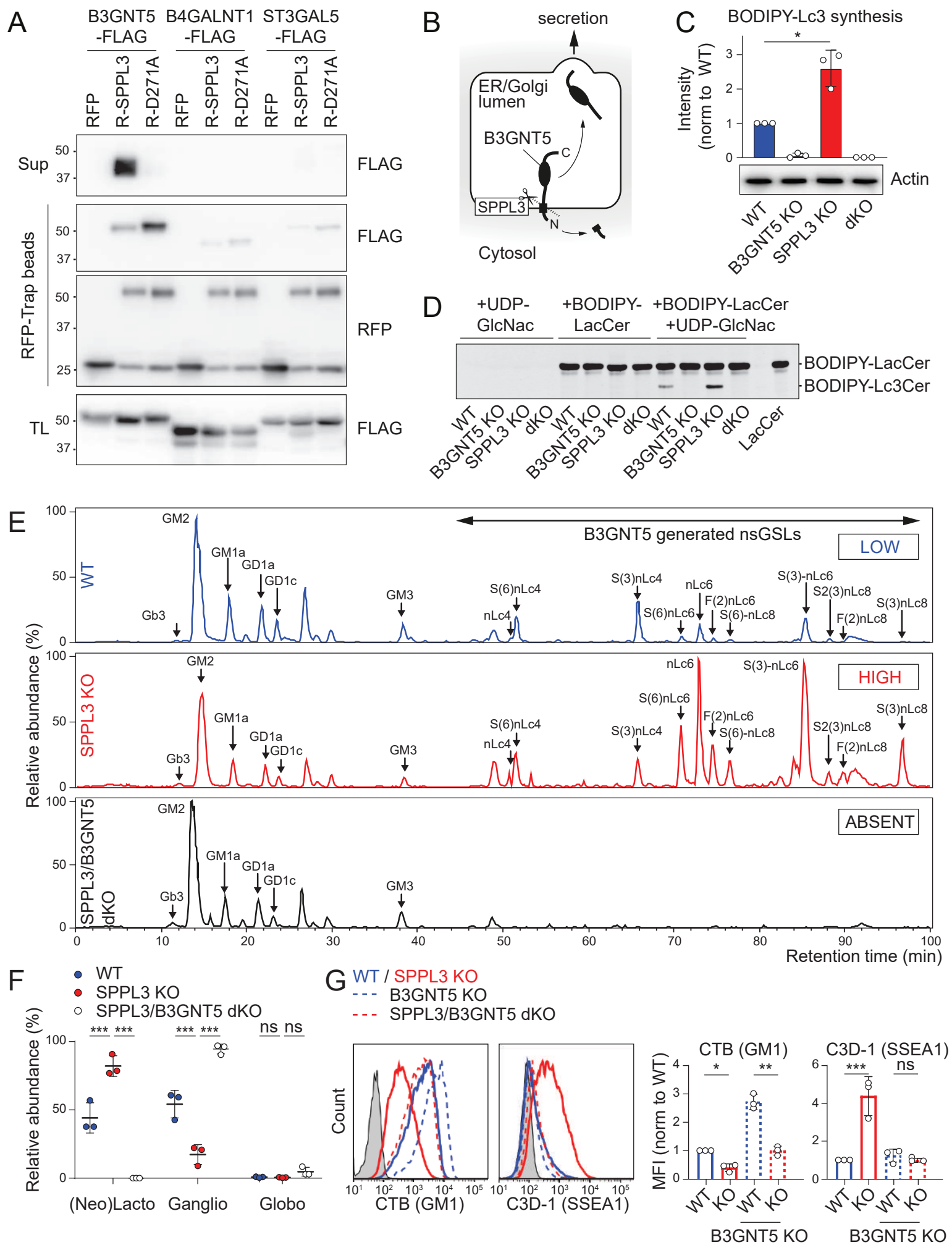


Figure 6

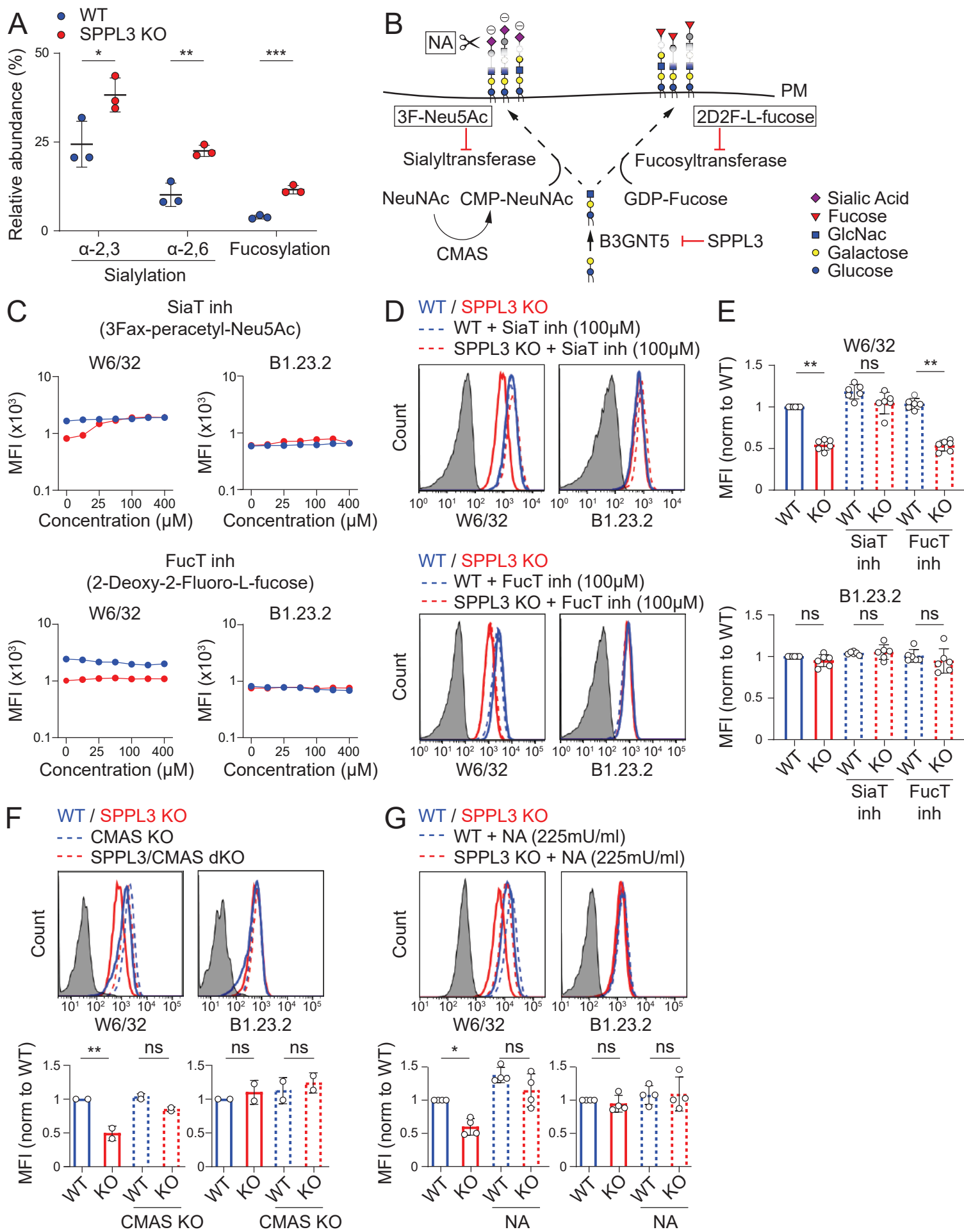
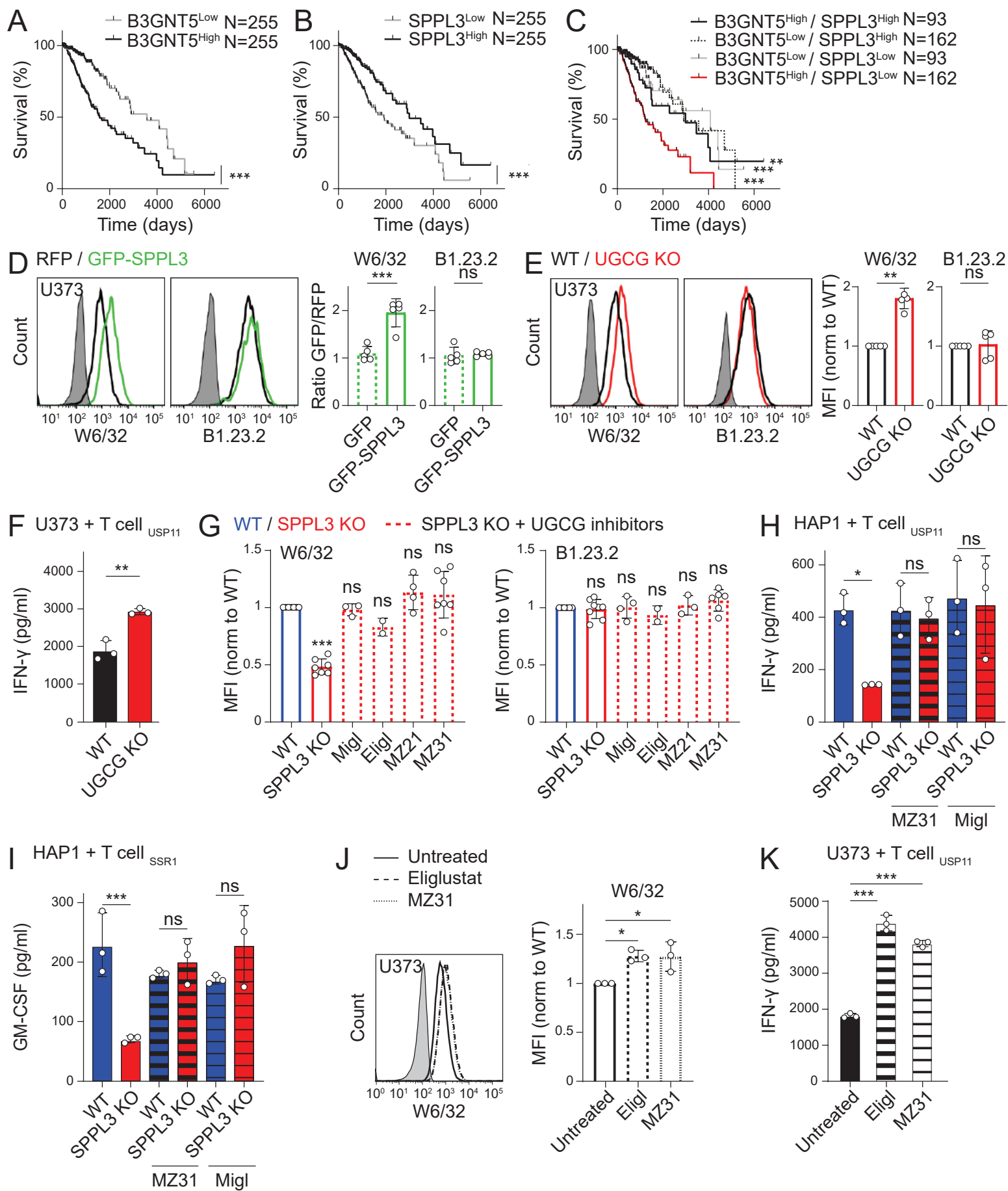


Figure 7



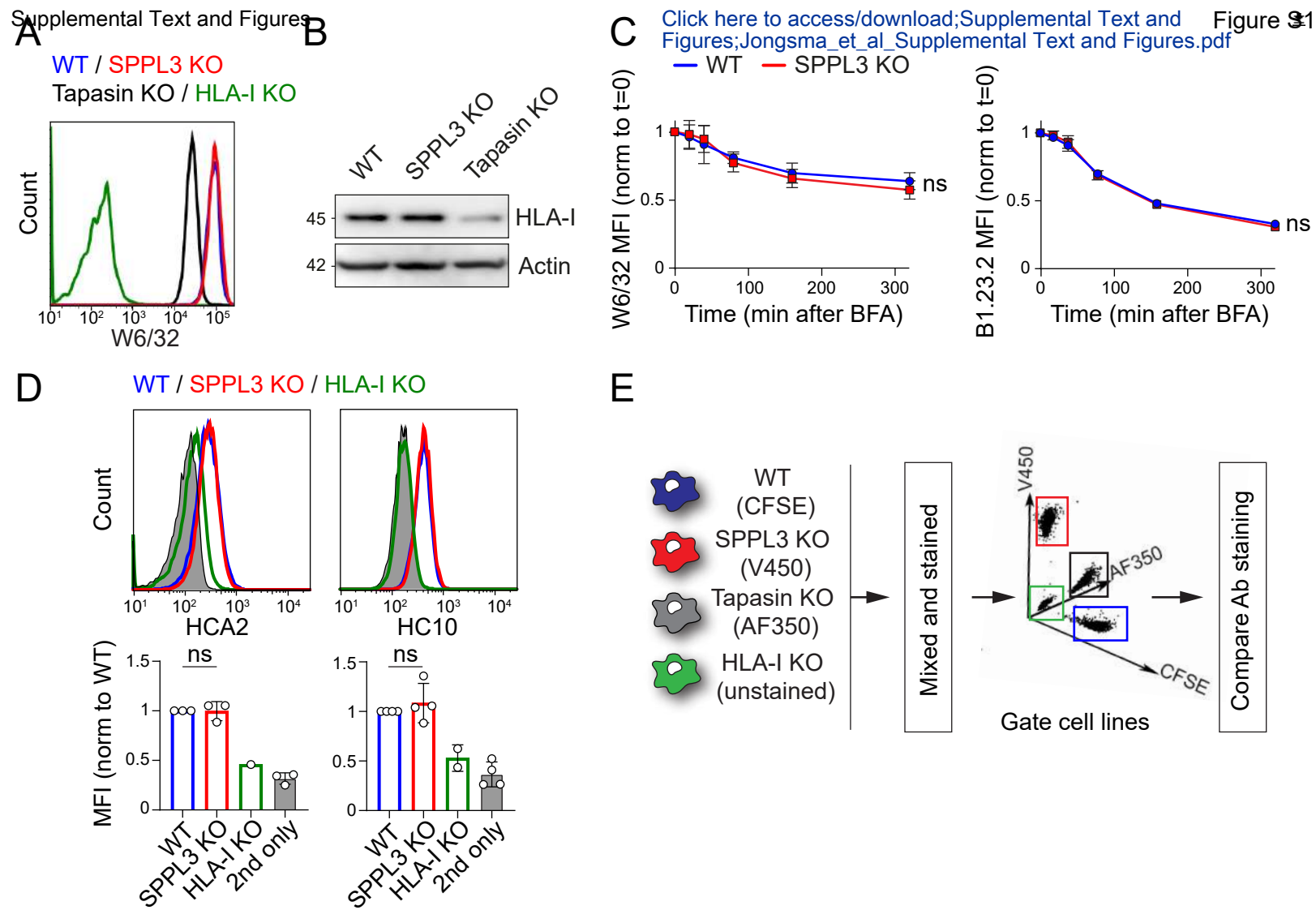


Figure S1. SPPL3 activity does not affect total HLA-I levels, HLA-I uptake and peptide stability (Relates to Figure 1) (A) Representative histograms of saturating W6/32 stain of WT (*blue*), SPPL3 KO (*red*), tapasin KO (*black*) and HLA-I KO (*green*) HAP1 cells. n=3. (B) Immunoblot showing the levels of total HLA-I (HC10) and actin (AC-15, loading control) in WT, SPPL3 KO and tapasin KO HAP1 cells. n=2. (C) Cell surface HLA-I levels detected at different timepoints after BFA addition by W6/32 and B1.23.2 staining (mean fluorescence intensity (MFI)) of WT (*blue*) and SPPL3 KO (*red*) cells. Normalized to t=0. Data are represented as mean \pm SD, n=3. (D) Representative histograms of HCA2 (HLA-A) and HC10 (HLA-B and HLA-C) surface staining of peptide free HLA-I heavy chains on WT (*blue*), SPPL3 KO (*red*) and HLA-I KO (*green*) HAP1 cells, indicating the relative stability of the peptide-HLA-I interaction. Quantified MFI are represented as \pm SD, n=3-4. The gray histogram represents the condition without primary antibody. (E) Schematic overview of fluorescent cell barcoding procedure. The depicted cell lines were barcoded using Alexa Fluor 350, Violet Proliferation (V450) or CFSE dyes, mixed and stained for flow cytometry (see Figures 1C and S2A). The cell lines were gated based on their barcoding before comparative analysis of antibody staining.

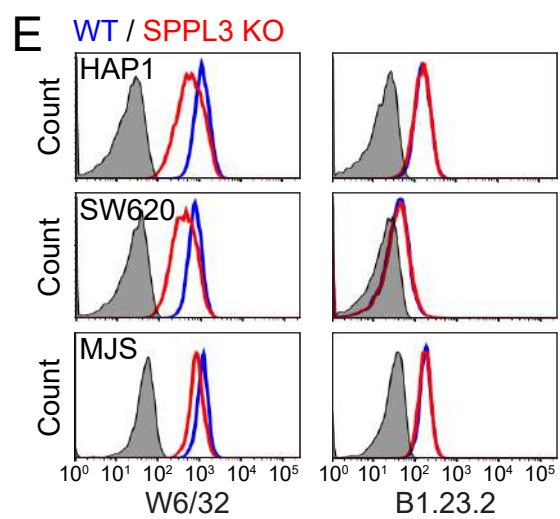
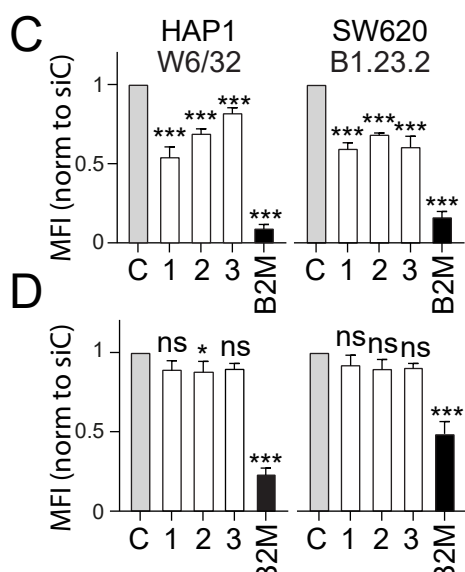
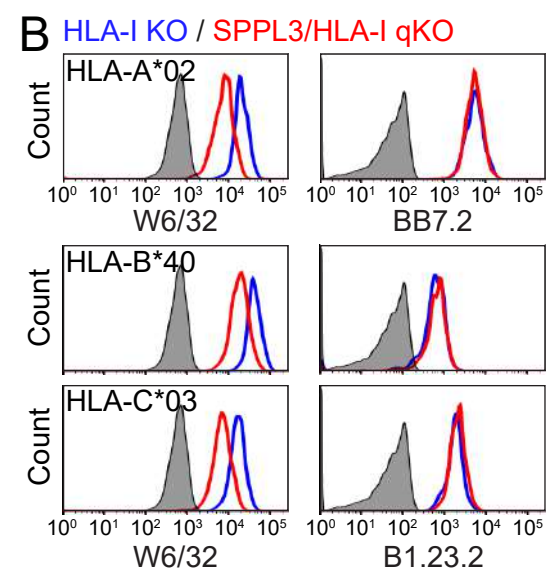
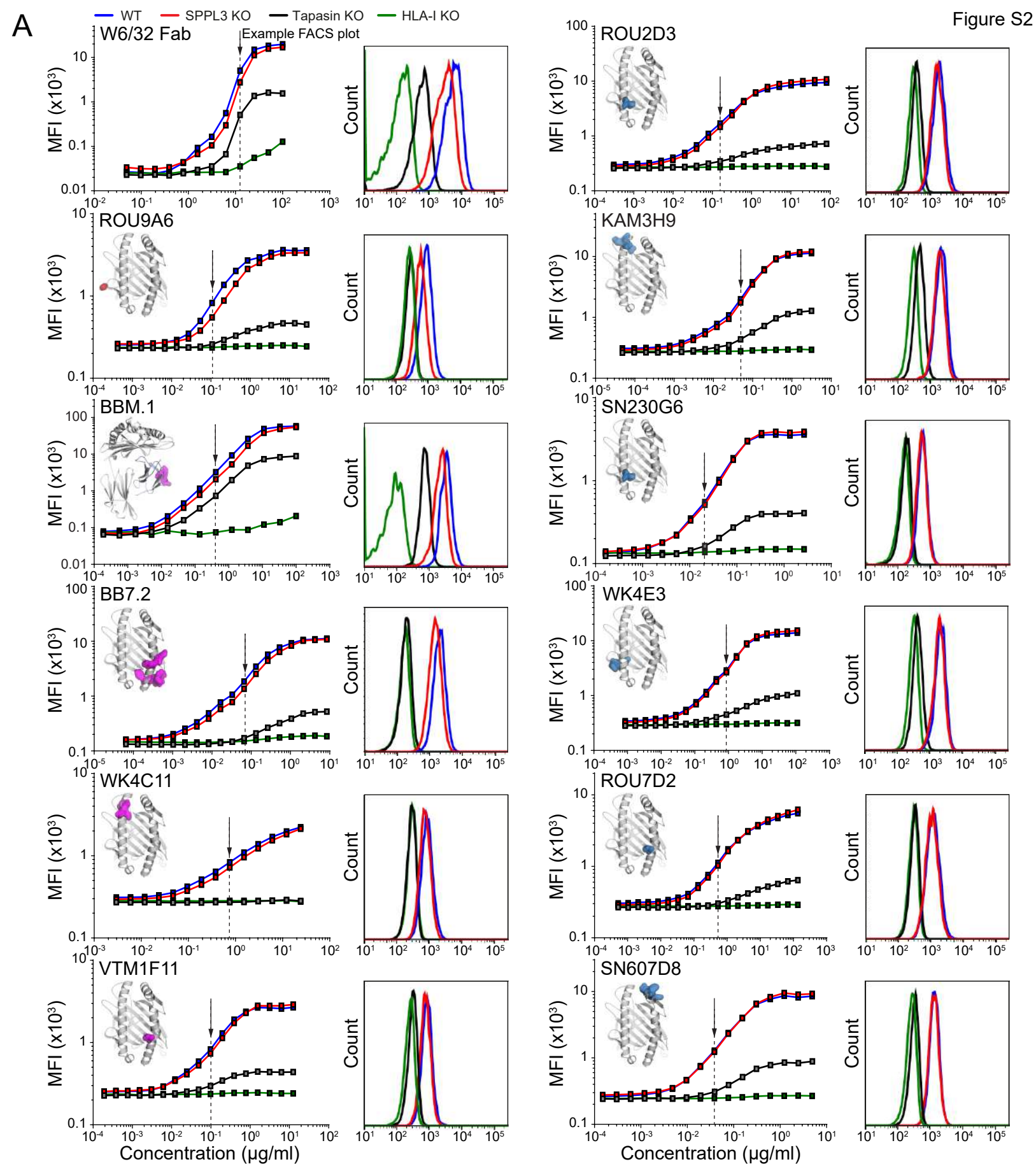


Figure S2. SPPL3 determines the accessibility of HLA-A, -B and -C alleles (Relates to Figure 1) (A) (*left*) Representative titration curves of AF647-labeled W6/32 Fab fragments and 11 HLA-I / B2M-specific antibodies on WT (*blue*), SPPL3 KO (*red*), tapasin KO (*black*) and HLA-I KO (*green*) HAP1 cells. (*inset*) Essential amino acids for binding of the respective antibody depicted on the HLA-I / B2M crystal structure in red (SPPL3-susceptible epitopes), purple (mildly affected epitopes) or blue (SPPL3-independent epitopes). (*right*) Representative histograms of non-saturating antibody staining (as indicated by the arrow). n=3. (B) Histograms of W6/32 and either BB7.2 (HLA-A) or B1.23.2 (HLA-B and -C) cell surface staining of HLA-A, -B and -C triple KO (HLA-I KO) (*blue*) or SPPL3/HLA-I quadruple KO (qKO) (*red*) HAP1 cells transduced with HLA-A*02:01, HLA-B*40:01 or HLA-C*03:03. n=1. (C/D) MFI of W6/32 (C) and B1.23.2 (D) cell surface staining of HAP1 or SW620 cells transfected with three individual siRNAs targeting SPPL3 (1,2,3) or one siRNA targeting B2M relative to control (C). Data are represented as mean \pm SD, n=2. (E) Representative histograms of W6/32 (*left panels*) and B1.23.2 stain (*right panels*) on either WT (*blue*) or SPPL3 gRNA (lentiCRISPR_v2) transduced and puromycin selected (*red*) HAP1, SW620 or MelJuSo cells. n=2. For flow cytometry data, the gray histogram represents an unstained control cell line.

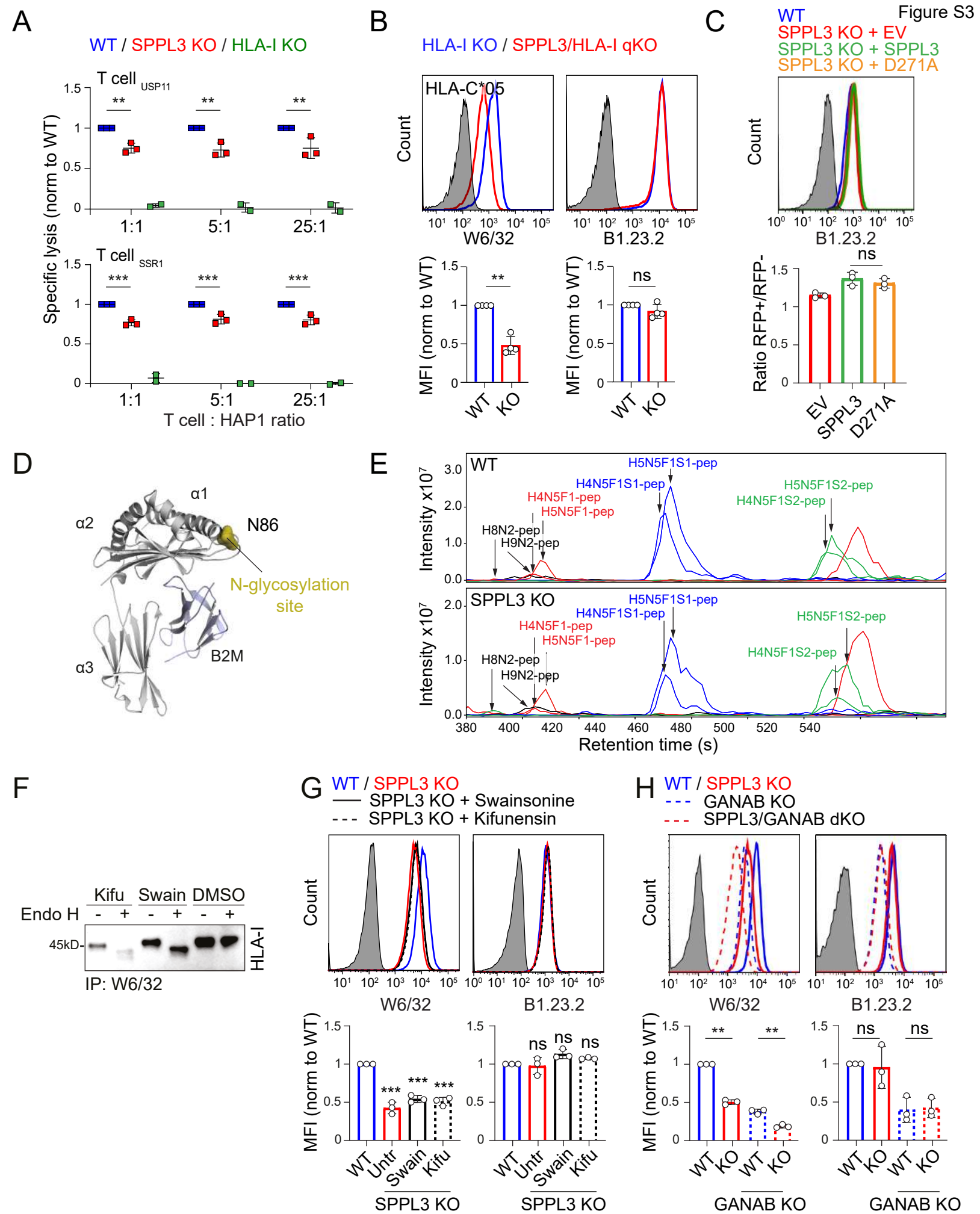


Figure S3. SPPL3 affects T cell mediated killing, but not HLA-I N-glycosylation (Relates to Figure 2)

(A) Specific lysis (as detected by chromium-51 (^{51}Cr) release) of SPPL3 KO (*red*) and HLA-I KO (*green*) cells after coculture with HLA-A*02:01-restricted USP11- or SSR1-specific T cells at indicated effector – target cell ratios, normalized to lysis of WT (*blue*) HAP1 cells. (B) Representative histograms of W6/32 and B1.23.2 cell surface staining of HLA-C*05:01 transduced HLA-I KO (*blue*) and SPPL3/HLA-I qKO (*red*) cells. Quantifications (MFI) are represented as \pm SD, n=4, 'KO' is SPPL3 KO. (C) Representative histogram of non-saturating B1.23.2 stain on HAP1 WT (*blue*) or SPPL3 KO cells transfected with either RFP-empty vector (*red*), RFP-SPPL3 (*green*) or catalytically inactive RFP-SPPL3 D271A (*orange*). RFP+ gate of transduced samples is shown. Quantification (MFI ratios RFP+/RFP-) are represented as mean \pm SD, n=3. (D) Crystal structure of HLA-I showing its N-glycosylation site. (E) Extracted ion chromatogram showing the eight most abundant glycopeptides derived from tryptic digest of immunoprecipitated HLA-I (BB7.2) from WT (*upper panel*) and SPPL3 KO (*bottom panel*) HAP1 cells analyzed by RP nanoLC-ESI-MS(/MS). The two most abundant high-mannose glycopeptides (*black*), neutral complex glycopeptides (*red*), monosialylated glycopeptides (*blue*) and disialylated glycopeptides (*green*) are shown. (F) Immunoblot of immunoprecipitated HLA-I by W6/32 from the depicted mannosidase inhibitor-treated SPPL3 KO cells followed either or not by Endoglycosidase H treatment to show modification of the N-linked glycan on HLA-I. HLA-I was detected by HC10 on western blot. Position marker protein is indicated. (G) Representative histograms of W6/32 (*left*) and B1.23.2 (*right*) cell surface staining of WT (*blue*), SPPL3 KO (*red*) and SPPL3 KO HAP1 cells cultured in the presence of mannosidase I and II inhibitors kifunensine and swainsonine (*black*). Quantification (MFI) is represented as mean \pm SD, n=3, 'KO' is SPPL3 KO. (H) Histograms of W6/32 (*left*) and B1.23.2 stain (*right*) on either WT (*blue*), SPPL3 KO (*red*), GANAB KO (*blue dashed*) or SPPL3/GANAB double KO (dKO) cells (*red dashed*). Quantification (MFI) is represented as mean \pm SD, n=3, 'KO' is SPPL3 KO. For all flow cytometry data, the gray histogram represents an unstained control cell line.

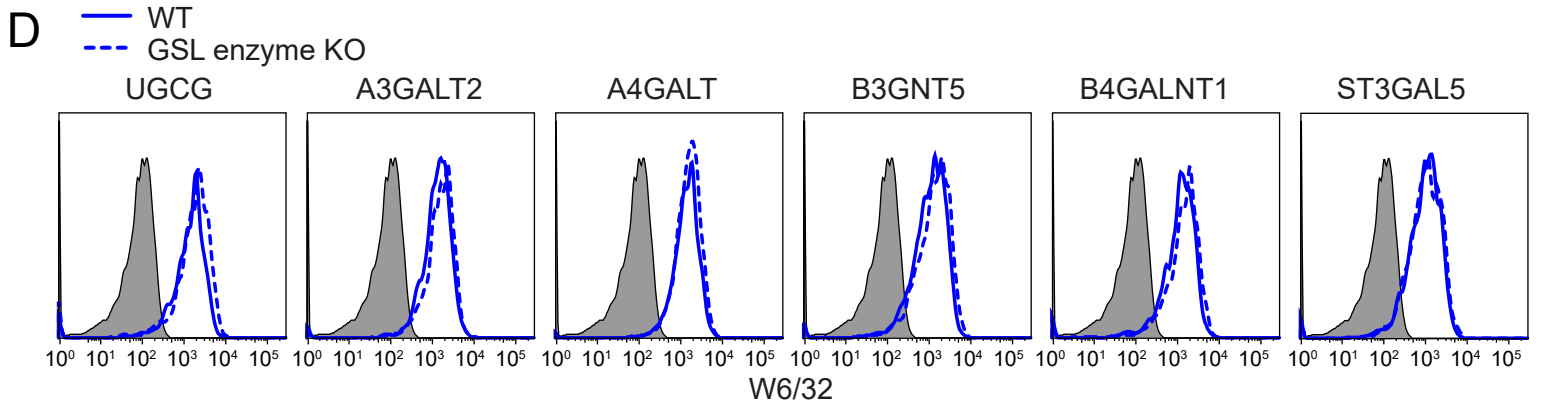
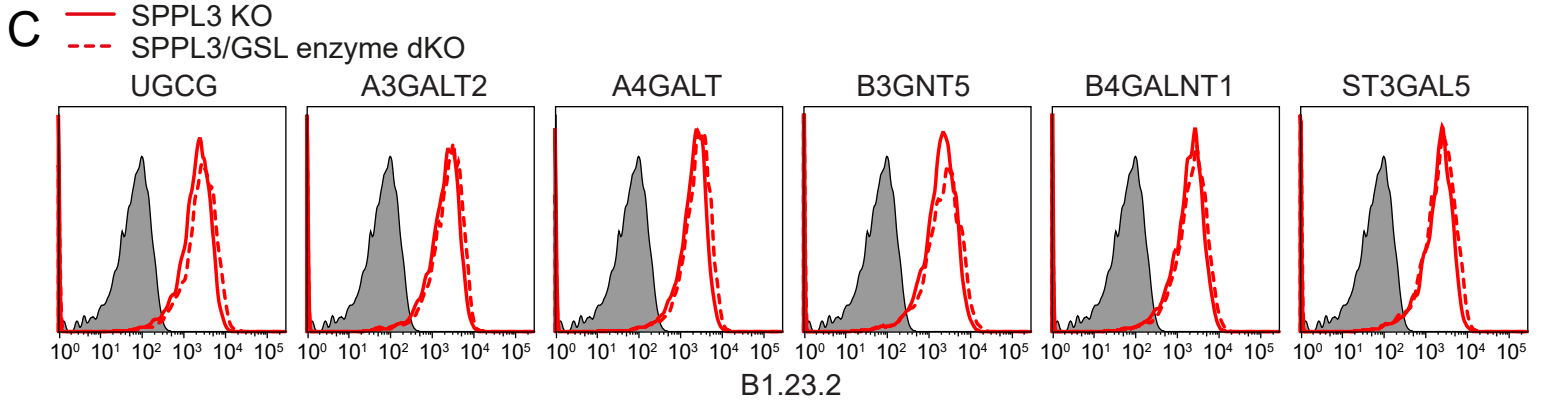
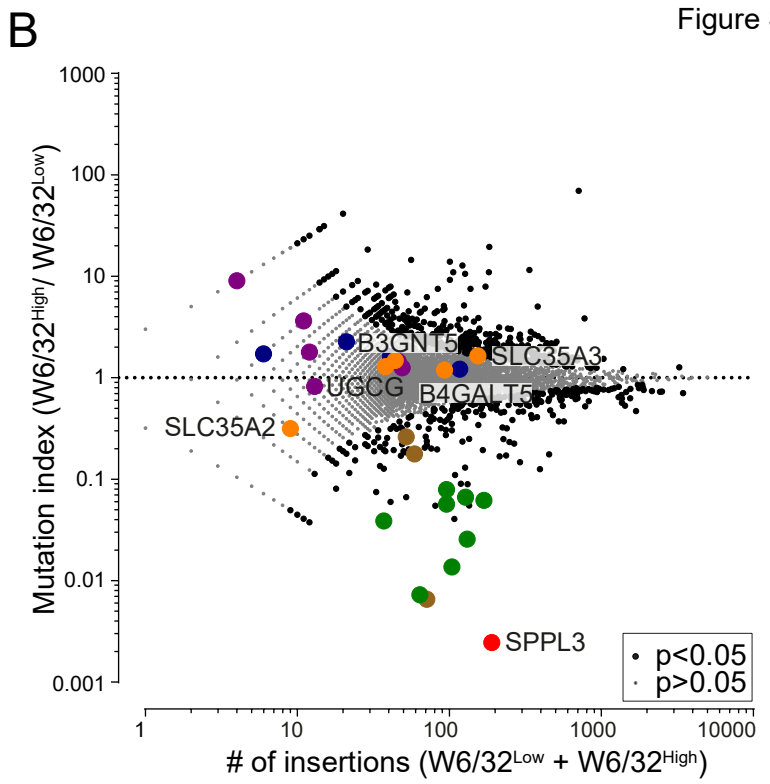
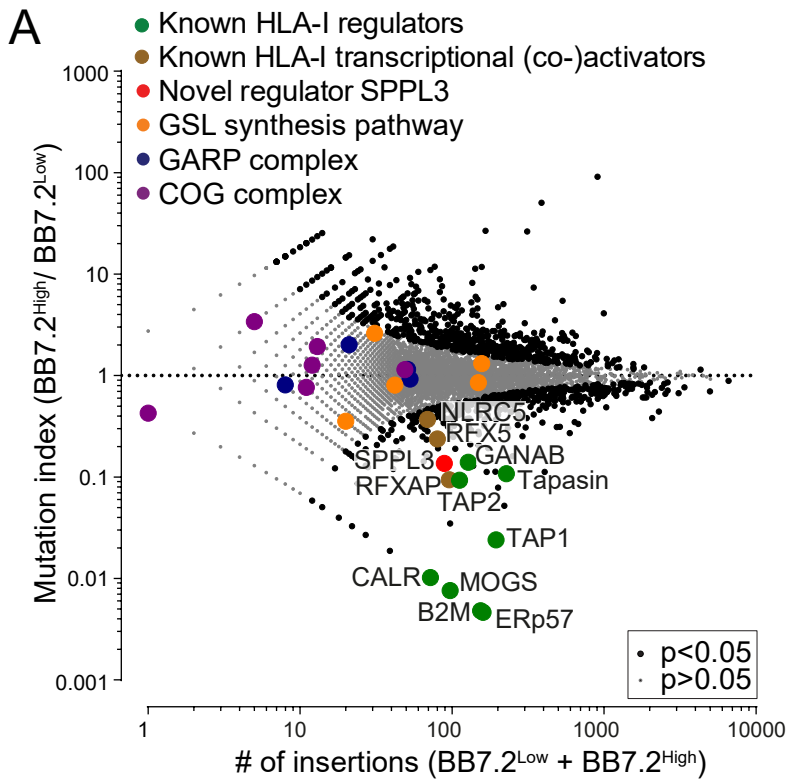


Figure S4. Additional haploid genetic screens carried out using different HLA-I antibodies revealing the contribution of GSL synthesis (Relates to Figures 3 and 4)

(A) Fish-tail plot, the mutation index shows the relative frequency of unique disrupting gene trap integrations in the BB7.2^{High} versus the BB7.2^{Low} sorted cell populations plotted against the total number of unique disrupting integrations (BB7.2^{High} + BB7.2^{Low}) mapped per gene. Positive and negative regulators of HLA-I (*black*) were determined by two-sided Fisher's exact test, FDR (Benjamini-Hochberg) corrected $p < 0.05$. Known HLA-I regulators are depicted in green ($p < 0.05$), known HLA-I transcriptional activators in brown ($p < 0.05$), the novel regulator SPPL3 in red ($p < 0.05$), proteins involved in the glycosphingolipid synthesis pathway in orange and members of the GARP and COG complex in blue and purple, respectively. (B) Fish-tail plot (same as in Figure 1B but with additional genes depicted), The mutation index shows the relative frequency of unique disrupting gene trap integrations in the W6/32^{High} versus the W6/32^{Low} sorted cell populations plotted against the total number of unique disrupting integrations (W6/32^{High} + W6/32^{Low}) mapped per gene. Positive and negative regulators of HLA-I (*black*) were determined by two-sided Fisher's exact test, FDR (Benjamini-Hochberg) corrected $p < 0.05$. Color legend in (A). (C) Representative histograms of non-saturating B1.23.2 cell surface staining of SPPL3 KO cells (GFP-: *red, solid*) or polyclonal populations of SPPL3 KO cells additionally knocked out for the core enzyme UGCG or one of the branching enzymes A3GALT2, A4GALT, B3GNT5, B4GALNT1 or ST3GAL5 (GFP+: *red, dashed*). (D) Representative histograms of non-saturating W6/32 cell surface staining of HAP1 WT cells (GFP-: *blue, solid*) or polyclonal populations of HAP1 WT cells additionally knocked out for the core enzyme UGCG or one of the branching enzymes A3GALT2, A4GALT, B3GNT5, B4GALNT1 or ST3GAL5 (GFP+: *blue, dashed*). For all flow cytometry data, the gray histogram represents an unstained control cell line.

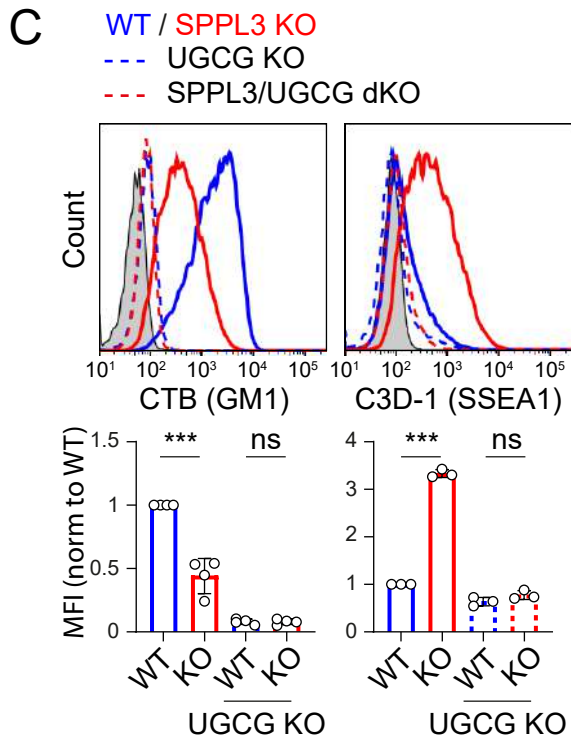
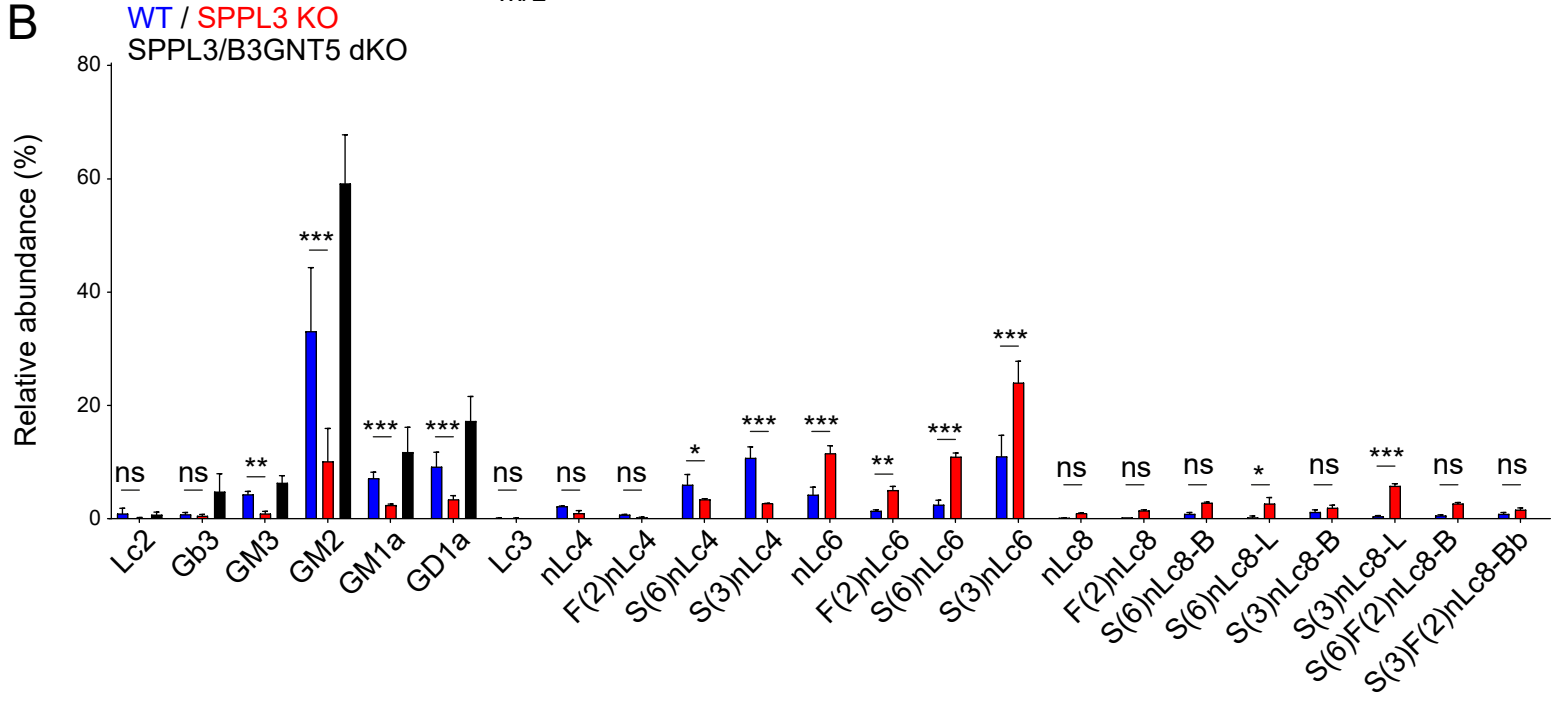
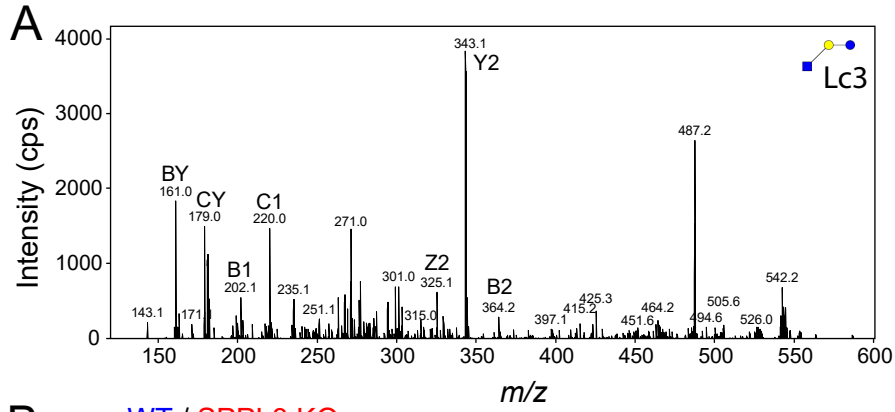


Figure S5. Characterization of the GSL composition and effect on HLA-I accessibility of HAP1 cells (Relates to Figure 5) (A) MS/MS spectra of the enzymatically released glycan from the lower band GSL(s) in the SPPL3 KO sample scratched from the TLC plate (Figure 5D), identifying this product as BODIPY-Lc3Cer. (B) Mean relative abundance of the 23 most abundant GSL glycans derived from WT (*blue*), SPPL3 KO (*red*) and SPPL3/B3GNT5 double KO (dKO) (*black*) cells (see Figure 5E and Table S3). Proposed structures were assigned based on MS/MS fragmentation (where possible) and biological GSL pathway constraints. Statistics shown compare GSL levels between WT and SPPL3 KO cells. n=3. (C) Representative histograms of flow cytometry of cholera toxin B (CTB; anti-GM1) and C3D-1 (anti-SSEA-1) stained WT (*blue*), SPPL3 KO (*red*), UGCG KO (*blue dashed*) and SPPL3/UGCG double KO (dKO) (*red dashed*) HAP1 cells. The gray histogram represents an unstained control cell line. Quantification (MFI) is represented as mean \pm SD, n=4 (CTB) and n=3 (C3D-1), 'KO' is SPPL3 KO.

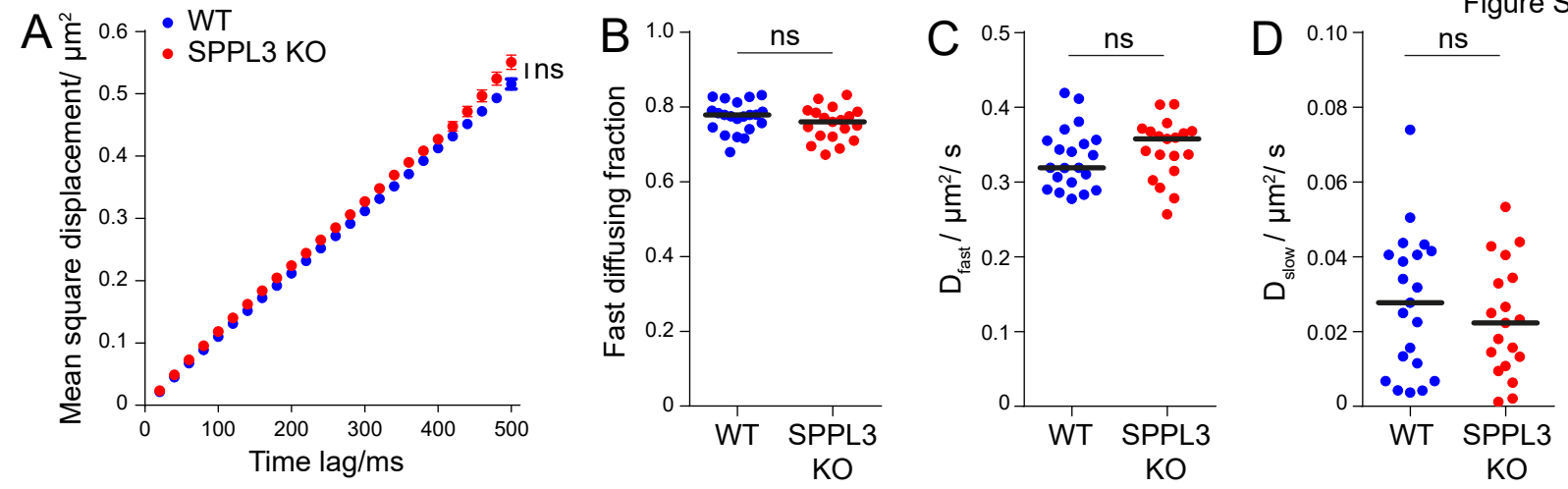


Figure S6. HLA-I membrane dynamics are unaffected by SPPL3 manipulation. Single particle tracking of individual HLA-I molecules was performed on WT and SPPL3 KO cells using SPPL3-independent HLA-I-specific Alexa Fluor 555-conjugated BB7.2 Fab fragments. Single HLA-I molecules were tracked at room temperature with a time lag of 20ms. Representative example of n=3 is shown. (A) Mean square displacement plot of recorded HLA-I trajectories (mean and standard deviation are shown). Relative fractions (B) and diffusion constants of fast- (C) and slow-diffusing (D) HLA-I molecules on WT (n=21) or SPPL3 KO (n=20) cells were calculated by fitting the recorded HLA-I trajectories to a binary diffusion model representing a fast and slow moving fraction. Statistics: median; Mann-Whitney U test.

Figure S7. Pharmacological inhibition of GSL synthesis in glioma improves anti-tumor immune responses (Relates to Figure 7) (A) Expression distribution of SPPL3 versus B3GNT5 in Low Grade Glioma (LGG) derived from TCGA. (B) Representative histograms of CTB (anti-GM1) cell surface staining of WT (*black*) and UGCG KO (*red*) U373 cells. Quantification (MFI) is represented as mean \pm SD, n=5. (C/D) Representative histograms of non-saturating W6/32 (*left*) and B1.23.2 (*right*) cell surface staining of WT (*blue*), SPPL3 KO (*red*) HAP1 cells, (C) SPPL3 KO cells cultured in the presence or absence of UGCG inhibitors (*black*) and (D) WT cells cultured in the presence or absence of UGCG inhibitors (*black*). The red area indicates fluorescence of SPPL3 KO cells. The blue area indicates fluorescence of WT cells. (E) Plotted are MFIs of WT cells stained with non-saturating W6/32 or B1.23.2 precultured with the UGCG inhibitors miglustat (Migl), eliglustat (Eligl), MZ21 or MZ31 (*blue dashed*). Data are normalized to WT (*blue solid*). Quantification (MFI) is represented as mean \pm SD, n=2-5. (F) Representative histograms of CTB (anti-GM1) and C3D-1 (anti-SSEA-1) cell surface staining of WT (*blue*), SPPL3 KO (*red*) precultured with (*dashed*) or without (*solid*) UGCG inhibitors miglustat (Migl), eliglustat (Eligl), MZ21 and MZ31. n=2. (G) IFN- γ secretion by HLA-A*02:01-restricted T cells recognizing endogenously presented FDPS (n=2), or ADIR (n=2) antigens on HAP1 WT (*blue*) or SPPL3 KO cells (*red*) either (*dashed*) or not (*solid*) precultured with indicated UGCG inhibitor (MZ31 or miglustat). IFN- γ secretion was determined by ELISA. Data is represented as mean \pm SD, n=3. (H) Representative histogram of B1.23.2 and CTB cell surface staining of WT (*solid*) U373 cells cultured in the presence of UGCG inhibitors eliglustat (*dashed*) or MZ31 (*dotted*). Quantification (MFI) is represented as mean \pm SD, n=3. For all flow cytometry data, the gray histogram represents an unstained control cell line.

Table S1. Sanger sequencing data of clonally derived CRISPR/Cas9 generated KO cell lines (Relates to all Figures).

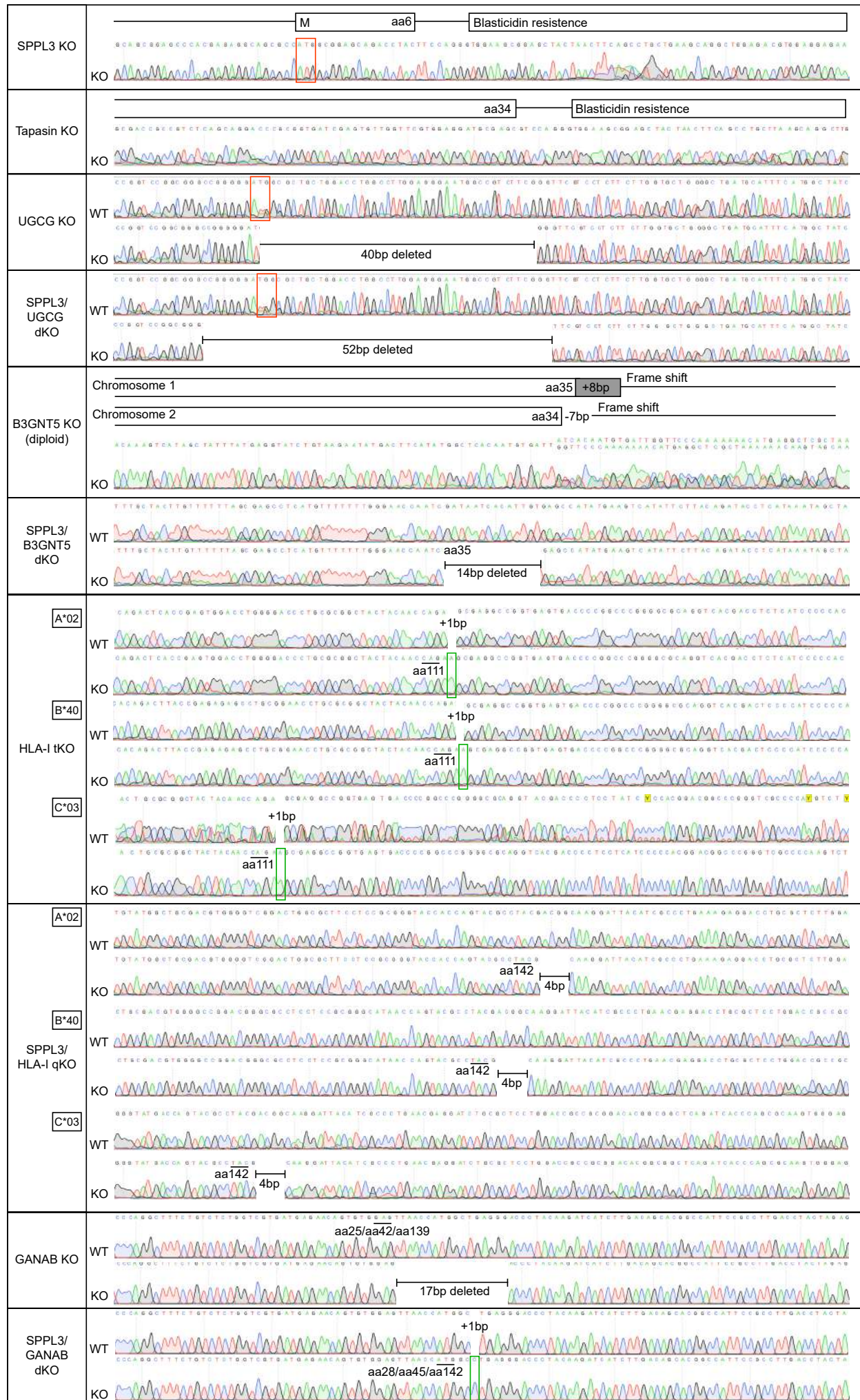


Table S2. Epitopes of HLA-I-specific antibodies (*Relates to Figures 1 and S2*).

Antibody	Recognized HLA Epitope**	Affected by SPPL3?	Reference
W6/32	121K; and 3R on the B2M chain	Yes	(Ladasky et al., 1999)
TP25.99	194V 195S 196D 197H 198E	Yes	(Desai et al., 2000)
ROU9A6*	41T	Yes	(Duquesnoy et al., 2012, Mulder et al., 2010)
BBM.1	38D 44E 45R on the B2M chain	Yes	(Trymbulak and Zeff, 1997)
WK1D12*	73T 76E 163E 167W	Slightly	(Mulder et al., 2010, Marrari et al., 2010)
VTM1F11*	163E	Slightly	(Mulder et al., 2010)
WK4C11*	76V 77S 79R 80N	Slightly	(de Groot et al., 2016, Hiby et al., 2010)
BB7.2	107W 161E 162G 163T 169R 171Y	Slightly	(Hogan and Brown, 1992, Taketani et al., 1983)
SN607D8	143T 144K 145H	No	(Mulder et al., 2010)***
WK4E3	44R 45M 46E	No	***
ROU2D3	62G 63E	No	(Mulder et al., 2010, Duquesnoy et al., 2013)
SN230G6	62G 63E		(Mulder et al., 2010)
ROU7D2*	163E	No	(Mulder et al., 2010)
KAM3H9*	80N 81L 82R 83G	No	(Duquesnoy et al., 2012, de Groot et al., 2016)
B1.23.2*	80N	No	(Achdout et al., 2008)****



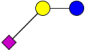
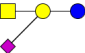
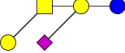
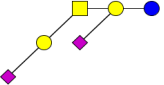

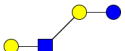
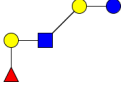
* Conserved positions of the epitopes are shown on the HLA-A2 crystal structure in Figures 1C, 1E and S2A, but residue identity differs between HLA alleles.


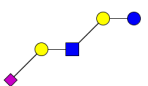
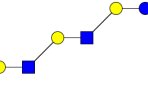
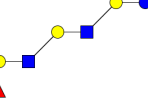
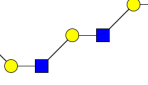
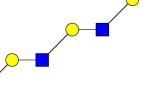
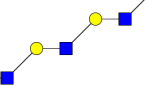
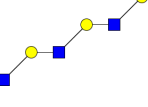
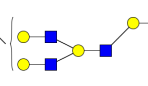
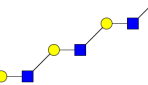
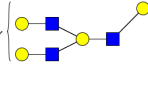
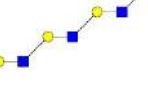
** Epitopes are defined as amino acids known to be important for binding of the respective antibody. Additional dependencies may still be identified in future studies.

*** Personal communication with Dr. R. Duquesnoy.

**** Based on blocking of KIR2DL1 binding.

Table S3. Relative quantification of glycans released from GSLs of WT, SPPL3 KO and SPPL3/B3GNT5 double KO (dKO) cells as detected by PGC LC-ESI-MS/MS (Relates to Figure 5). Proposed structures were assigned based on MS/MS fragmentation (where possible) and biological GSL pathway constraints. Structures are depicted according to the CFG (Consortium of Functional Glycomics). Average from n=3, not detected (n.d.).

Name	$[M-H]^{-1}$ ($[M-2H]^{-2}$)	Proposed structure	Type	Average relative abundance % (SD)		
				WT	SPPL3 KO	SPPL3/ B3GNT5 dKO
Lc2	343.12		LacCer	0.9(1.0)	0.1(0.1)	0.7(0.5)
Gb3	505.17		Globoside	0.8(0.4)	0.5(0.2)	4.7(3.2)
GM3	634.22		Ganglioside	4.3(0.6)	0.9(0.4)	6.3(1.3)
GM2	837.31		Ganglioside	33.1(11.2)	10.1(5.8)	59.2(8.6)
GM1a	999.34		Ganglioside	7.2(1.0)	2.4(0.3)	11.8(4.4)
GD1a	1290.39 (644.69)		Ganglioside	9.2(2.5)	3.4(0.7)	17.3(5.4)
Lc3	546.20		nsGSL	0.1(0.1)	0.1(0.1)	n.d.
nLc4	708.28		nsGSL	2.2(0.1)	0.9(0.5)	n.d.
F(2)nLc4	854.31		nsGSL	0.7(0.1)	0.2(0.1)	n.d.

S(6)nLc4	999.35		nsGSL	6.0(1.8)	3.4(0.1)	n.d.
S(3)nLc4	999.35		nsGSL	10.8(1.9)	2.7(0.0)	n.d.
nLc6	1073.38 (536.2)		nsGSL	4.2(1.4)	11.5(1.4)	n.d.
F(2)nLc6	1219.42 (609.21)		nsGSL	1.4(0.2)	5.1(0.6)	n.d.
S(6)nLc6	1364.44 (681.72)		nsGSL	2.5(0.8)	11.0(0.7)	n.d.
S(3)nLc6	1364.44 (681.72)		nsGSL	11.0(3.7)	24.0(3.8)	n.d.
nLc8	1438.54 (718.77)		nsGSL	0.1(0.0)	1.0(0.1)	n.d.
F(2)nLc8	1584.50 (791.75)		nsGSL	0.2(0.0)	1.5(0.1)	n.d.
S(6)nLc8-B	1729.53 (864.27)		nsGSL	0.8(0.3)	2.8(0.1)	n.d.
S(6)nLc8-L	1729.53 (864.27)		nsGSL	0.2(0.3)	2.7(1.1)	n.d.
S(3)nLc8-B	1729.53 (864.27)		nsGSL	1.2(0.4)	1.9(0.5)	n.d.
S(3)nLc8-L	1729.53 (864.27)		nsGSL	0.4(0.1)	5.8(0.4)	n.d.

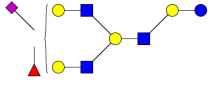
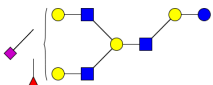
S(6)F(2)nLc8-B	1875.62 (937.31)		nsGSL	0.6(0.1)	2.7(0.2)	n.d.
S(3)F(2)nLc8-B	1875.62 (937.31)		nsGSL	0.9(0.3)	1.6(0.3)	n.d.

Table S4. gRNA primers used for CRISPR/Cas9 mediated genome editing (Relates to Table S1)

gRNAs were handpicked using online tools (Doench et al., 2016, Hsu et al., 2013). The HLA-A, -B, -C specific gRNAs target common sequences of the three HLA alleles expressed in HAP1 cells (HLA-A*02:01, HLA-B*40:01 and HLA-Cw*03:04).

Gene	Forward	Reverse
SPPL3*	CACCGCCCCGCACTCACCACGAGT	AAACACTCGTGGTGAGTGCGGGGC
HLA-ABC#1*	CACCGCGGCTACTACAACCAGAGCG	AAACCGCTCTGGTTGTAGTAGCCGC
HLA-ABC#2*	CACCGATGTAATCCTTGCCGTCGT	AAACACGACGGCAAGGATTACATC
Tapasin*	CACCGCGTGGAGGATGCGAGCGGAA	AAACTTCCGCTCGCATCCTCCACGC
UGCG#1*	CACCGTGGAGGGAATGGCCGTCTTC	AAACGAAGACGGCCATTCCCTCCAC
UGCG#2	CACCGAAGAGGACGAACCCGAAGA	CACCGAAGACGGCCATTCCCTCCA
UGCG#3	CACCGAAGACGGCCATTCCCTCCA	AAACTGGAGGGAATGGCCGTCTTC
B3GNT5#1*	CACCGCTCACAATGTGATTATCGAT	AAACATCGATAATCACATTGTGAGC
B3GNT5#2	CACCGCTCTTAAGCACACCTCAGCG	AAACCGCTGAGGTGTGCTTAAGAGC
B3GNT5#3	CACCGTGAGGTGTGCTTAAGAGACA	AAACTGTCTCTTAAGCACACCTCAC
B3GNT5#4	CACCGTTGAGTGGATATGAGAATGT	AAACACATTCTCATATCCACTCAAC
A3GALT2#1	CACCGCCCTCCTTGAGAGCCATATG	AAACCATATGGCTCTCAAGGAGGGC
A3GALT2#2	CACCGTCCCATATGGCTCTCAAGG	AAACCCCTTGAGAGCCATATGGGGAC
A3GALT2#3	CACCGCCGAAGGGCAGACGCCCATG	AAACCATGGGCGTCTGCCCTTCGGC
B4GALNT1#1	CACCGACGGCGCAAGAGGTAGCCGG	AAACCCGGCTACCTCTTGCGCCGTC
B4GALNT1#2	CACCGCCCCACCTAGGATGTGGCT	AAACAGCCACATCCTAGGTGGGGGC
B4GALNT1#3	CACCGCGCGTACAGGAGCCCCAGCG	AAACCGCTGGGGCTCCTGTACGCGC
ST3GAL5#1	CACCGAACTGAGAAGTGATTGCTCG	AAACCGAGCAATCACTTCTCAGTTC
ST3GAL5#2	CACCGATCACTTCTCAGTTTCACAT	AAACATGTGAAACTGAGAAGTGATC
ST3GAL5 #3	CACCGTTCACATAGGTGTACTIONACT	AAACAGTGAGTACACCTATGTGAAC
A4GALT#1	CACCGAACGTGCCAGTAGATCATGA	AAACTCATGATCTACTGGCACGTTC
A4GALT#2	CACCGGTGCAGACCCGCTGCCTTG	AAACCAAGGCAGCGGGTCTGCACC
CMAS	CACCGCTGAATCCAGGGCCGCACGC	AAACGCGTGCGGCCCTGGATTACAGC
GANAB*	CACCGAACAGTGTGGAGTTAACCA	AAACTGGTTAACTCCACACTGTTC

* used to create monoclonally derived KO cell lines.

Table S5. PCR and sequencing primers (Relates to Table S1)

Gene	PCR Forward	PCR Reverse	Sequencing
SPPL3	AGCGAGCAAGCAAGCAAG	CGACATGGTGCTTGTTGTCC	TGGTGATCTTCTCAGTGGCG
HLA-A#1&2*	TTCTTCACATCCGTGTCCCG	TTCCTCTCCCTCAGGACCAG	TCCAATTGTCTCCCCTCCT
HLA-B#1&2*	CCGGGAGACACAGATCTCCA	CAGCTTGTCTTCCCGTTCT	GAGCCACTCCACGCACTC
HLA-C#1*	ACTTCATCGCAGTGGGCTAC	GGATCTCAGACCGGGAGACT	ACACAGAAGTACAAGCGCCA
HLA-C#2*	GTTTAGGCCAAAATCCCGC	TCCATTTTCTCCCCTCCT	GCCAGGGTCTCACATCATCC
Tapasin	TCGCCAAGAAGTAGAGGGA	CGACATGGTGCTTGTTGTCC	TGGTGATCTTCTCAGTGGCG
UGCG	TTTCTCTCCCCACCTTCT	AAACCAAGCCACCACCTTCA	AACGTTTCCCATTCTCGCCT
B3GNT5	GGCGGCATTGGTGTCAAAT	ACCACGATGAACACGACCAA	ACCACGATGAACACGACCAA
GANAB	ATGCTTGGGTCTGTTCTGG	GCCCTCTGATGCTCAAACCTC	TTCCCCGGTCTTCTAAAGT

*primers to allele-specifically amplify regions targeted by the HLA-A, -B and -C-targeting gRNAs HLA-ABC#1 and/or HLA-ABC#2.